DURBAN UNIVERSITY OF TECHNOLOGY
INYUVESI YASETHEKWINI YEZOBUCHWEPHESHE

POWER FLOW AND FAULTS ANALYSIS OF A HYBRID DC MICROGRID: PV SYSTEM AND WIND ENERGY

By

Musawenkosi Lethumcebo Thanduxolo Zulu

Student Number: 21750894

A dissertation submitted in fulfilment of the requirements for the degree of Master of Engineering in Electrical Power Engineering

In the Department of Electrical Power Engineering, Faculty of Engineering and the Built Environment

Supervisor: **Dr Evans E. Ojo**

Co-Supervisor: **Dr Ajibola O. Akinrinde**

October, 2021

DECLARATION

I hereby declare that this dissertation is my work, and each text has been correctly referenced or cited. Moreover, this work has not been previously published in portion or whole for another degree at any other University.

This research was duly supervised by Dr Evans E. Ojo and Dr Ajibola O. Akinrinde at the Durban University of Technology.

Submitted by:

04/10/2021

……. ……..……..

Musawenkosi L. T. Zulu Date

Student Number: 21750894

Approved for Final Submission by:

25/10/2021

……. …….

Supervisor: Dr Evans E. Ojo Date

26/10/2021

……. …….

Co-Supervisor: Dr Ajibola O. Akinrinde Date

Dedication

This dissertation is dedicated to my beloved parents, Mr Bonginkosi and Mrs Olgah Zulu, and also to the Almighty God, the saviour of my life, who made all grace fall upon me and who has been my source from the beginning to the completion of this work.

Acknowledgement

First and foremost, I would like to express my sincere and deep appreciation to the man above all, the Lord God Almighty, for granting me power and for making this dream a reality. Secondly, with deep regard and profound respect, I wish to extend my sincere gratitude to my supervisors, Dr Evans E. Ojo and Dr A.O Akinrinde, for their enthusiasm, constant encouragement, persistent unending support, guidance, suggestions, positive criticism and valuable suggestions throughout the entire period of study- it is acknowledged. I humble myself and express my deep sense of gratitude and indebtedness. Many thanks and deep love go out to my parents, Mr Bonginkosi M Zulu and Mrs Olgah T Zulu, my siblings Thembinkosi, Sithembiso, Ntando, Nomalungelo and Sinqobile Zulu and extended family members Phiwokuhle Ndaba and the entire family who supported me, whose invaluable encouragement to me meant more than they will ever know.

I am truly indebted to my colleagues, best friends and staff in the Department of Electrical Power Engineering and the Durban University of Technology family for their support in many different ways. I am enormously grateful to Dr Elutunji Buraimoh for his endless support in all circumstances and for his guidance. I am also equally indebted to all those who have contributed directly or indirectly.

To all of you, may God shower his blessings upon you, show you mercy and grant you His favour all the time. You have given me the gift of believing in myself.

Abstract

Rural electrification has become a very important means of improving the standard of living of rural dwellers, a process which also helps in the electrification of remote and isolated regions. Presently, the electrification of such regions can be achieved through the use of renewable energy. The use of renewable energy sources such as PV and wind energy is gaining popularity as the solution to achieving the electrification of rural areas, such as the use of the microgrid, which can be in the form of an AC or DC microgrid. The DC microgrid can be used to connect distributed energy resources and its energy storage is considered to be an economical system to meet consumer demand due to its benefits, namely environmental friendliness, reliability and good performance in load distribution. The power system may experience many faults when transferring power via overhead transmission lines to the load. When these faults occur, it is important to detect the location and isolate the part that had experienced the fault quickly, without de-activating the whole microgrid. The main aim of this study was to conduct a power flow and faults analysis on a hybrid DC microgrid model with battery storage. The hybrid energy sources for the DC microgrid are the PV system and wind energy system. Firstly, this research conducted a power flow analysis for the hybrid DC microgrid. Secondly, a fault analysis was carried out on the system and both the power flow and the fault analysis were formulated through implementation in a MATLAB/Simulink environment under various conditions in order to ascertain the stability and reliability of the system. Various MATLAB/Simulations were carried out, including the DC single-line-ground fault and DC line-line fault and are analysed in a designed hybrid DC microgrid power system. The results showed that DC line-to-line and DC line-to-ground faults lead to the imbalance of DC voltage, which is difficult to re-balance and stabilize in the system after the existence of these faults. When these faults occurred in the system, there was immense fluctuation and unsteadiness of output load power delivered to consumers. Moreover, wind-generated power on the generation side was severely affected.

Based on the results and analysis of those results, the hybrid DC microgrid is seen as a satisfactory and optimum concept for the generation and transmission of power for rural and isolated area electrification, i.e. it can provide power to remote areas that cannot be reached by the national grid. The study revealed, based on the analysis of results, that it has an effective response under fault conditions. Results for a hybrid DC microgrid revealed that high quality of power is experienced in load distribution. Also based on the results, when DC faults occurs there is disturbance to output.

Table of Contents

List of Figures

List of Tables

List of Acronyms

AC	Alternating Current
BDC	Bidirectional Converters
BESSs	Battery Energy Storage Systems
CSP	Concentrated Solar Power
DC	Direct Current
DERs	Distributed Energy Resources
DG	Distributed generation
EDLCs	Electric Double-Layer Capacitors
ESS	Energy Storage System
FF	Fill Factor
HAWT	Horizontal Axis Wind Turbine
HES	Hybrid energy systems
HV	High Voltage
HVAC	High Voltage Alternating Current
HVDC	High Voltage Direct Current
IGBT	Insulated Gate Bipolar Transistor
IEEE	Institute of Electrical and Electronics Engineers
LCC	Line Commutated Converters
LVDC	Low Voltage Direct Current

MG	Microgrid
MPPT	Maximum Power-Point Tracking
PMSG	Permanent Magnet Synchronous Generators
PV	Photovoltaic
SOC	State of Charge of the battery
STC	Standard Test Condition
STE	Solar Thermal Energy
VAWT	Vertical Axis Wind Turbine
VSC	Voltage Source Converters
WG	Wind Generator
WTs	Wind Turbines

List of Symbols

I	Cell current (the same as the module current) (A)
Isc	Short Circuit Current which is equal to photocurrent (A)
Io	Dark Saturation Current (A)
q	Electronic charge (1.602x10-19C)
k	Boltzmann's constant (1.381 × 10−23 J/K)
A	Idealizing Factor
T	Cell Temperature (K)
V	Cell Voltage (V)
Rs	Shunt Resistance (Ω)
Rp	Parallel resistance (Ω)
Id	Diode current (A)
Ip	Parallel Resistance Current (A)
Vd	Diode Voltage (V)
Δt	Time step
d(t)	Duty ratio at the present time step
d(t- Δt)	Duty ratio at the preceding time step and
Δd	Incremental duty ratio
Ew	Energy generated by wind turbine
Pw	Output power
ρw	Density of air in is Kg/m^3
A	Swept Area of rotor blades,

Cp	Power coefficient represent generator and turbine efficiency
μ_g	Generator Efficiency
μ_t	Turbine Efficiency
$P_4(k)$	Power flow from the battery (discharge);
$E_{nominal}$	Nominal Energy
η	Battery efficiency
$L_{\min}$	Minimum inductance required for continuous operation
D	Duty cycle
R	Load resistance
f	Switching frequency.
β	Pitch angle of blades in degree
δ	Tip speed ratio of turbine

Chapter One
Introduction

1.1 Background

The energy crisis experienced in recent times, coupled with the deterioration of the world ecology and global warming are critical problems facing the world. This is mostly due to the fact that there is an increasing use of the energy resources like fossil fuels which is directly adversely affecting the natural environment as a result of the emission of carbon dioxide (CO_2) [1]. The effects of using fossils fuels, coupled with its depletion, highlight a need to explore alternative sources of energy such as distributed energy resources (DERs), which are regarded as clean and renewable. The demand for electricity has increased significantly over the last few decades, which has necessitated the establishment of more power generation stations with the corresponding expansion of the power grid to convey power to the load centres.

In addition, population growth has led to an increased demand for electricity, which means the use of more coal-fired power stations. The operation of these power stations have adverse effects on the environment, which directly result in pollution. To mitigate this situation and avoid the use of long transmission lines which usually stretch for several kilometres, the use of the concept of the direct current (DC) microgrid is explored. A microgrid is an incorporated power co-ordination that generates power from a variety of sources in order to achieve energy efficacy, environmental friendliness, sustainability, consistency and cost benefits [2], [3]. The DC microgrid has proved to be a powerful distribution network solution to remedy this problem due to its level of operation and also based on the fact that DC microgrids provide significant benefits for electricity consumers and power grid operators. Consequently, DC hybrid microgrid power systems are highly recommended for consideration for the future in order to achieve low gas emission from power generation stations. The DC microgrid hybrid system also offers the advantage of providing the bases for the interconnection of systems, i.e. for

meshing networks that are normally complex. Despite these advantages, DC microgrids experience many faults which pose great challenges in using this form of power transfer in distribution networks. The use of DC microgrids (MG) for power transmission has already been proposed, as documented in [4].

Around the world, new generation capacities are being installed at phenomenal rates, driven mainly by wind and solar energy are primary source of power. Wind and solar energy are the primary sources of power. With the generation of more than 1000 gigawatts of wind and solar energy in the middle of 2018, the world reached a landmark [5]. Figure 1.1 shows the rapid increase in terms of generation capacity for the last two decades of global wind and solar installations.

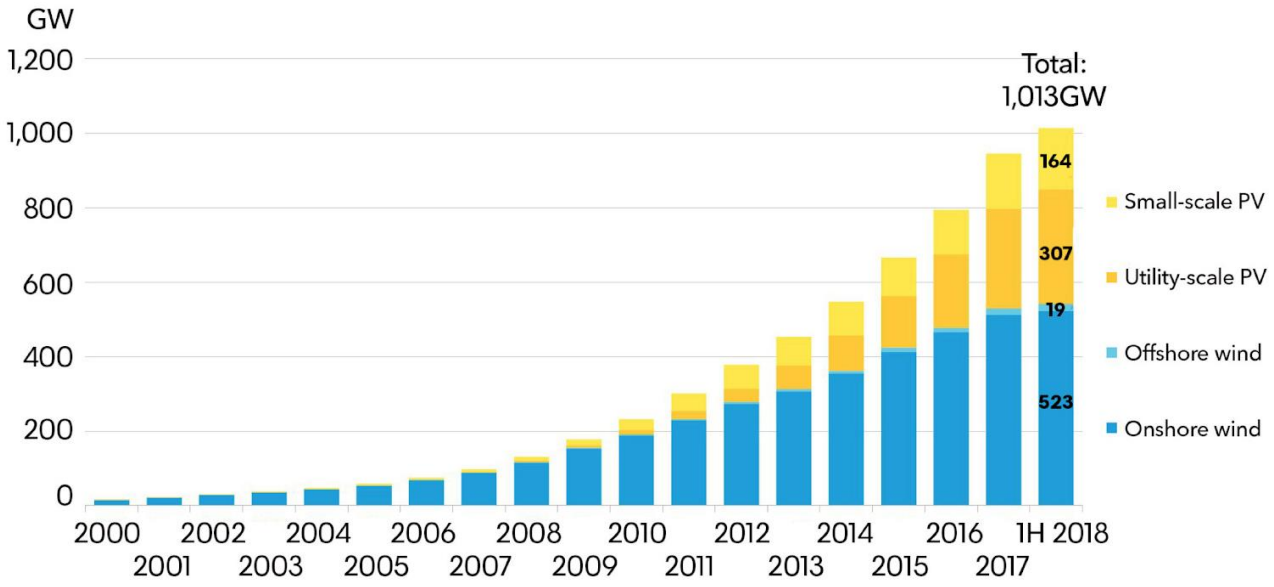

Figure 1.1: Global wind and solar installations (2000 - 2018) [5]

A microgrid can function as a stand-alone arrangement in island mode or as part of the grid in grid connected mode. In order to connect a microgrid to the main grid in grid connected mode, it must be according to the IEEE 1547 standard [6] which lays out the guiding principle and necessities for doing so. Intentionally or inadvertently, the microgrid may transform from grid to island mode. The isolating system can isolate the microgrid from the grid if a failure occurs on the main grid, which is an unintentional scenario. The microgrid may be deliberately

detached from the grid for repairs purposes in the event of grid maintenance. The above-mentioned migration and accelerating investment in renewable energy clearly reveal that renewable energy is the way of the future.

1.2 Problem Statement

There is an evolving trends in which the use of distributed energy resources (DERs) for power generation is gaining popularity. This has drawn much attention because it is a viable means to cater for the constantly increasing demand for electricity consumption, which is greater than the generation capacity. Moreover, the use of the DC microgrid has revealed a speedy development to cater for DC load distribution. DC, when compared to AC, provides the benefits of a no power conversion process in conventional power systems. Furthermore, there is effective energy conversion, improved transportation capability and it can be used to access new energy sources easily. The DC microgrid has become a new trend for the transfer of power due to its simplicity and reliability, which is achieved through connected micro-source, battery storage source and load distributed by the transmission of DC lines. However, the implementation of the DC microgrid comes with many challenges and many investigations are conducted with the goal being to develop methods to reduce or mitigate these challenges [7]. The major challenges are when faults occurs in a power system and the occurrence of these faults necessitate the disconnecting of faulty parts in the system for the clearance of this fault. This problem also applies to power systems used for the DC microgrid.

For this study, the hybrid DC microgrid consisting of power sources from solar and wind was investigated. This investigation will comprise the design, modelling and simulation of the power network. For this network, power flow analysis will be conducted on the designed system as well as the fault analysis in order to determine the efficiency of the system.

1.3 Purpose of this Study

The increased damaging effect of fossil-fuelled power generators has necessitated the diversification of the power industries, with emphasis on the use of renewable energy resources. Renewable energy based on distributed generators (DGs) has the potential to plays a significant part in power generation while also assisting in the fight against global warming. The use of renewable energy provides various advantages such as suppleness, environmental friendliness and expandability. These advantages have made DGs power-driven by numerous renewable and non-conventional micro-sources an attractive and suitable option for reducing global warming and also for configuring modern electrical grids. Microgrids are proposed as a solution for using DGs since they are controllable and can work in together or separately from the national grid as an integrated energy distribution system. Nevertheless, many challenges arise in the use of microgrids, namely the stability of the system and fault occurrences.

The purpose of this study is to conduct a power flow analysis and carry out a fault analysis in a hybrid DC microgrid: PV system and wind energy system, as well as to promote the use of renewable energy. The hybrid DC microgrid was designed, modelled and simulated to evaluate these tasks. The PV and wind energy systems are modelled separately and merged to form the hybrid DC microgrid to power the system. The performance of a hybrid is analysed to assess the stability, productivity and reliability of the system with the aid of power flow. The DC faults analysis of the DC line-to-line fault and DC line-to-ground fault is carried out in a hybrid DC microgrid for the purpose of ascertaining the robustness of the system. The results obtained are from the formulation, modelling and simulations implemented on MATLAB/SIMULINK software.

1.4 Aim and Objectives

The aims of this study in relation to the purpose for this research are highlighted as follows:

- To conduct, analytically, a power flow analysis of a hybrid DC microgrid powered by a PV system and wind energy;
- To carry out a fault analysis on the hybrid DC microgrid: PV system and wind energy; and
- To model a combined PV system and wind energy as a hybrid DC microgrid.

In line with the aforementioned aims, this thesis seeks to achieve the following objectives:

- To further an understanding of a hybrid DC microgrid using distributed energy resources (DERs);
- To model, separately, a DC PV system and the DC wind energy system;
- In line with the above, to combine the two systems to develop a hybrid DC microgrid;
- To conduct a power flow analysis and evaluate the efficiency of hybrid DC microgrid; and
- To analyze performance and power stability of power supply in the hybrid DC microgrid.

1.5 Research Questions

On completion of this research, this investigation document in this report will be used to answer the following questions:

- What is the most energy-efficient and cost-effective way of connecting a PV system with wind energy to form a Hybrid DC microgrid?
- How does conducting a power flow analysis assist to reveal the effectiveness and reliability of a hybrid DC microgrid system?

1.6 Dissertation Outline

The thesis is structured into five chapters:

Chapter 1-Introduction: This chapter introduces and orientates the study with respect to the general background, problem statement, motivation and aims and objectives of the study. It also highlights the research questions for revealing the implementation of DC microgrid.

Chapter 2-Literature Review: Chapter 2 discusses the published peer-reviewed related work. It gives an introduction to different theories for modelling a hybrid DC microgrid. The chapter also provides an in-depth review to the generation, transmission and supply of DC power to the load of PV and wind energy connection. This chapter also further explains the detailed modelling a PV and wind energy arrangement using MPPT, merging into a hybrid DC microgrid. It also presents a review of hybrid powered power systems. In the faults that occur in the system are also discussed.

Chapter 3-Modelling and Computer Simulations: This third chapter discusses the analytical modelling and the computer simulations of PV systems, wind energy systems and hybrid DC microgrid. It presents the methodology and strategies for the modelling of a hybrid DC microgrid. The chapter also gives a detailed explanation of computer simulations of the modelled hybrid DC microgrid, including the implemented strategies of MPPT, with the simulations in the MATLAB/SIMULINK.

Chapter 4-Results and Discussion of Results: This chapter presents the simulations and the results, which was implemented in the MATLAB/SIMULINK environment. Power flow and fault analysis results of a hybrid DC microgrid are presented and discussed in this chapter. Steady state performance during faults are analysed in a hybrid DC microgrid with the aid of a power flow study and transient studies respectively. The results of the faults analysis are presented for the three components of the hybrid DC microgrid: the generation, DC transmission and the DC load.

Chapter 5-Conclusion and Recommendation: Finally, this last chapter is a conclusion of the thesis. It provides a comprehensive summary of the study undertaken. Recommendations on future research based on the results of the study are also highlighted.

Chapter Two
Literature Review

2.1 Introduction

This chapter delivers a general review of the literature in terms of the significance and states the reasons why the use of distributed energy resources (DERs) should be encouraged. It gives a detailed explanation for the use of renewable energies explored in this study: PV solar energy and wind energy. The chapter provides a broad review of the fast-developing distributed energy technology and its application. Thus, the review of research related to this study will serve as the basis for improving the application of renewable energy resources. Several of control strategies and its enhancement for DC microgrid deployment are presented in this chapter. Distributed, hierarchical, distributed and intelligent control strategies are presented. Reviewing distribution systems, renewable resources which are PV solar energy, wind energy and the energy storage systems. Furthermore, it reviews the previous modelling and simulation of a DC microgrid powered by PV solar and wind energy to highlight motivations, limitations, viewpoints, advances, contributions to system flexibility and expandability, as well as their relevance to the current study.

2.2 DC Microgrid

A microgrid is defined as a power systems unit which is made up of one or more collections of distributed energy resources, including the energy storage sources, and a microgrid can operate independently as an isolated power source from the main power system grid [8]. This form of power system needs to be monitored to deliver desired power as it is intended for specific loads [9]. The use of a microgrid, due to its good performance, is recommended for use in distributed energy resources, like wind energy, fuel cells, PV, power generators and combined heat [10]. This requires the knowledge of its accurate size and design for better performance. Microgrids

have the ability to function as well-intended islanding without interrupting the grid reliability to advance the performance under the case of power inconsistency [7].

There are two systems in an electricity network, namely: transmission and distribution systems. In conventional networks, the system consists of a main power being transported to the distribution system and delivered towards the load [11]. The biggest challenges accompanying this system are that the load side is far away from the power generation stations. This results in unreliability. Thus, it will be difficult to cope with unsteadiness arising at the load end. A microgrid is capable and more suitable for these needs since it consists of DERs. The majority of the world is still dominated by AC networks, but recently the DC microgrid network is gaining popularity due to its excellent consistency and high effectiveness when connected with renewable energy, together with the energy storage system [12].

The network of a microgrid is made up of the following components: wind energy, rectifiers and DC-DC converters which are required to deliver DC loads. In this network, an AC microgrid distribution line is connected with a voltage of 230 V angle phase AC system, then AC loads can be directly connected [13], [14].

Shown in Figure 2.1 are the DERs and other devices such as the rectifiers, which play a role of converting the AC to DC and then the inverter converts the direct current to alternating current. The energy made from different resources, including the grid to the distribution line, is co-ordinated in the microgrid system.

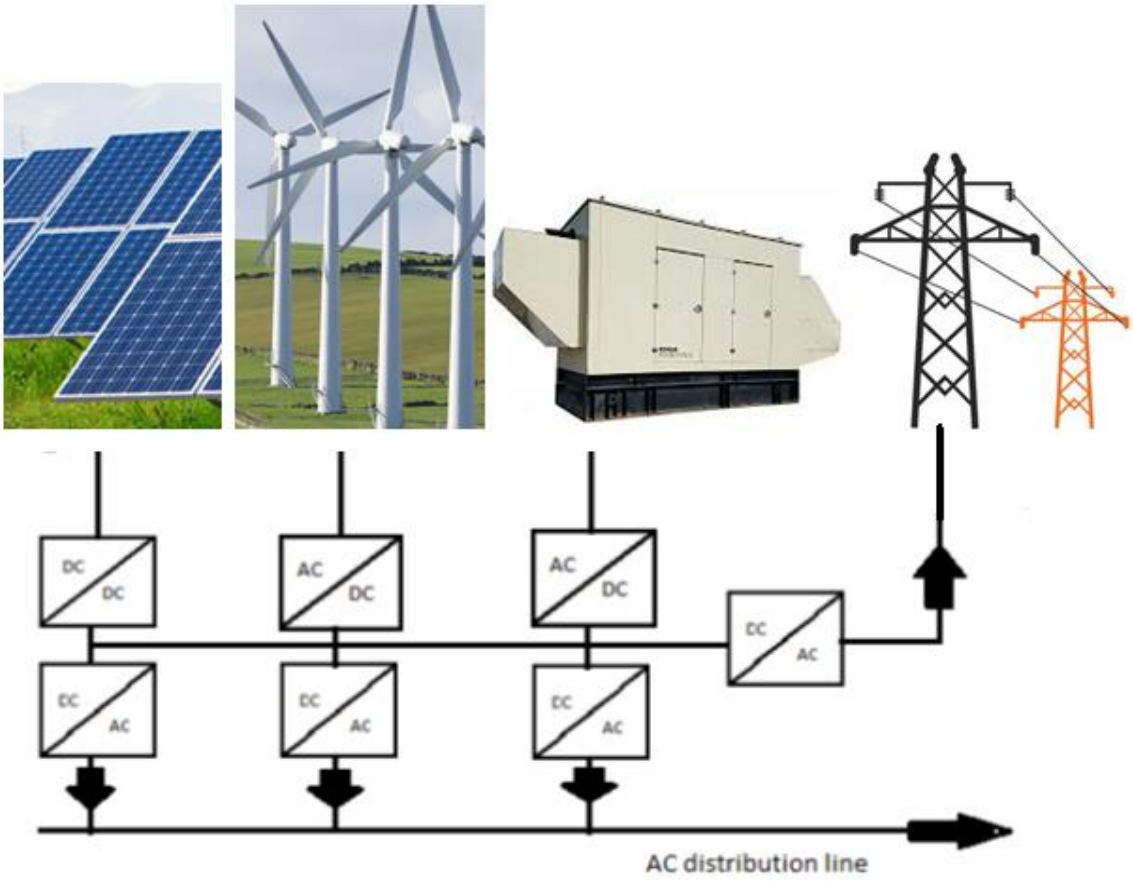

Figure 2.1: Microgrids with distributed energy resources components included

2.3 Distribution system

To construct a well-organized microgrid, it is important to plan a distribution system since it contribute in developing a system. The planning of distribution structure does not only contribute to power reliability, but it is also environmentally friendly while it remains economically affordable.

For utility grid and microgrid, there are three different categories of distribution, namely:

- Radial Distribution;
- Loop Distribution; and
- Network Distribution.

Radial and loop type distribution are the most commonly used in the distribution in microgrids [15]. These two types of distribution are easy to plan and construct. As a result, the cost needed in their implementation is low.

2.3.1 Radial Distribution

Radial distribution has good power distribution and is regarded as the best system in load distribution. In most countries around the world, radial distribution is deployed for power distribution. About 90% of all distribution in South Africa uses the radial distribution network. A majority of the microgrids that are installed and constructed prefer the radial distribution system because of affordability, ease of design and modesty. Radial distribution is designed such that there is only one pathway between the generation point and the houses, as shown in Figure 2.2.

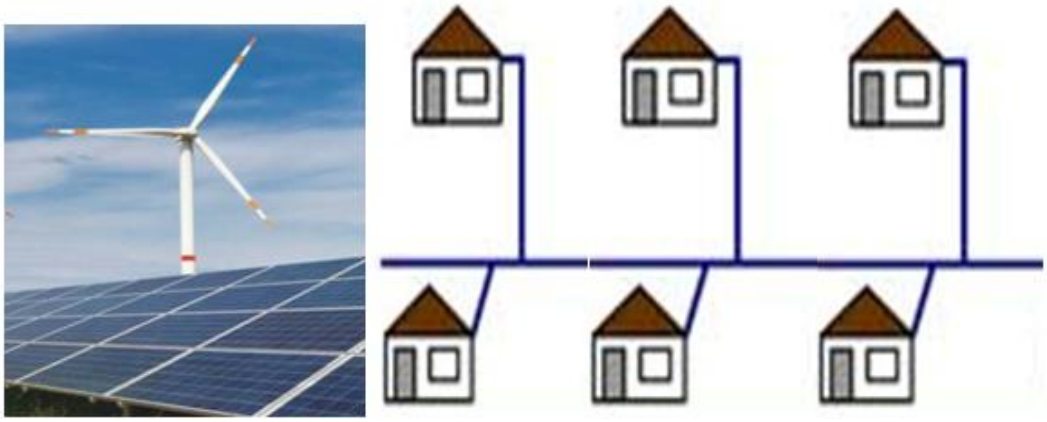

Figure 2.2: Typical radial distribution

This indicates that there is only a single path that the power flows through, which if disturbed will cut off power to the households linked to distribution. In a radial distribution system bus lines to be used are determined by the type of power that is being transmitted to the households connected through bus lines. The crucial shortcoming of this radial distribution arrangement is that it is less reliable since this system can only distribute power in one direction, thus consumers connected to the system will have a blackout when the power line is interrupted or breaks down [15].

2.3.2 Loop Distribution

Recently, when constructing the microgrid, the loop distribution system has been regarded as a substitute to the radial type distribution system. Depending on the most suitable distribution for that area, loop type distribution is leading in most parts of Europe[15]. Loop type distribution can be defined as a loop which supplies all the households connected to it. The loop formation approach is that from the point of generation, power must be transmit in both bi-directional ways. Loop type distribution, , means that there is only one direction of power flow at the time and at the point of generation, and where the transmission line starts and ends not like radial distribution, as shown in Figure 2.3.

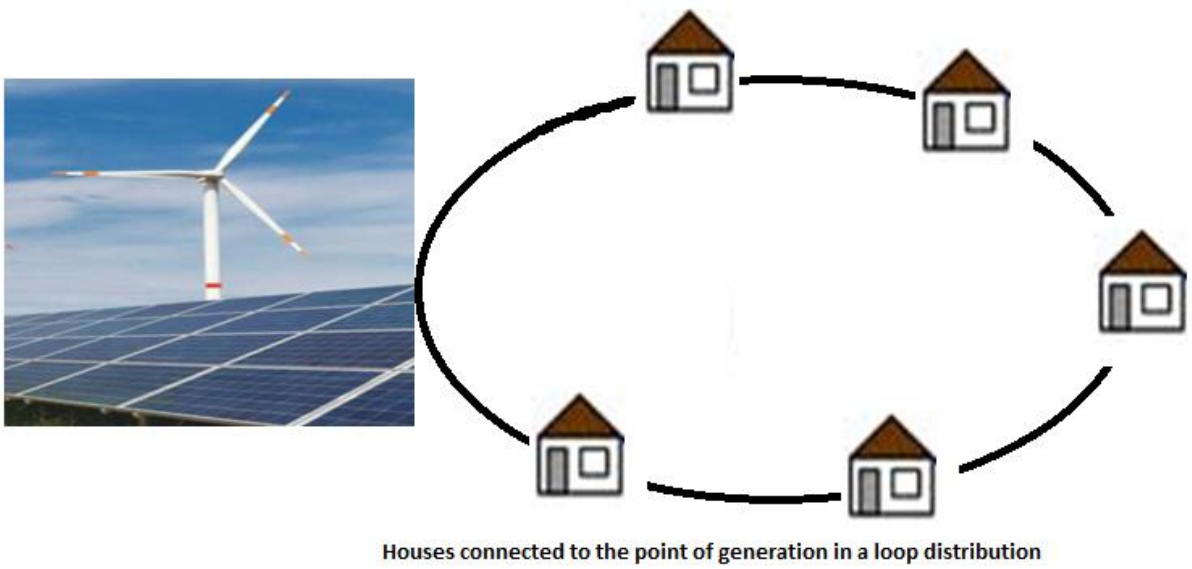

Figure 2.3: Loop type distribution

The advantage of a loop distribution system is that it is more reliable and improves the electrical network. For such networks, loop distribution operation is such that if there is a power failure in one path, then power can be fed to the consumers through other path switches automatically or manually. However, the loop type distribution is more expensive as compared to the radial distribution since more switches and conductors are required [15].

2.3.3 Network Distribution

A network distribution system is also referred to as mesh distribution. It is the most consistent amongst others and it is usually used for major establishments in a crowded, high load density municipal areas. Network distribution is a combination of radial and loop distribution types. The network type distribution can be supplied from two or more power supplies and if one of the supplier ceases feeding due to breakdowns or other reasons, then other generators as a loop type will continue feeding power with the aid of switches and circuit breakers. Figure 2.4 shows a network type distribution system connected in a DC microgrid.

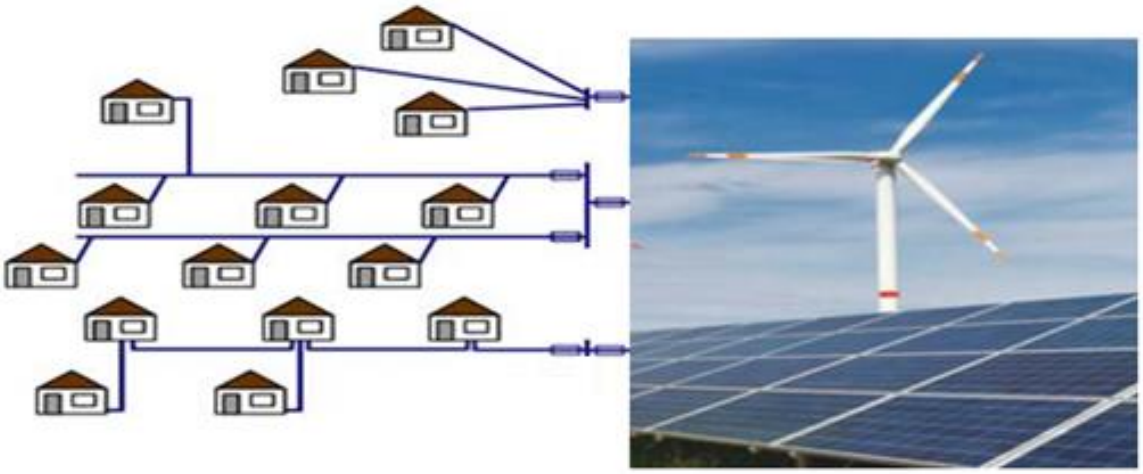

Figure 2.4: Network type distribution

Network type distribution is a more reliable system. However, it is the most expensive and complicated system and is not suitable for microgrids[15]. Furthermore, most microgrids are not more than a few 100 kW. Considering all these reasons, it is more appropriate for the purpose of microgrids to deploy radial and loop type distributions.

Presently, many scholars are researching all these types for implementing them in microgrids. They all have advantages and disadvantages. Common bus used in the microgrids has all these types represented. Recently, DC distribution is more reliable and recommended since as PV, wind system, fuel cells and other distributed generation technologies are adopted easily due to

their characteristic is in DC. For this type, most of appliances in an AC system are all made up to be connected to it. Therefore, it remains useful for a variety of applications.

A 50/60 Hz alternative current line is the most frequently used distribution bus type and has been used for a very long time. Frequency supply for each country is different. AC power supplies all the household appliances manufactured to run with it. Due to Frequency control, power loss and harmonic distortions disadvantage the system since it results in cost increments because it uses expensive inverters in microgrids, since the majority of distributed generation resources are also DC systems [16], [17].

2.4 DC Transmission Lines

DC electrification has shown many benefits compared to AC. Hence, DC is recommended as the best in the field of supply [18]. DC has shown a variety of advantages [18], namely:

- DC distribution does not necessitate synchronization compared to AC distribution.
- Renewable energy resources and the grid can be directly or indirectly distributed to DC.
- DC investment is low on equipment such as wires, conductors etc. as compared to AC.
- Phase balancing is not necessary.
- No harmonics technical drawbacks.
- It delivers more efficient and superlative distribution as compared to AC distribution.

There are also indirect benefits such as:

- DC systems are well suited for loads that are power electronics, i.e. laptops and computers. It shows great advantages to employ DC in applications like telecommunication systems and data interiors.
- The use of storage compatibility such as flywheels and batteries improve the efficiency of the system.
- Improved efficiency, since one requires few conversion stages in a DC distribution.

However, a major disadvantage of DC distribution is that the safety measurements are not yet accessible at the moment. In DC distribution, the most predominant voltage level is attained due to its benefits such as reducing conductor costs, ability to provide safe transmission and standardized safety [19].

2.5 DC in Transmission and Distribution

2.5.1 Application of HVDC

Power electronics devices have gained more technological improvements and the result currently is that there are so many changes within the power industry. In the past, power transmission was AC based since AC voltages remained, and was suggested, as reliable, effective and having the ability to be raised as compared to DC transmission. Normally thermal power plants and solar power plants are used to generate power, which is stepped up by a transformer to precise high voltages ranging in kV, and it is distributed over transmission lines. This kind of method has been used for years and years. However, the world is changing and deploying more renewable energy to generate power.

Due to the intermittent nature of renewable energy, it comes with many difficulties accompanying the stability and power loss in the power plants. Adopting HVDC transmission can be the solution to the aforementioned problems [20]. The HVDC transmission arrangement is made up of two converters, arranged as follows:

- Alternating current is converted to direct current by means of a rectifiers using one converter.
- Other one on the receiving side serve to transforms direct power to alternating power.

Figure 2.5 shows a HVDC transmission connected to the sending side, which is solar PV and wind sources and also connected loads.

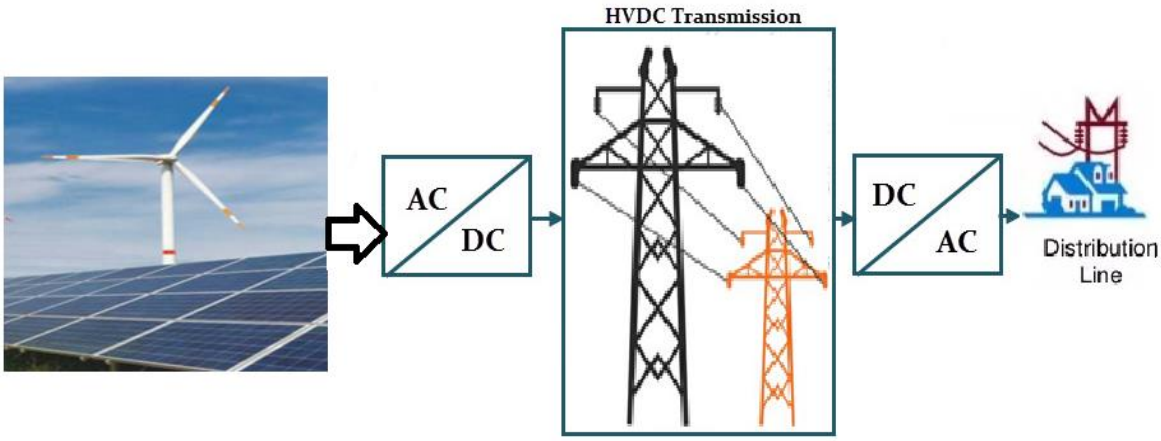

Figure 2.5: HVDC transmission

The HVDC are divided into two main parts on the planning used, which are voltage source converters (VSC) and line commutated converters (LCC). LCC is suitable for large-scale projects, while VSC is suitable for small-scale size projects such as established renewable energy power plants.

2.5.2 Application of LVDC

DC microgrids have gained popularity due to excellent performance. DC microgrids have more benefits such as reliability as they have the ability to function autonomously while maintaining grid flexibility. DC microgrids are not only an intelligent solution for rural electrification, but also for use in building offices, information technology and data centres. The adoption of DC microgrids has a variety of advantages such as efficiency and being environmentally friendly [21]. The three-phase supply is dominant in many buildings as the three-phase AC power can be converted into low voltage DC in the range of 12V to 48V through an AC–DC converter. It is a system that involves DERs such as PV systems, wind energy systems, battery storage and a distribution panel for a building with low demands [22].

2.6 DC Microgrid Control Strategies

The power from grid interfacing converter and load linked parallel coordinated to DC bus system supplies a DC microgrid development [23]. Divergent voltage levels occurs at altered

converters and load stations due to line resistance of the connected system. Voltages are different at converters and load terminals due to wires connecting elements in the system undergoing line resistance. Generated and consumed power levels should be adjusted to manage a voltage balance to acceptable nominal value [24] to make sure that the voltage is controlled within the limits and microgrid.

2.6.1 Hierarchical Control

The structure flexibility and expandability is influenced by the communication between different control levels. Hierarchical control arrangements contribute. This kind of system is considered as an effective technique for diverse coordination functioning modes, for instance grid connected modes, isolated modes and load-shedding modes [24]. There are three levels in hierarchical control strategy. There is a primary control level that is presumed by the power sources and load converters that deploys a droop control method that controls the DC system voltages.

2.6.2 Distributed Control

Distributed control strategies use converters depending on attained feedback signals to control each component of the system. For this kind of a system, it is unnecessary to have autonomous distributed control, which is a communication system. Nevertheless, some intelligent distributed control strategies to reduce controller's complexity use communication between distributed controllers.

2.6.2.1 Autonomous Distributed Control

This system does not necessitate communication between the distributed controllers to sustain adequate scheme set-up in a range of functioning modes. The deployment of an autonomous distributed control strategy minimizes difficulties and has an uncomplicated system while increasing the consistency, reliability of the system and improving expandability due it being unnecessary to have added system components in the progress controllers.

Autonomous control strategies commonly use droop control schemes, mostly in order to control the parallel set-up of converters. Droop features of the converters is deployed in DC microgrid for controlling power sharing and droop constants of the inverters for output resistance variation. Separate converter switches amongst functioning modes grounded on deviation from the nominal values to obtain terminals voltages and power evaluation limits helps to consider the variation of system operating conditions [24], [25]. In [26] , a four-operating modes, separate control strategies is presented with the four levels of DC voltage variety discussed. Figure 2.6 and Table 2.1 show four predefined levels in a microgrid functioning mode where DC voltage is regulated.

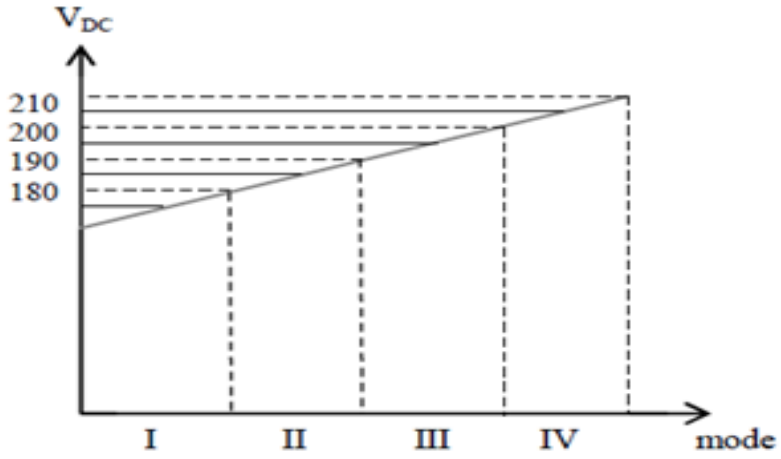

Figure 2.6: Four functioning modes autonomous control strategy [26]

Table 2.1: Four functioning modes autonomous control strategy [26]

I	Isolated	Energy storage system control
II	Grid-connected	DC/AC converter control (rectification)
III	Grid-connected	DC/AC converter control (Inversion)
IV	Isolated	DG control

In [27], a five-operating modes autonomous control strategy is suggested. Voltage range corresponds to five operating modes and is separated into five levels. Converters are used as a slack terminal that controls DC voltage on each levels, as shown in Figure 2.7.

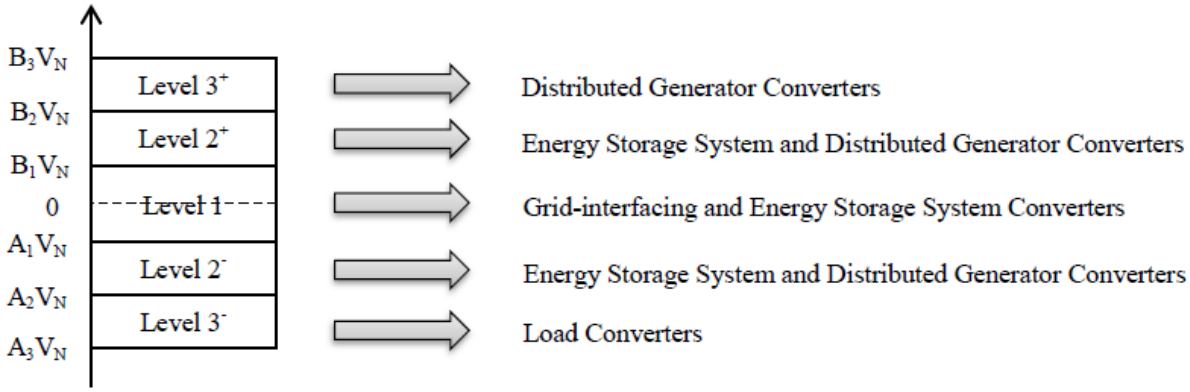

Figure 2.7: Five-operating-modes autonomous control strategy[27]

2.6.2.2 Multi Agent Control

Communication is the key multi-agent control. This strategy of distributed control involves many different agents that have restricted abilities. However, having the ability to communicate individually is essential to implement adequate distribution. The emergence of fast communication devices facilitates the use of a multi-agent control to improve the system [24]. In [28], a hybrid microgrid is discussed and the use of generation scheduling and the management of the demand side is presented. A multi-agent control strategy is used for modelling power system elements [28]. In [29], for the DC microgrid, the emergency demand response control is implemented. A multi agent system is a proficient control method for enormous power distribution system [29].

2.6.3 Intelligent Control

Intelligent control theory can comprehend distinct system. Nevertheless, fuzzy logic refers to intelligent control systems that function well for tremendously complex and ambiguous systems [24]. In DC microgrid, intelligent control, the application of fuzzy logic control gives the benefits of the integration of human best put into controller designs practise. In [30], the researchers describe how they used fuzzy logic and gain controlling to track electric double-

layer capacitor storage systems. To correspond the power deposited into energy storage system Fuzzy logic control is used and done with arranging the droop gains of the storage system controllers provide DC voltage [30].

2.7 Hybrid of Solar-Wind System

The modern electric grid is more secure and sustainable by collecting the maximum possible energy distributed energy resources [31]. Hybrid PV and wind energy systems turn out to be a precise smart way out by means of standalone coordination. PV and wind systems are two sources combined offers improved consistency in the power supply; consistency of renewable energy generation supplying power to the load; and it is more economical. Hybrid systems of these two sources turn out to be more beneficial and are cost-effective to adopt due to the advantages. For example, during the faintness of one system, it can be supplemented by other one. Furthermore, a benefit of integrating hybrid solar PV and wind power is that it supplies the power continuously while energy storage size is minimized. There are two operation approaches of a microgrid, namely the standalone approach and grid connected approach. The harvested output power produced by PV units is defined through the use of instance energy. The increase in light intensity that will result in the increase in photocurrent reduces open circuit voltage [32]. There is a decrease in the efficiency of PV cells when there is an inconsistent increase in temperatures across the cell [33]. Solar panels distributed across various geographical areas can produce consistent solar output power [34]. According to the Global Wind Report (2012), there is about a 10% annual market growth to reach 45 GW and about 19% increasing market growth. Wind turbines (WTs) are divided into two categories: vertical axis WTs (VAWTs) and horizontal axis WTs (HAWTs). The optimum energy that can be harvested by WT is approximately 59 %, of the total hypothetical wind power [35].

In Figure 2.8, hybrid supplied by PV and wind systems, which are distributed energy resources, are connected in grid with the power plant. The load is delivered to supply factory, commercial and also residential.

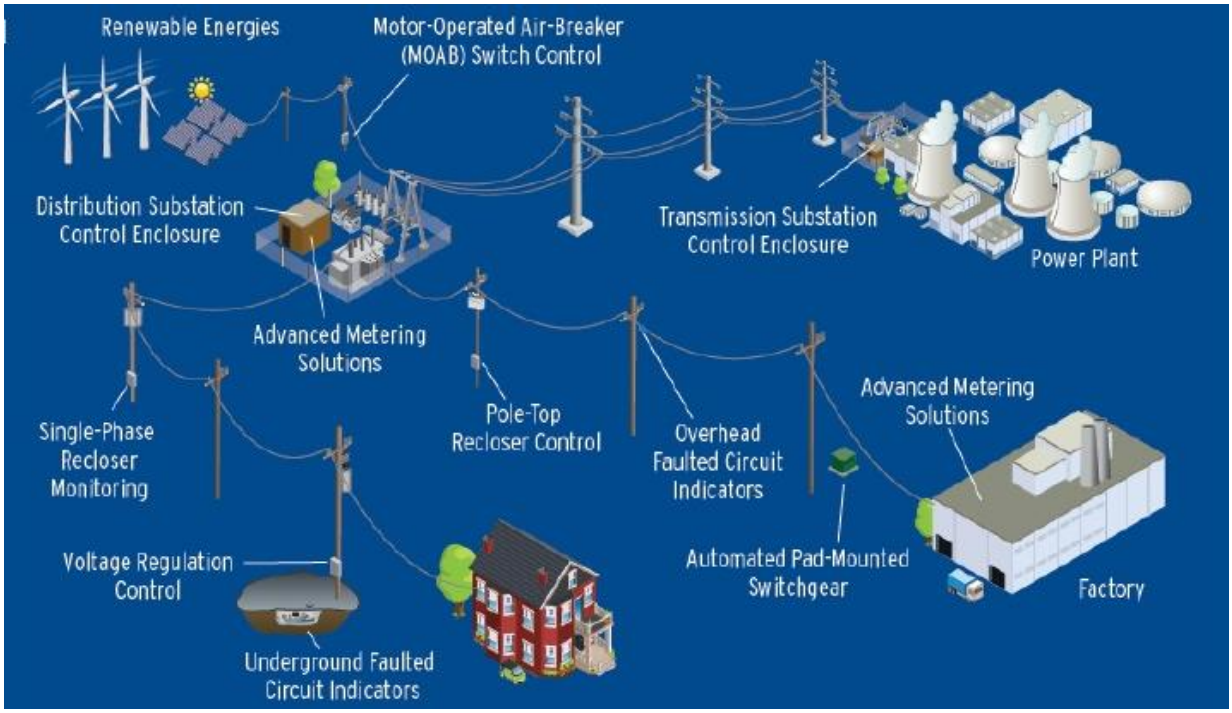

Figure 2.8: Hybrid PV-wind systems with grid connected[36]

2.8 Wind Power Sources

Wind energy is the energy extracted from the wind. Windmills are used for the extraction of this type of energy. The generation of electricity using wind energy is more economical since its costs are very low. Wind is existent throughout the whole day for 24 hours. With wind energy, emission is less. For wind systems, the initial cost is less. The speed of wind empowers an efficient process for the electrical energy generation.

The use of independent renewable energy resources is not recommended due the power not being available all the time. To overcome this, the use of both wind and solar energy together is more appropriate as it will make the system more reliable. This makes the system more trustworthy and leads to the continuation of generation. The ultimate encounters with this

system are that the initial cost is high. However, it has more advantages such as a long lifespan and the maintenance cost is less.

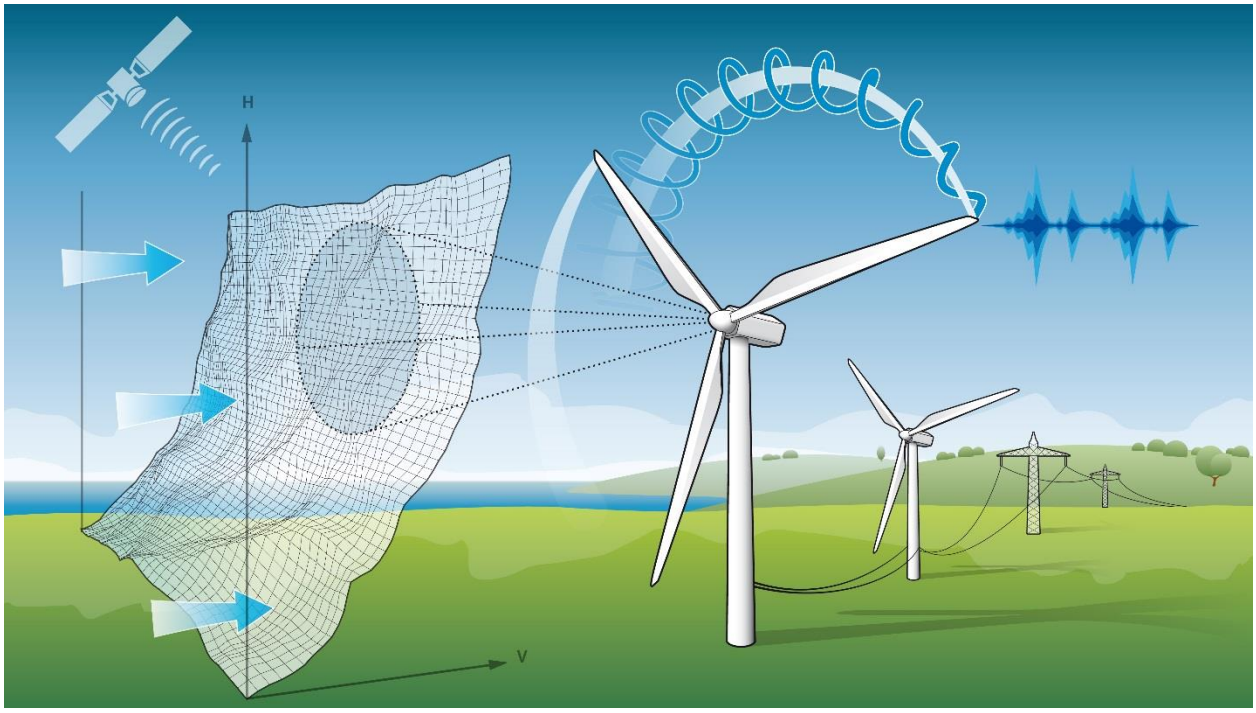

Figure 2.9: Wind turbines with wind direction [35]

In Figure 2.9 above, the diagram shows the direction of the wind blowing the blades to improve the harvesting process in wind turbines. The angular displacement is aligned correctly for better performance. Wind energy is regarded as the leading superior source of renewable energy and considered as the most capable source of alternate energy. In recent times, researchers have been interested in the operation of different wind farms, focusing on its design and control. Many researchers in the field of wind power discovered advantages, such as by increasing turbines of different sizes, it lowers the costs per mounted production capability of electricity [37]. Recently, many scholars have been interested in the development of improved approaches and methodologies to find an optimal design, control and to advance the performance in the wind energy [38]. Nevertheless, the weather conditions cause wind technology not to be dependable since it is not technically sustainable in all locations and the speed is also not

consistent. Due to these disadvantages, one can say that it is unpredictable as compared to PV solar systems.

2.9 Solar energy sources

The operation of solar energy sources is through converting radiation from solar into electrical power. There are two kinds of solar sources which use different technology to convert energy. In a photovoltaic (PV) solar system, when panels are irradiated by sunlight, the solar energy is converted straight to DC electrical power [36]. In solar thermal systems, the system produces energy as conventional thermal power plants by using heat converted from solar energy. PV systems can be operated with a few sections situated in residential building rooftops. The size and the capacity has increased to large PV systems made up of many panels fixed on a huge ground area. This system is capable of supplying power equivalent to the existing thermal power plant. The PV system panels allows concentrators to be used for the purpose of increasing the solar radiation, hence the required dimensions of the panels to produce certain electrical power is minimized [39]. Concentrated solar power (CSP) is a technology which turns the light into heat by employing mirrors to concentrate sunlight against a tube. Figure 2.10 shows a PV solar system connected to produce energy.

Figure 2.10: PV solar panels connection [39]

In a DC microgrid, a PV system is supplementary recommended as compared to solar thermal systems since the PV solar system extracts DC electrical power directly. The solar thermal arrangement produces AC electrical power by employing conventional power generators. The use of PV systems for DC microgrids results in many benefits such as fewer power alteration being required in the electrical system.

The author used MPPT for the output power from the PV solar system to be maximized [40]. It is the remote renewable DC microgrid that uses PV sources to distribute energy. The approach shown appears to be effective, employing obtainable low-cost renewable energy [40].

2.10 Wind energy conversion

The kinetic energy of the wind is converted into mechanical energy by aerodynamic blades on the rotor, efficiently providing the Torque T_r on the rotor presented in equation (2.1) as follows:

$$T_r = \frac{P_r}{\omega_r} \tag{2.1}$$

Where ω_r is the angular speed of the rotor and P_r is the power of the rotor, given by the following relation in equation (2.2) as presented:

$$P_r = \frac{1}{2}\pi\rho R^2 v^3 c_p(\lambda,\theta) \tag{2.2}$$

Where ρ is the air density, R is the radius in wing , c_p is the efficiency coefficient, , θ is the function of the blade pitch angle, λ is the tip speed ratio between the wind speed and blade tip and v is the effective wind speed. Equation (2.3) represent tip speed ratio.

$$\lambda = \frac{v}{v_{tip}} = \frac{v}{R\omega_r} \tag{2.3}$$

Where the speed at the tip of the blades is v_{tip}, c_p is the wind turbine performance coefficients attained over mathematical calculations and date table. Assume that no loss in the generator.

Hence, rotor power P_r would be equal to electrical power generated P_e as presented in equation (2.4).

$$P_r = P_e \tag{2.4}$$

Where P_e is power in the generator, given by the following equation (2.5)

$$P_e = T_g \omega_g \tag{2.5}$$

Where T_g is the torque of the generator and ω_g is the generator speed.

2.11 Grid-Connected System

Microgrids have been recognized as the best solution as they resolve a variety of power problems in the world. DC microgrids have also been projected as a way forward due to the benefit that it minimizes the conversion from DC power to AC power. Microgrids come with many advantages, namely that it offers solutions to carbon caps and allows the use of renewable energy as a standard technique to conduct business worldwide. One of the best things about the microgrid is that it is versatile since it can be also connected to the national electric grid [41]. The microgrid is well suited since the distributed generation (DG) units are capable of improving the steadfastness of the electricity distribution system and supplying electricity without any interruption. Moreover, in the case whereby there is a widespread outage, the microgrid is capable of disconnecting from the national grid and carrying on operating independently and supplying electricity to consumers. Figure 2.11 below shows a complete hybrid microgrid connected to a grid in which *PV* solar and wind generate DC power. There is battery storage which plays a vital role as a backup in the system. This power is then fed to the consumers.

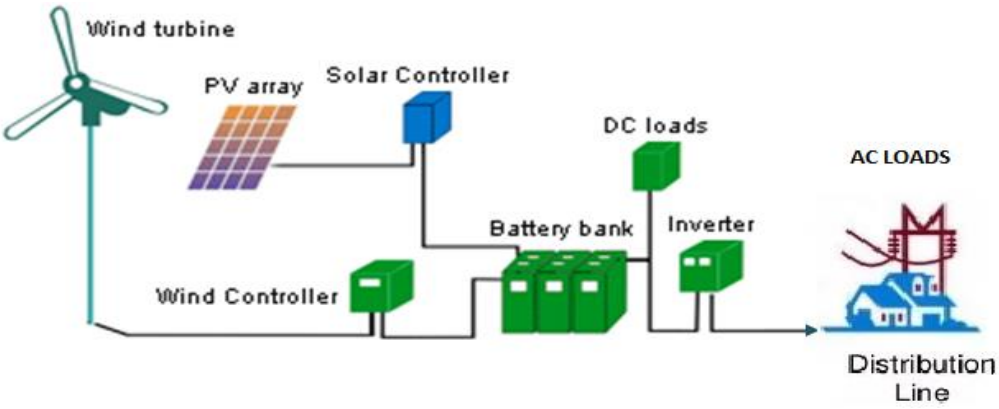

Figure 2.11: Grid connected hybrid

2.12 Energy Storage Systems

The energy storage system (ESS) is more important in a DC microgrid. ESS is used to provide power or close the gaps amongst the load and generation. The application of this function is more significant in a DC microgrid due to the random and improbable natural state of distributed energy resources. Since the power available can be stored and supplied to the consumers when it is required to meet the local load needed by customers, the implementation of ESS supports the independent operation of microgrids. Superconducting magnetic energy storage, flywheels, batteries and electric double-layer capacitors are among the storage devices that can be used with DC microgrids.

2.12.1 Batteries

The universally used ESS because of the benefits such as long life span, low cost and high density is battery energy storage systems (BESSs). BESSs in a microgrid, commonly use lead-acid batteries since they have high power density and cost-effective benefits. It is more reliable to use lead acid batteries that their valve is controlled, which are closed batteries, as compared to flooded lead-acid batteries, as they require no regular maintenance [42], [43], [44].

2.12.2 Electric Double-Layer Capacitors

Ultra-capacitors and super capacitors are terms used to describe Electric Double-Layer Capacitors (EDLCs). The structure of EDLC and a battery are similar to each other: each has

double electrodes put in into an electrolyte, as well as a dielectric separator between them. These electrodes have a large number of microspores on their surface, resulting in a large surface area where the charges are produced. The dielectric material stores energy as electrostatic energy [43]. EDLCs have many benefits, namely lower maintenance, longer life-span and quicker responses. The residential DC microgrid ELDC storage system is discussed in [45] with transmitted distributed generation units.

2.12.3 Flywheels

Flywheels ESS store power in the spinning mass of a flywheel connected to an electrical machine. The machine can be operated in motor mode with the purpose of accelerating the flywheel shaft, which that results in the energy being transferred to the flywheels. Energy can be transmitted back to the electrical system when the mechanism is powered with regenerative braking to reduce rotation of the shaft. This system offers great benefits such as fast operations and the high efficiency with flywheels offers significant capacity. On the other hand, energy cannot be stored for extended periods of time and the energy can be recovered from flywheels over short periods of time [42], [43]. In a DC microgrid based on wind generation, the author used a hybrid flywheel energy storage system [1], [46].

2.12.4 Superconducting Magnetic Energy Storage

In superconducting magnetic energy storage (SMES), the magnetic field is deployed to store energy. It is created by passing current through an inductor. To sustain its superconducting properties, the inductor is fabricated by means of superconducting material while retaining a very low temperature. The use of positive voltage across the conductor helps to transfer energy to the storage and then transfers it back to the electrical system using reverse voltage [39]. SMES offer awesome benefits such as quick responses, high efficiency and grid frequency support. However, SMES has a rather short bridging time, between one and two minutes and its costs are very high [36], [42].

2.13 AC Faults

An alternating current fault is any failure that disrupts the normal activity of the system. The most common faults in the system are unsymmetrical faults.

2.13.1 Unsymmetrical Faults

Unsymmetrical faults, which may involve single line to ground faults, are the most common faults that occur on power system overhead lines. A few assumptions must be taken into consideration in order to do an effective fault analysis. Figure 2.12 represents a faulted segment, where the faulted point by voltage will be indicated by VF and phase faulted by current are I_R, I_Y and I_B. This research will study how the system operates when these faults take place. Alternatively, R = a, Y = b and B = c and $I_R = I_a$, $I_Y = I_b$ and $I_B = I_c$.

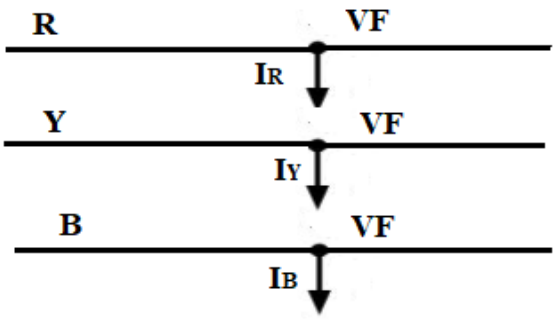

Figure 2.12: Representation of faulted segment

As a purpose of sequence impedances and the positive sequence voltage source, the symmetrical component relational equations derived from the three sequence networks equivalent to a given unsymmetrical system in the prearrangement equation (2.6) are as follows [47]:

$$\begin{aligned} V_{a0} &= - I_{a0} Z_0 \\ V_{a1} &= E_a - I_{a1} Z_1 \\ V_{a2} &= - I_{a2} Z_2 \end{aligned} \qquad (2.6)$$

The sequence equations are the names given to these equations. The sequence equation (2.7) can be considered in matrix arrangement as follows:

$$\begin{pmatrix} V_{a0} \\ V_{a1} \\ V_{a2} \end{pmatrix} = \begin{pmatrix} 0 \\ E_a \\ 0 \end{pmatrix} - \begin{pmatrix} Z_0 & 0 & 0 \\ 0 & Z_1 & 0 \\ 0 & 0 & Z_2 \end{pmatrix} \begin{pmatrix} I_{a0} \\ I_{a1} \\ I_{a2} \end{pmatrix} \quad (2.7)$$

This equation (2.7) is used in conjunction with the equations obtained to describe the fault under consideration, i.e. conditions under fault (c.u.f.), in order to evaluate the sequence current I_{a1} and thus the fault current I_f , in terms of E_a and the sequence impedances, Z_1, Z_2 and Z_0. Thus, in order to obtain the necessary fault parameters during unsymmetrical fault analysis of any given type of fault, two sets of equations are considered for solving simultaneously:

- Condition under fault equations
- The sequence components Equation (2.7).

2.13.1.1 Single line-to-ground fault

There are approximately 65%-70% of asymmetric line-to-ground faults that occur in transmission line faults. Mostly, they arise due to many factors such as physical contact that can be caused by lightning or other storm damage. This fault occurs when lightning strokes strike the distribution line and at that point the conductor may breakdown, also negatively or positively, and fall on the earth. In industrial distribution systems, single L-G faults are mostly incidences in industrialised distribution and provide line to ground for current [48]. In Figure 2.13, a single line to ground fault is presented.

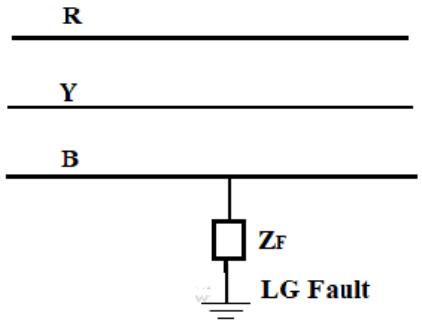

Figure 2.13: Single line-to-ground fault

Let E_a, E_b and E_c be the produced voltages internally and Z_n. Segment 'a' is presumed as fault line. Now consider the conditions under fault as follows in equation (2.8):

$$Ib = 0 \; ; \; Ic = 0 \; ; \text{ and } Va = 0 \tag{2.8}$$

Considering $Ib = Ic = 0$, prearranged by equation (2.9):

$$\begin{pmatrix} I_{a0} \\ I_{a1} \\ I_{a2} \end{pmatrix} = \frac{1}{3} \begin{pmatrix} 1 & 1 & 1 \\ 1 & a & a^2 \\ 1 & a^2 & a \end{pmatrix} \begin{pmatrix} I_a \\ 0 \\ 0 \end{pmatrix} \tag{2.9}$$

Solving equation (2.9), one gets equation (2.10):

$$I_{a1} = I_{a2} = I_{a0} = (I_a/3) \tag{2.10}$$

Furthermore, using equations (2.9) and (2.10), one gets equation (2.11):

$$\begin{pmatrix} V_{a0} \\ V_{a1} \\ V_{a2} \end{pmatrix} = \begin{pmatrix} 0 \\ E_a \\ 0 \end{pmatrix} - \begin{pmatrix} Z_0 & 0 & 0 \\ 0 & Z_1 & 0 \\ 0 & 0 & Z_2 \end{pmatrix} \begin{pmatrix} I_{a1} \\ I_{a1} \\ I_{a1} \end{pmatrix} \tag{2.11}$$

Pre-multiplying equation (2.11) throughout by matrix $[111]$, one gets equation (2.12):

$$I_{a1} = \left[E_a / Z_1 + Z_2 + Z_0 \right] \tag{2.12}$$

2.13.1.2 Line-to-line fault

Approximately 5%-10% of asymmetric L-L faults occur in transmission line faults. A line-to-line fault is an extremely dangerous fault, but uncommon to arise in the power system compared to single L-G faults. Insulation failures can be the main cause for this fault to occur in underground cables due to Ionization of air or when there is physical contact between the lines, which causes a short circuit between them [49]. Arrangement of the fault is shown in Figure 2.14.

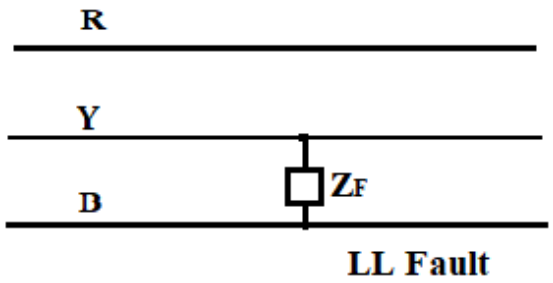

Figure 2.14: Line-to-line fault [49]

Now consider a line-to-line fault at the terminals, through a reactance, neutral is grounded. Then let's consider fault under fault as in equation (2.13)

$$I_a = 0;\ I_b = -I_c;\ \text{and}\ V_b = V_c \qquad (2.13)$$

Considering the symmetrical elements of the voltage V_a where $V_b = V_c$, given by equation (2.14):

$$\begin{pmatrix} V_{a0} \\ V_{a1} \\ V_{a2} \end{pmatrix} = \frac{1}{3}\begin{pmatrix} 1 & 1 & 1 \\ 1 & a & a^2 \\ 1 & a^2 & a \end{pmatrix}\begin{pmatrix} V_a \\ V_b \\ V_b \end{pmatrix} \qquad (2.14)$$

Solving equation (2.14), one gets equation (2.15)

$$V_{a1} = V_{a2} \qquad (2.15)$$

Furthermore, study the symmetrical elements of current I_a with $I_b = -I_c$ and $I_a = 0$ as given by equation (2.16):

$$\begin{pmatrix} I_{a0} \\ I_{a1} \\ I_{a2} \end{pmatrix} = \frac{1}{3}\begin{pmatrix} 1 & 1 & 1 \\ 1 & a & a^2 \\ 1 & a^2 & a \end{pmatrix}\begin{pmatrix} I_a \\ I_b \\ -I_b \end{pmatrix} \qquad (2.16)$$

Resolving the equation (2.16) matrix, equation (2.17) is obtained:

$$I_{a0} = 0;\ \text{and}\ I_{a2} = -I_{a1} \qquad (2.17)$$

Using equations (2.15) and (2.17) in equation (2.7), and since $V_{a0=0}$ (I_{a0} being 0), the following equation is obtained:

$$\begin{pmatrix} 0 \\ V_{a1} \\ V_{a1} \end{pmatrix} \begin{pmatrix} 0 \\ E_a \\ 0 \end{pmatrix} - \begin{pmatrix} Z_0 & 0 & 0 \\ 0 & Z_1 & 0 \\ 0 & 0 & Z_2 \end{pmatrix} \begin{pmatrix} 0 \\ I_{a1} \\ -I_{a1} \end{pmatrix} \quad (2.18)$$

Solving and pre-multiplying equation (2.18) throughout by the matrix $\begin{bmatrix} 0 & 1 & -1 \end{bmatrix}$, equation (2.19) is obtained:

$$I_{a1} = \left[E_a / (Z_1 + Z_2) \right] \quad (2.19)$$

2.13.1.3 Double-line-to-ground

Approximately 15-20% of asymmetric double L-L-G faults occur in transmission line faults. These faults are mainly caused by storm damage and when two lines come into contact with the ground [49]. The arrangement of the line-to-line ground fault is displayed in Figure 2.15.

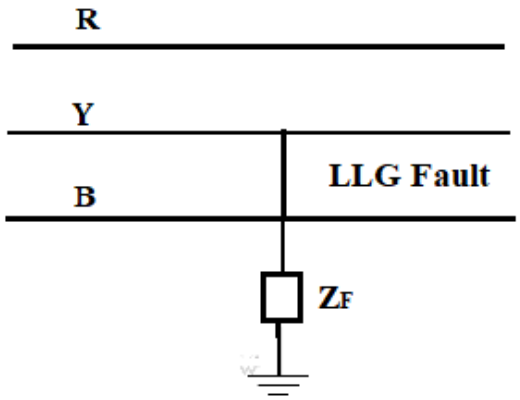

Figure 2.15: Line-to-line-to-ground fault

Consider L-L-G fault, whose neutral is grounded ‘b’ and phase ‘c’. Let’s now consider the condition under fault in equation (2.20):

$$I_a = 0 \text{ and } V_b = V_c = 0 \quad (2.20)$$

Considering $V_b = V_c = 0$ prearranged by equation (2.21) with the symmetrical elements of the voltage:

$$\begin{pmatrix} V_{a0} \\ V_{a1} \\ V_{a2} \end{pmatrix} = \frac{1}{3}\begin{pmatrix} 1 & 1 & 1 \\ 1 & a & a^2 \\ 1 & a^2 & a \end{pmatrix}\begin{pmatrix} V_a \\ 0 \\ 0 \end{pmatrix} \quad (2.21)$$

Solving equation (2.21), one gets equation (2.22):

$$V_{a1} = V_{a2} = V_{a0} = Va/3 \quad (2.22)$$

Considering the sequence in Equation (2.7), having equation (2.23):

$$\begin{pmatrix} V_{a0} \\ V_{a1} \\ V_{a2} \end{pmatrix} = \begin{pmatrix} 0 \\ E_a \\ 0 \end{pmatrix} - \begin{pmatrix} Z_0 & 0 & 0 \\ 0 & Z_1 & 0 \\ 0 & 0 & Z_2 \end{pmatrix}\begin{pmatrix} I_{a0} \\ I_{a1} \\ I_{a2} \end{pmatrix} \quad (2.23)$$

Solving, pre-multiplying Equation (2.23) throughout by equation (2.24),

$$Z^{-1} = \begin{pmatrix} 1/Z_0 & 0 & 0 \\ 0 & 1/Z_1 & 0 \\ 0 & 0 & 1/Z_2 \end{pmatrix} \quad (2.24)$$

Results in equation (2.25):

$$\text{“}Z^{-1}\begin{pmatrix} V_{a1} \\ V_{a1} \\ V_{a1} \end{pmatrix} = Z^{-1}\begin{pmatrix} 0 \\ E_a \\ 0 \end{pmatrix} - Z^{-1}\begin{pmatrix} Z_0 & 0 & 0 \\ 0 & Z_1 & 0 \\ 0 & 0 & Z_2 \end{pmatrix}\begin{pmatrix} I_{a0} \\ I_{a1} \\ I_{a2} \end{pmatrix}\text{”} \quad (2.25)$$

Using the character: $Va1 = (E_a - I_{a1}Z_1)$ in equation (4.19), solving the equation by the matrix $[1\ 1\ 1]$ and finally adding, the following equation will be obtained:

$$\text{“}E_a/Z_0 - I_{a1}(Z_1/Z_0) + (E_a/Z_1) - I_{a1} + E_a/Z_2 - I_{a1}(Z_1/Z_2) = E_a/Z_1 - (I_{a0} + I_{a1} + I_{a2})\text{”} \quad (2.26)$$

Since for $Ia = 0$, solving the equation (2.26), the following equation will be obtained:

$$I_{a1} = \{E_a/[(Z_1 + Z_2 * Z_0)/(Z_2 + Z_0)]\} \quad (2.27)$$

2.13.2 Short circuit faults

A short circuit is a fault that occurs in a normal load when the current bypasses standard capacity. When the circuit is intermittent by failure, then an open-circuit fault takes place. These faults occur in a three-phase system, which may include only between phases, one or more phases and ground. A short circuit fault in the transmission lines is the main cause of under-voltage within the equipment terminal.

2.14 DC Fault in a DC microgrid

External mechanical tension, pollution, and lighting strikes are the most common causes of DC transmission line faults. The most common types of faults in HVDC transmission systems are line to line faults and line to ground faults. Repairs on faulty parts is necessary since these faults tend to be permanent [4]. Converters should be detached instantly after discovering faults in the system. These faults must be cleared immediately and restored because they are capable to occur shorter. The two DC faults are as follows:

2.14.1 DC Line To Line Fault

Insulation failure between the two DC conductors triggers DC L-“L faults. Both converters must be disabled. DC L-L faults are an unusual accidents. When a line-to-line fault occurs in DC transmission lines, the capacitor must be immediately discharged. A three-phase short circuit occurs simultaneously at the fault point in the AC system. IGBTs can be obstructed for self-defence by faults exiting reverse diodes exposed to over-current when faults occur on the DC side [50]. The equivalent circuit of a DC L-L fault is shown in Figure 2.16.”

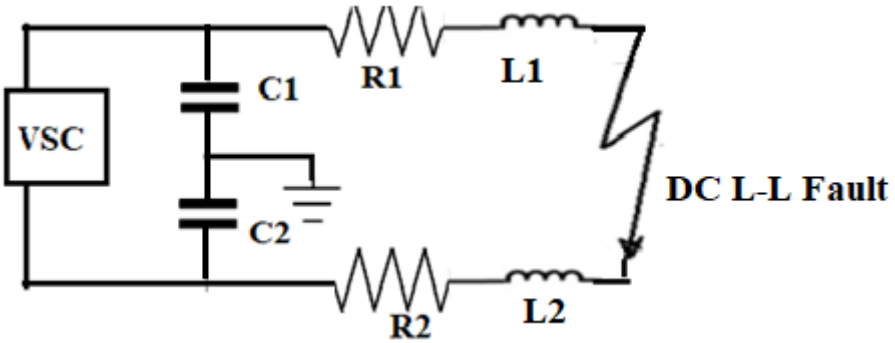

Figure 2.16: Equivalent Circuit of DC Line-to-Line Fault

There are three stages of a DC short circuit fault, which is classified as follows:

a. Capacitor Discharge Stage

When a DC L-L faults takes place, it forms a loop circuit with no source. The capacitor discharge stage is triggered during fault occurrence. At this point, the capacitor voltage has fallen to zero.

b. Diode Freewheel Stage

When a DC line voltage fallen to zero at rapid speed, a loop circuit is formed by cable inductance and the free-wheel diode. Primarily, The IGBT is obstructed for self-defence, and there is a strong initial over-current flowing through the diodes, posing a major risk of diode failure. The DC current and diode current would then rapidly decrease [51].

c. Capacitor Recharging Stage

The DC link capacitor, AC form and cable inductance form enforced reaction and capacitor will be charged at the capacitor recharging stage, where there is an increase in the DC voltage [4].

2.14.2 DC Line-to-Ground Fault

The DC L-G fault in the overhead line is defined by the insulation failure between the DC L-G. In the overhead line, strikes of lightning and pollution can result in impermanent DC line to ground in the HVDC transmission system. The occurrence of DC L-G faults is common in the underground HVDC transmission system. Figure 2.17 shows the equivalent circuit of DC line to ground faults. Aside from the mid-point of the DC link capacitor and the neutral ground link of the transformer, the DC line to ground fault results in a ground point [51].

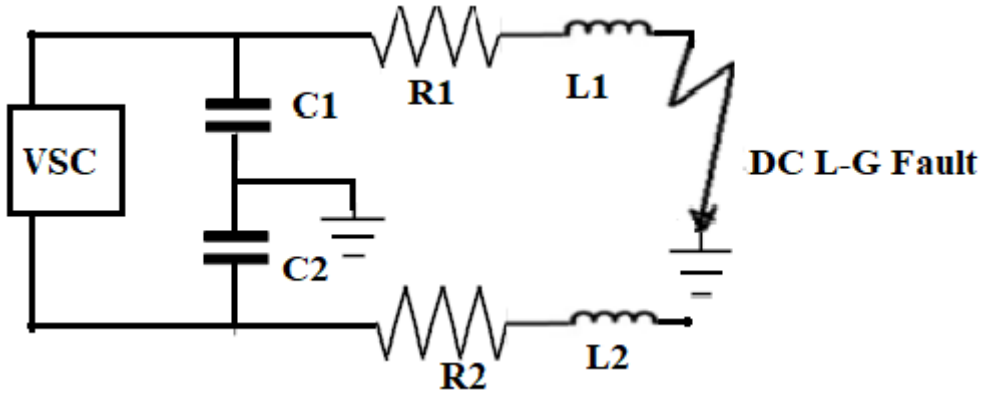

Figure 2.17: Equivalent Circuit of DC line-to-ground fault

The DC short-circuit fault is divided into three phases, as shown below:

a. DC Side Capacitor Discharge

In the occurrence of DC L-G fault, discharge circuit is made by the faults in pole capacitor and impedance through the fault line. The DC side capacitor discharge stage is experienced in the system after the fault has occurred.

b. Grid-Side Current Feeding Stage

During DC L-G fault occurrence, the DC voltage drops continuously and leads to the DC side capacitor discharging. This stage will occur when the voltage drops below any grid phase voltage due to the line to ground fault taking place in the system.

c. Voltage Recovery Stage

The capacitor discharge is directly proportional to the fault pole, capacitor voltage drops drastically and non-fault pole capacitor voltage increasing. The voltage recovery stage occurs when the DC voltage progressively gets restored [52].

2.15 The Review of Literature on Hybrid Systems

They are different sources, conventional and renewable sources, in the power system analysis. A hybrid system can be formed by combining more than two sources, i.e. solar and wind. The dependability and reliability of renewable energy sources is the major key factor in ensuring continuity of supply in the renewable industry. This applies to different sectors of the industry, whether the load is domestic, commercial or industrial. In regions far from the equator, commercialized standalone set alight the street coordination create conventional configuration of PV cells and batteries cannot run all year [1], [53]. The technologies in the renewable energy industry must improve their performance, especially the stability of their output. It is also necessary to connect renewable energy sources to conventional sources [54]. Recently scholars are attracted in the optimization and management of standalone hybrid power generation systems where they are balancing power between the optimum power harvested and the consumed energy [55].

An optimal hybrid system design adds more effectiveness and reliability to the system compared to a single system, hence there is growing interest in defining the essential environments to install PW/PV power plants because of their operational and economic advantages [56]. The objective to optimise the mix of renewable energy systems to reduce the demand for power during the peak period, while minimising the combined intermittence at a lowest costs, resulted in some objective functions being suggested [57]. In [58], Katsigiannis et al. worked a combinatorial objective model to minimise the energy with the cost implication of the system, while the total greenhouse gas emissions of the system during its lifetime are also minimised as presented, it was found that conventional optimisation methods are unable to solve the problems because of local optimum solution convergence. In [59], Mahor et al. used a PSO to determine the problem and the results showed improved performance as compared to conventional optimisation techniques. In [60], Brini et al. presented the cost-

effective environmental dispatching of a hybrid power system consisting of wind and solar thermal energies by means of MOEA, which is presented as a multi-objective function that simultaneously minimises fuel costs and pollution. In [61], Kanhukamwe proposed MOEA to the multi-objective model for isolated hybrid systems, taking into consideration different control variables, which are the total cost and pollutant ejections. The results attained when planning a PV-wind-diesel system reveal the design method's practical usefulness. In addition to the two control variables, the load variations in the hybrid system were taken into consideration [62] by Dufo-Lopez and Bernal-Agustín. In [63], Bilal et al. presented an objective function for scaling a hybrid system with the aim of lowering the annual cost and loss of power. In [64], Pachori and Suhane presented a Pareto-based objective function for sizing a solar-wind-battery system with a combinatorial objective function to minimise the annual cost and the probable loss of power supply. In [65], Montoya et al. presented a paper on a multi-objective function of a meta-heuristic that combines PAES with SA and TS to minimise voltage and power losses.

The optimisation techniques, including LP have been discussed in [66] by Cormio, Dicorato, Minoia and Trovato and in [67], Courtecuisse et al. reviewed the fuzzy system. Some scholars explore how to assess the best renewable energy technology arrangement by not only considering the renewable energy tools, but also technology characterisation, encouragements and economic parameters [1]. Once again in [68], Lee and Chen proposed a PSO for a TOU rate industrial consumer to use for wind-PV power coordination, with the intention of optimizing the economic benefits of investing in both a wind and a PV generation system. In [69], Kaviani et al. presented an objective function to optimise a hybrid wind-PV-fuel cell generation system and PV generation. In [53], Lagorse, et al. presented the GA to optimise the hybrid system. In [70], Eke et al. apply an optimisation technique for a hybrid power generation system's configuration and operation. In [71] , the authors Giannakoudis et al. presented an

optimisation development and application of a hybrid power generation method. From an economic point of view, renewable energy can be used as an alternative to electricity in remote areas. The solution to have an isolated network is hybridising renewable energy power sources such as wind, solar and micro-hydro systems [72]. In [73], Bernal-Agustín and Dufo-Lopez compare and contrast the key research techniques for optimizing hybrid systems with dynamic battery storage systems. In [74], Martiskainen and Coburn present a basic overview of the current state of the art in the optimal setting embedded with simulations and controls strategies for standalone hybrid PV-wind energy, energy storage systems, with the results demonstrating the wide range of technologies available for accurately predicting their performance. Other scholars looked at renewable energy sources like wind, solar, battery, and DG, and used the GA to figure out the best power system configuration for islands [75]. In [76], Balamurugan et al. present a hybrid system that incorporates biomass, wind, solar PV, and battery to optimize energy during peak times when solar radiation is poor or non-existent, as well as low wind periods."

In [77], Nema and Rangnekar present a review of the current state of the design, operation and control requirements of the stand-alone PV solar-wind hybrid energy systems with conventional back-up sources such as a DG or grid, and highlight further research in the field. To achieve an optimal design in the hybrid system, the sizing and control strategies must be the main considerations [78]. In [79],"Garcia and Weisser present LP and load dispatch to study the size of grid units and dispatch in a wind-diesel power system with the goal of cost minimization, using a one-year time series of hourly wind speeds as data and electricity demand as the main model's control variable. In [80], Koutroulis et al. present GA optimisation for the sizing of standalone PV-wind generator systems, which selects the optimal number and type of units to minimise the cost and is taken as an objective function, whilst the energy requirements are taken as constraints to the model. In [81],"Yang Zhou and Fang propose the

GA for optimisation for the sizing of the configuration of a hybrid solar-wind system using a battery as a storage system, where the number of PV modules, wind turbines, batteries, PV module slope angle, and wind turbine installation height are all control variables. In [82], Arce et al. propose a method for the assessment of the optimal element sizing of a hybrid power system that combines a wind turbine with two storage systems. In [83], Bernal-Agustín and Dufo-López propose a control and design applying EA for an efficient electrical energy generation system comprised of a PV wind turbine -diesel-battery-hydrogen-system. In [84], Zervas et al. analyse a hybrid system that consists of the use of a PV system, proton exchange membrane fuel cells and metal hydride tanks has advantages over stand-alone PV systems, but the optimization technique for its operation is a rather complex task. In [85], Diaf et al. using the cost of energy as a constraint, compare the estimation of the appropriate dimensions of a stand-alone hybrid PV-wind system that guarantees the energy autonomy of a typical remote consumer."

In the paper presented in [86], Hakimi and Moghaddas-Tafreshi demonstrated the ability of the PSO in renewable energy to minimise the total cost of distributed energy resources that powers a hybrid power generation system. It makes use of biomass as an available energy resource to meet the demand for an entire control horizon. The same authors use the PSO model to size the hybrid power system in order to minimize the total cost of the system while meeting the demands in [86]. Several scholars have attempted to analyse the effect of renewable energy on the functioning of power systems. In [87], Razak et al. derived an optimal model to minimise surplus energy and energy costs in a hybrid green energy system that incorporates multiple energy sources. The results indicated the importance of considering the surplus power produced by hybrid system to minimize costs. In [88], Chakraborty et al. propose GA and PSO for the dispatch of the thermal units integrated with the hybrid system. While hydropower has priority for transmission energy , Matevosyan et al in [89], Matevosyan et al. present a day-ahead

schedule model for a multi-reservoir hydro-power system synchronized with wind power and utilizing the same transmission power lines. In [90], Castronuovo and Lopes present an optimal model to determine the optimum daily operational strategy, where wind turbines is combined with hydro generation pumping equipment. In [57], Mukhammadiev et al. propose an application to a neuro-fuzzy controller for a hybrid system composed with two different sources of renewable energy systems (wind generation and DG systems) and connected in parallel with a stall-regulated wind turbine to an induction generator, which are linked to an AC-bus bar. Compared to other approaches such as fixed parameters fuzzy logic controllers and PID controllers, the application of fuzzy controllers into new configurations presented in [57] show a better achievement of the results. In [91], Dufo-Lopez and Bernal-Agustin present a GA for the optimisation of the design and the operation control of a composed hybrid system (PV, DG, Wind generation, the hydro pump as storage system) which can be in remote or isolated areas, which they found to be better for the cost and the reliability of the system. In [92], Anagnostopoulos and Papantonis propose an algorithm for the simulation of the plant operator and automated optimisation EA software. In [93], Anarbaev et al. present a new configuration, applying a closed loop control algorithm for a solar system which is included with geysers to increase the temperature during any time of the day, as well as to increase the hot water load replacement factor.

The use of available renewable energy sources such as PV and wind energy to many scholars is gaining popularity as solution to achieve full electrification for rural areas such as the use of microgrid. DC microgrid can be considered as economical system to meet consumers demand due to its benefits of being environmental friendly and has virtuous performance. Nevertheless, microgrids experience numerous faults when transmitting power, it is vital to detect the location and isolate faulty part quickly.

CHAPTER THREE
Modelling and Computer Simulation

3.1 Introduction

This chapter presents the methodology and strategies used to do the modelling of a hybrid DC microgrid. The modelling of the PV solar system and modelling of wind energy is extensively discussed in this chapter. Renewable energy is considered a reliable substitute clean energy. Furthermore, in order to expand and advance the economic management of the system, it neccessitates the more incorporation of renewable resources. Poor set-ups management of the hybrid system results in incompetent systems. There are three factors affecting the PV systems's efficiency, namely: PV panel efficacy in commercial PV panels that is ranging 8-15% [94]; inverter efficiency of 95-98% [95]; and MPPT algorithm productivity that is above 98% [96]. The planned system in this research consists of a photovoltaic system and wind generator(WG) as a battery as most important component. PV systems have the foremost contribution as a primary source. WG comes as a secondary source since its contribution in the system is inferior. ESS play a vital part in the system, hence the battery is deployed to make the system more dependable by closing supply demand gaps between the sources and load.

3.2 Modelling of Solar PV System and Wind Energy

The PV system and wind energy are likely to be undependable because their supply is intermittent in nature. The hybrid system that is made up of solar and wind, the coupling of both systems is regarded to be a more reliable and superior arrangement. Regulating power generated by hybrid system prevent the variation of frequency and voltage power complementarity.

3.2.1 Modelling and Operating principle of Solar PV system

Photovoltaic cells convert sunlight into a voltage by means of a photo-electric effect [97]. A load connected across a PV array will draw current from the device and the PV array will deliver power to the load [97]. The construction of the PV array consists of n-type and p-type material so that current flow is generated in an exterior circuit. PV cells result in the absorption of photons due to light that smashes it. Due to the external circuit connecting the n-type and p-type material, the electron will travel from the N-type material to the P-type material through a connection by an external circuit generating current flow [98]. Figure 3.1 shows the definition of a single cell for the construction of a PV arrangement. A single cell only generates a voltage in the range of 0.5 V - 0.8 V which is not enough to power the load. Hence, many cells are connected in series and parallel to increase the voltage and current respectively [95] as shown in Figure 3.2 (a) and (b).

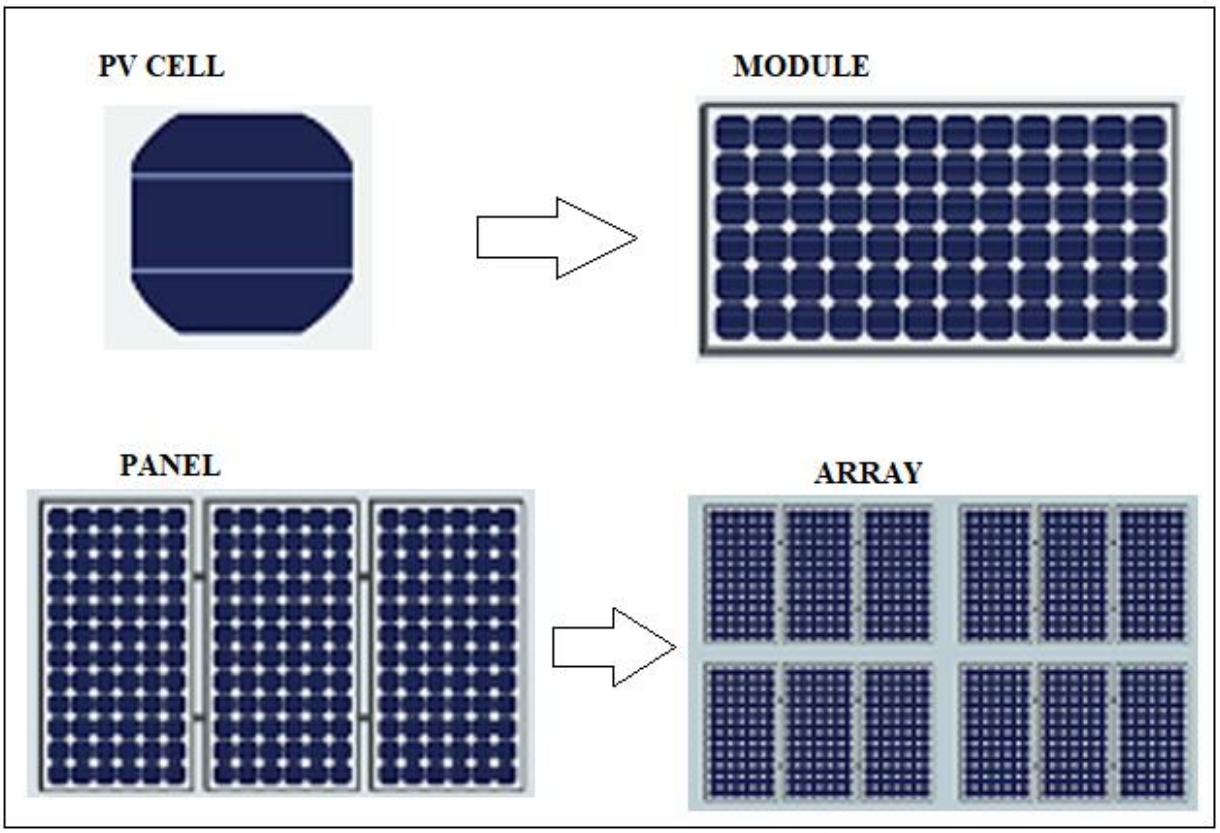

Figure 3.1: PV definitions

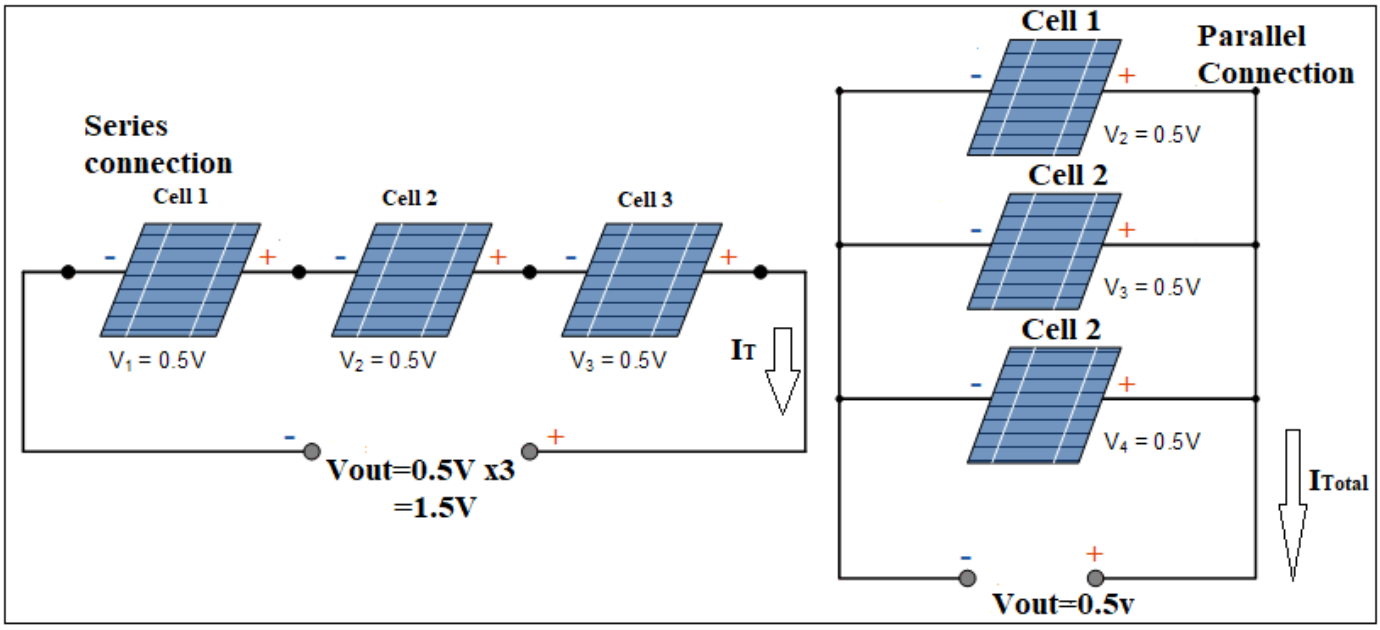

(a) PV Voltage increment (b) PV current increment

Figure 3.2: PV series and parallel connections to increase the voltage and current

Solar cells is the simple arrangement of any PV system. Best cell arrangement is also considered as a current source in which the current from the solar cells is related to the solar irradiation intensity striking [99], [100]. Solar cells represented in an electrical circuit are shown in Figure 3.3. The current in the solar PV system is expressed in equation (3.1):

$$I = I_{SC} - I_d - \frac{V}{R_p} \tag{3.1}$$

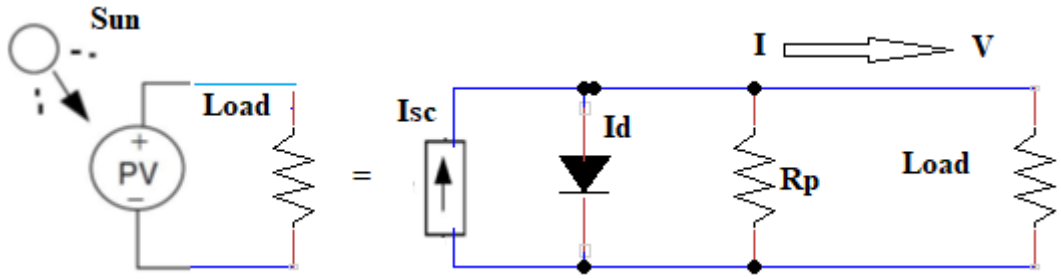

Figure 3.3: Equivalent circuit of the solar cell with the load connected

In Figure 3.3, the diagram shows a simple corresponding circuit of a solar cell generating electrical energy characterized by a real diode in parallel with an ideal current source. The

current delivered is proportional to the flux of insolation received by the solar cell [101]. equation (3.2) shows the current-voltage characteristic curve of the real PV cell:

$$I = I_{SC} - I_O \left(e^{q\left(\frac{V+IR_S}{AKT}\right)} - 1 \right) - \left(\frac{V + IR_S}{R_P} \right)$$

(3.2)

Where I is cell current (the same as the module current) (A), I_{SC} is a short circuit current which is equal to photocurrent (A), I_0 is a dark saturation current (A), I_d is a diode current, q is an electronic charge (1.602x10-19C), K is a Boltzmann's constant (1.381 × 10−23 J/K), A is the Idealizing factor, T is cell temperature (K), V is a cell voltage (V), R_S is a shunt resistance (Ω), R_P is a parallel resistance (Ω).

Retaining the sign convention shown in Figure 3.3 and relating Kirchhoff's Current Law to the node above the diode, using equation (3.3), one can presume that:

$$I_{SC} = I + Id + Ip \tag{3.3}$$

Where Id Is a diode current (A) and Ip is a parallel resistance current (A). Rearranging and substituting the Shockley diode equation into equation (3.3) at 25 °C, one obtains equation (3.4):

$$I = I_{SC} - I_O(e^{38.9Vd} - 1) - \left(\frac{Vd}{Rp} \right) \tag{3.4}$$

Where Vd is the diode voltage (V). With an assumed value of temperature in a spreadsheet, current I can be found from equation (3.4). The voltage across an individual cell can be found from equation (3.5):

$$I = Vd - IRs \tag{3.5}$$

3.2.1.1 Generalised equivalent circuit for a PV cell

The effect of parallel resistance is less important in a PV module compared to series resistance and only where a number of PV modules are connected in parallel to harvest an enormous current, will the effect become more observable merely in the bigger systems [100]. In Figure 3.4, one obtains the solar cell equivalent circuit one-diode model by arranging the parallel resistance Rp to ∞.

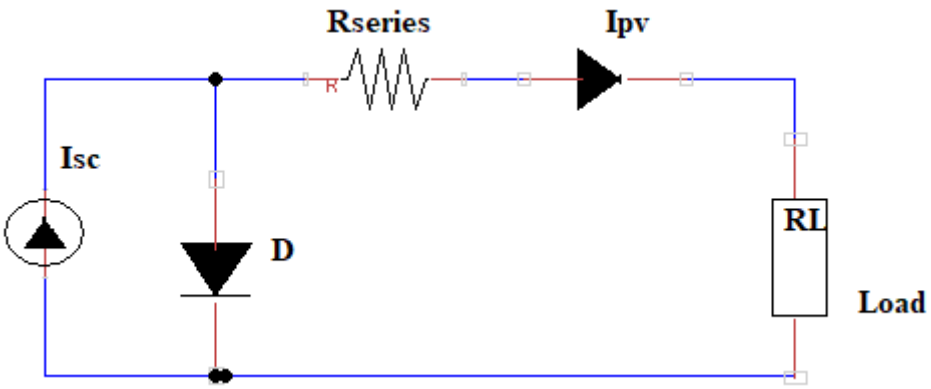

Figure 3.4: A simplified equivalent circuit of the solar cell

From equation (3.5), the current is given by the following equation:

$$I = I_{SC} - I_O \left(e^{q\left(\frac{V+IRs}{AKT}\right)} - 1 \right) \tag{3.6}$$

3.2.1.2 The PV I-V curve under standard test conditions (STC)

In the scheme of a PV array and in the determination of PV modules, imperative parameters for solar cells and PV modules are provided by manufacturers. Figure 3.5 represents these parameters.

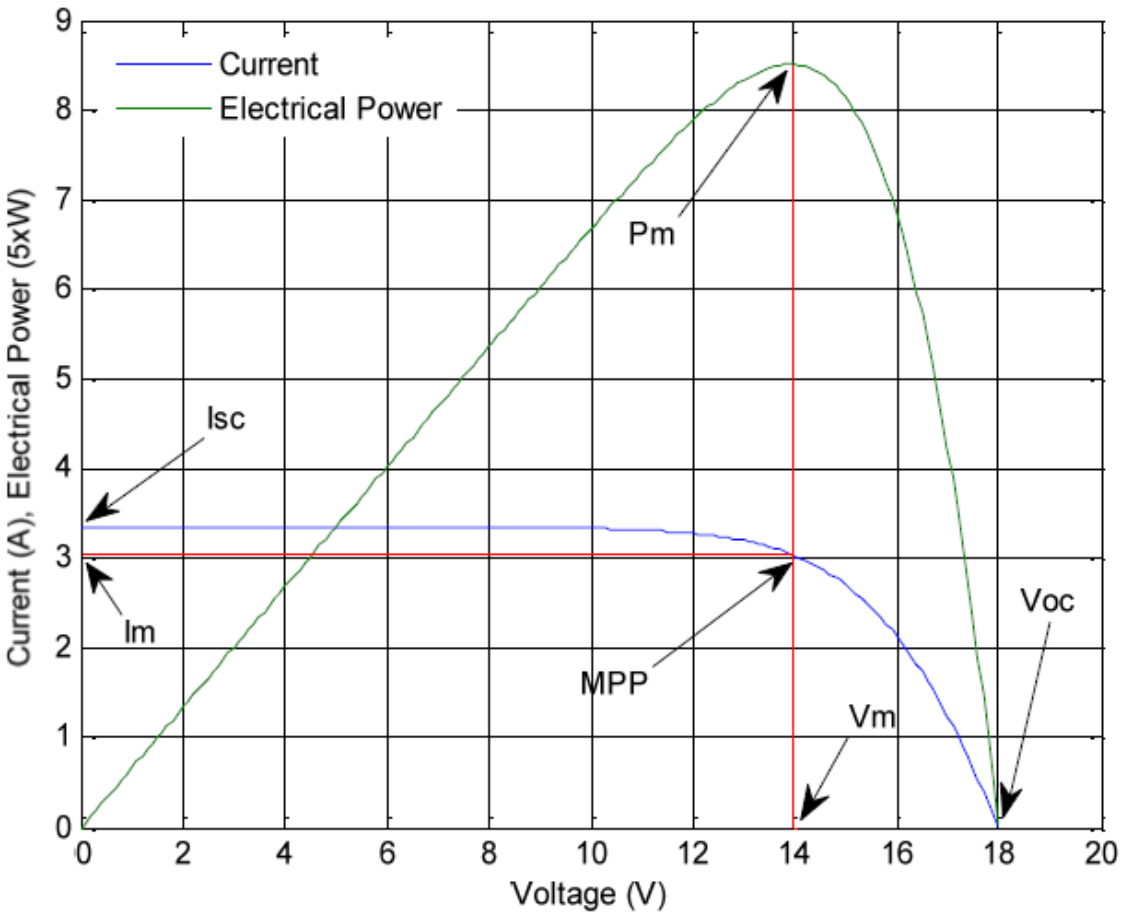

Figure 3.5: I-V curve of PV module [100]

3.2.1.3 Maximum Power Point Tracking (MPPT)

The manufacturers set the characteristicscs at Standard Test Conditions (STC), displaying that the PV module's output power is affected by irradiation, cell temperature, and voltage As a result, the MPPT unit is used to extract the full amount of power from the PV module. There have been many MPPT methods reported [102], [103]. In this research, the Sources IC method is deployed. As discussed in [102], the incremental conductance algorithm fast tracks the maximum power point under quick varying atmospheric environments. In the source, the output current and voltage are examined. In order for the MPPT controller to decide whether to decrease or increase duty ratio, it depends upon these outputs calculating the conductance and incremental conductance.

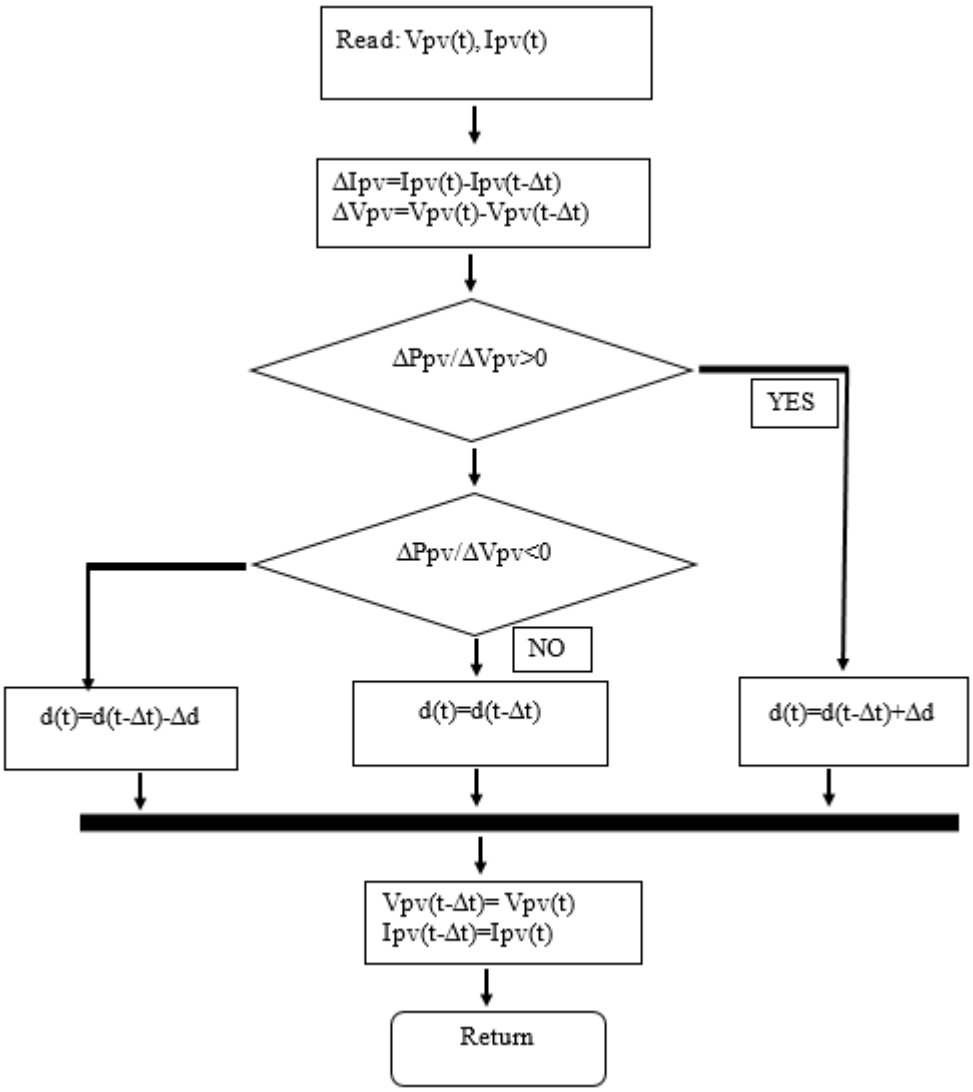

Figure 3.6: Incremental Conductance Algorithm flowchart

A described algorithm at every MPPT incremental conductance sampling is shown in Figure 3.6, where, d (t) is the duty ratio at the present time step, Δd is the incremental duty ratio, d(t-Δt) is the duty ratio at the preceding time step and Δt is the time step.

The output power from the PV source presented in equation (3.7) can be expressed as follows:

$$P_{PV} = I_{PV} * V_{PV} \tag{3.7}$$

Where P_{PV} the power from PV is, I_{PV} is the current from PV and V_{PV} is the voltage from the PV.

The equation (3.7) is differentiated to determine the algorithm, the:

$$\frac{I}{V}\frac{dP}{dv} = \frac{i}{v} + \frac{di}{dv} \tag{3.8}$$

G and ΔG respectively, define the source conductance and incremental conductance:

$$G = \frac{I_{pv}}{V_{pv}} \tag{3.9}$$

$$\Delta G = \frac{di_{pv}}{dv_{pv}} \tag{3.10}$$

MPPT algorithms are characteristically deployed in the schemes for PV systems. In features such as sunlight (variable irradiance) and temperature, algorithms version plays a vital role to ensure that at all times the PV system produces the maximum power harvested [103]. In Figure 3.7, the power voltage curve has I-V and P-V characteristics of a photovoltaic system. Irradiance effect on PV array performance, T=25.15ºC.

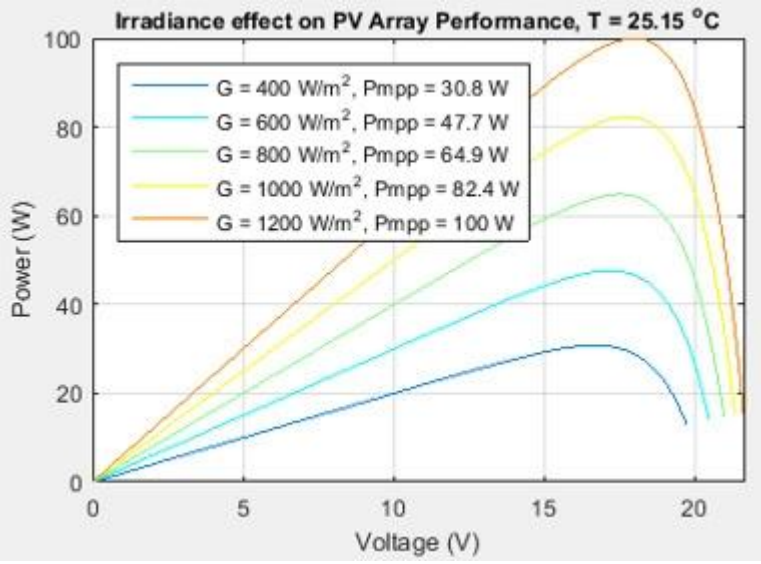

Figure 3.7: Power voltage curve with I-V and P-V characteristics of a photovoltaic system [104]

The fill factor (FF), is the ratio of the maximum power that can be supplied to the load to the product of I_{SC} and V_{OC}, is often used to define module efficiency, which is a measure of the real I-V characteristic. Its value is higher than 0.7 for good cells [105]. FF is around 70-75% for crystalline silicone solar modules are typical, while for multi-junction amorphous-Si modules, getting nearer to 50–60% [100].

3.2.1.4 DC-DC Converters

To help steady the voltage and maximum power generated, DC-DC converters arranged in conjunction with microgrid modules [106]. Three DC-DC converter types are as follows:

• Buck-converter

• Boost-converter

• Buck-Boost converter

These DC-DC converters function by opening and closing a switch on a regular basis. The input voltage is reduced by the buck converter, while the input voltage is increased by the boost converter. The output voltage is higher than the input voltage, so it's called a boost converter [106]. The buck-boost converter has the ability to increase or decrease the input voltage, but with a polarity reversal. These DC-DC converters circuits are shown in Figures 3.8(a), (b) and (c).

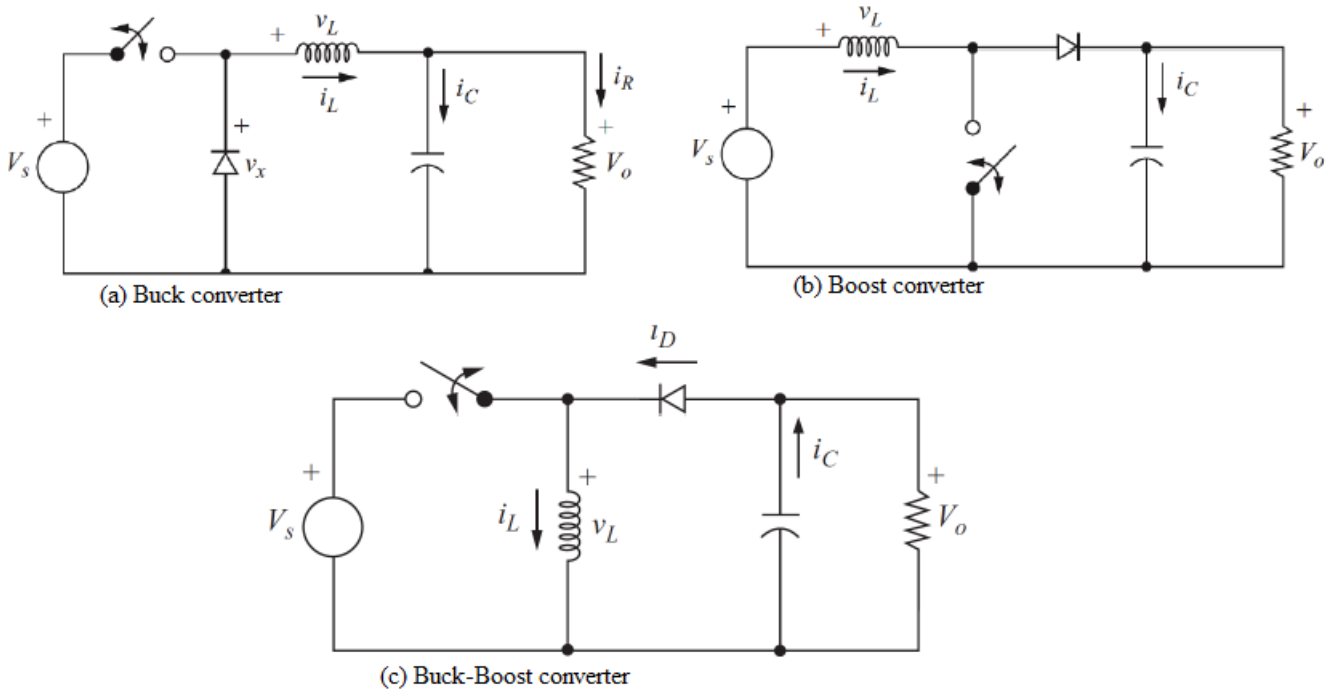

(a) Buck converter (b) Boost converter (c) Buck-Boost converter

Figure 3.8: DC-DC converter circuits

To attain a purely DC output, the converters have a small permit filter after the output switch. The service cycle is extended to change the output voltage. Equations (3.11) to (3.13) respectively are used to measure the performance of the buck, boost, and buck-boost converters, with the responses plotted in Figure 3.9(a) to (c).

$$Vo = VsD \tag{3.11}$$

$$Vo = \frac{Vs}{1-D} \tag{3.12}$$

$$Vo = -Vs\left(\frac{D}{1-D}\right) \tag{3.13}$$

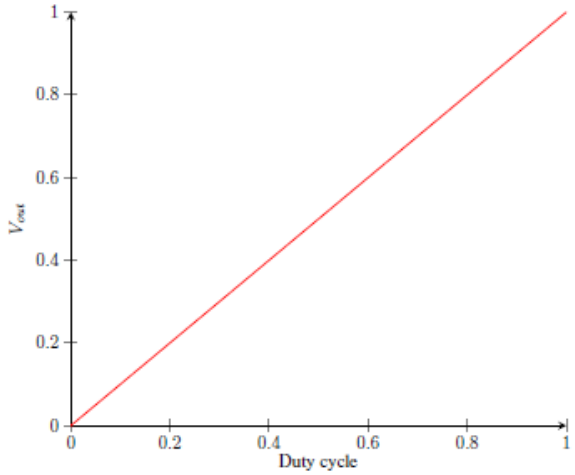

(a) Buck converter

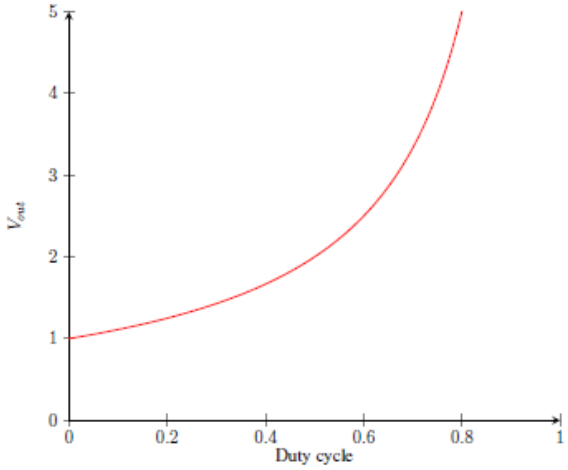

(b) Boost converter

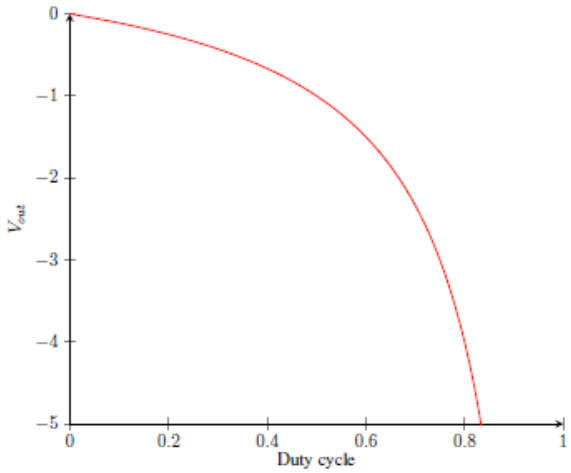

(c) Buck-Boost converter

Figure 3.9: DC-DC converter outputs [106]

The boost converter works by storing energy in an inductor when the switch is closed and delivering that energy to the load when the switch is open to boost the output voltage. The inductor needs to be large enough in order to keep the current positive and in continuous operation. When choosing the inductor size, equation (3.14) was used to find the minimum inductor size required in order for the current to be continuous [107]. A larger inductor was chosen to ensure that the current stays positive when the switch is open. The voltage ripple can be reduced by using a larger output capacitor. Equation (3.15) can be used to measure voltage ripple.

$$L_{min} = \frac{D(1-D)^2 R}{2f} \tag{3.14}$$

Where in Equation (3.14), L_{min} is the minimum inductance required for continuous operation, D is the duty cycle and R is the load resistance and *f* is the switching frequency.

$$\frac{\Delta Vo}{Vo} = \frac{D}{RCf} \tag{3.15}$$

Where *Vo* is the output voltage and C is the capacitance.

The boost converter is shown in Figure 3.9(b). The inductor value was calculated using equation 3.14. Then, Figure 3.10 shows the required minimum inductance versus the duty cycle for a load of $10\,\Omega$ at 5 kHz. It shows the largest minimum inductance of $150\ \mu H$ when the duty cycle is around 0.35. A larger inductance of $240\ \mu H$ was chosen to ensure that the boost converter operated in continuous current mode.

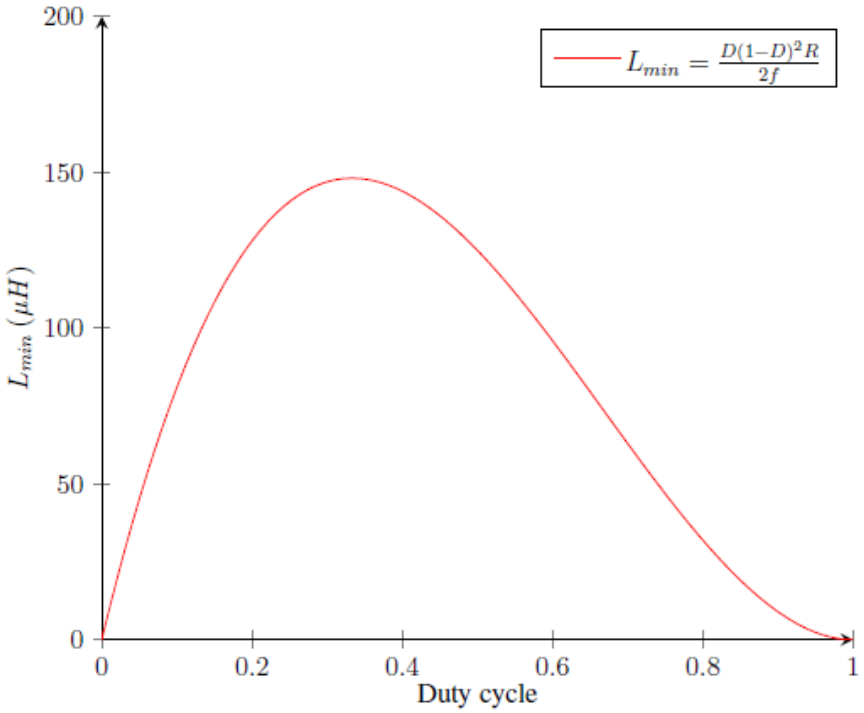

Figure 3.10: Boost converter minimum inductance for continuous current[106]

A buck-boost converter is also a great component. This converter works by storing energy in the inductor when the switch is closed and the energy is then transferred to the load when the

switch is open [108]. The duty cycle is adjusted to determine the output voltage, which can be higher than or lower than the input voltage. If the duty cycle is greater than 0.5, the output voltage is greater than the input voltage and if the duty cycle is less than 0.5, the output voltage is less than the input voltage as shown in Figure 3.9(c). The output voltage is calculated using equation 3.15. For continuous current in mode operation, the minimum inductance can be determined using equation (3.14) and the output voltage ripple can be calculated with equation (3.15). The inductor value was calculated using equation (3.14). Then, Figure 3.11 is the required minimum inductance versus the duty cycle for load 10 Ω ohms at 5 kHz.

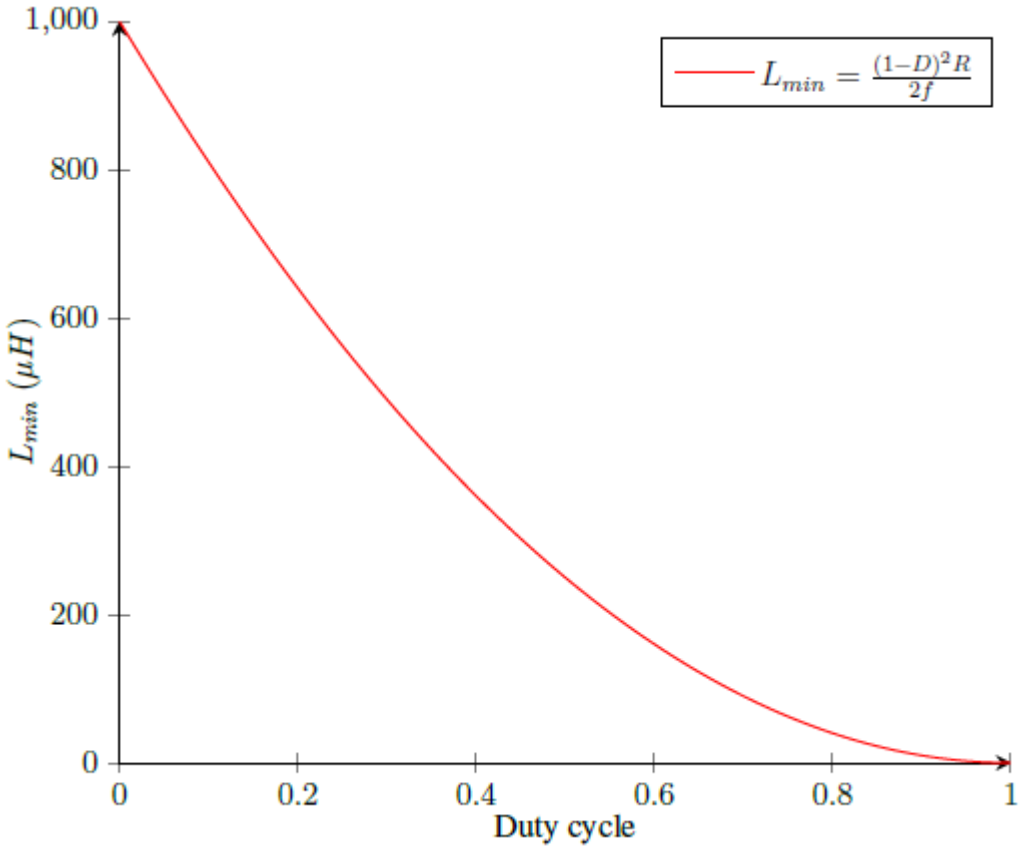

Figure 3.11: Buck-boost minimum inductance for continuous current

The output voltage is below the input voltage. When the duty cycle is 0.7, the output voltage was 840 V, as can be confirmed using equation (3.16).

$$Vo = -Vs\left(\frac{D}{1-D}\right) \tag{3.16}$$

3.2.2 The Bi-directional Converter

A bi-directional converter is required to permit the flow of power from and to the batteries in the microgrid. The previous buck and boost converters do not have the capability for bi-directional power flow. This is because they all have diodes in their designs which prevent reverse current flow [106]. In Figure 3.12, a bi-directional converter is achieved by cascading the buck converter and boost converters and substituting their diodes with switches. The top switch is used to operate the converter as a buck converter, transferring power from the high voltage side to the low voltage side and the bottom switch is used to operate the converter as a boost converter, transferring power from the low voltage side to the high voltage side.

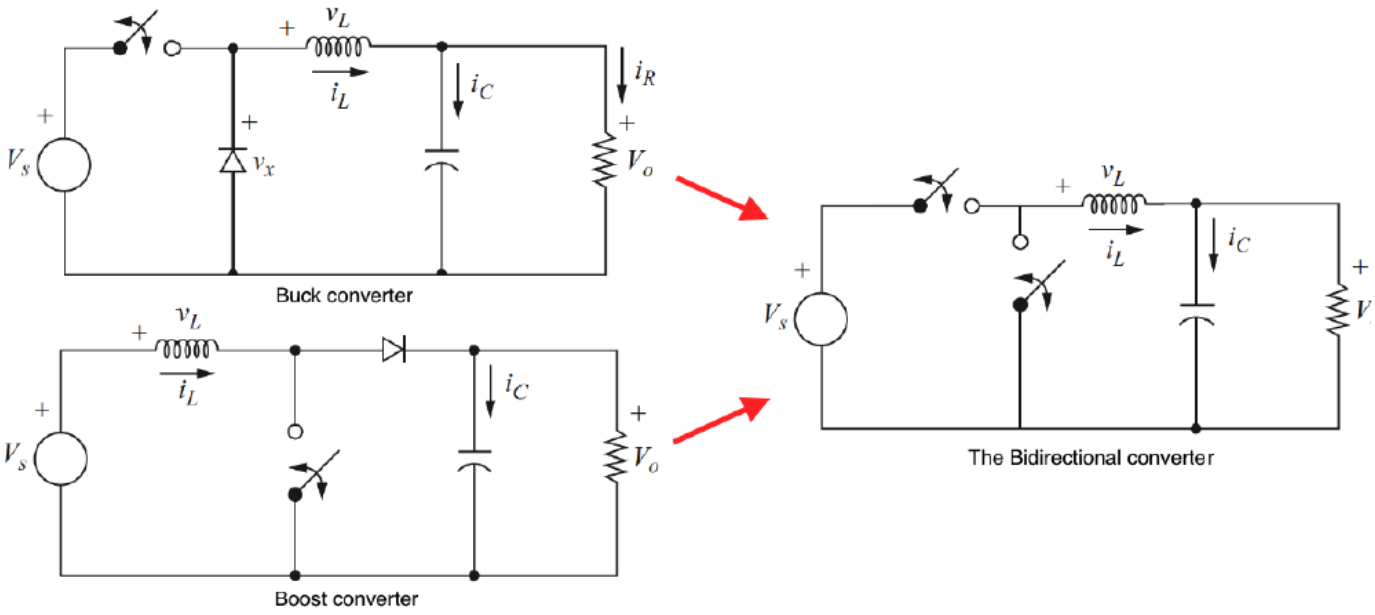

Figure 3.12: Bi-directional converter construction

The bi-directional converter will be controlled by a charge controller which will determine whether energy needs to be sent to or from the battery in order to smooth out the fluctuations of renewable energy sources and stabilize the voltage. The same values as the buck converter design were used for the bi-directional converter, except for the inductor value. It was found that having a large inductor value inhibits the voltage stability of the system, therefore a lower value was chosen. The lower ripple will help to charge and discharge the batteries with higher efficiencies, increasing their lifetime.

3.2.2.1 Matlab/Simulink model development of PV system

Figure 3.13 shows the MATLAB scheme implementation of the photovoltaic system, made up of MPPT and complemented with a boost converter.

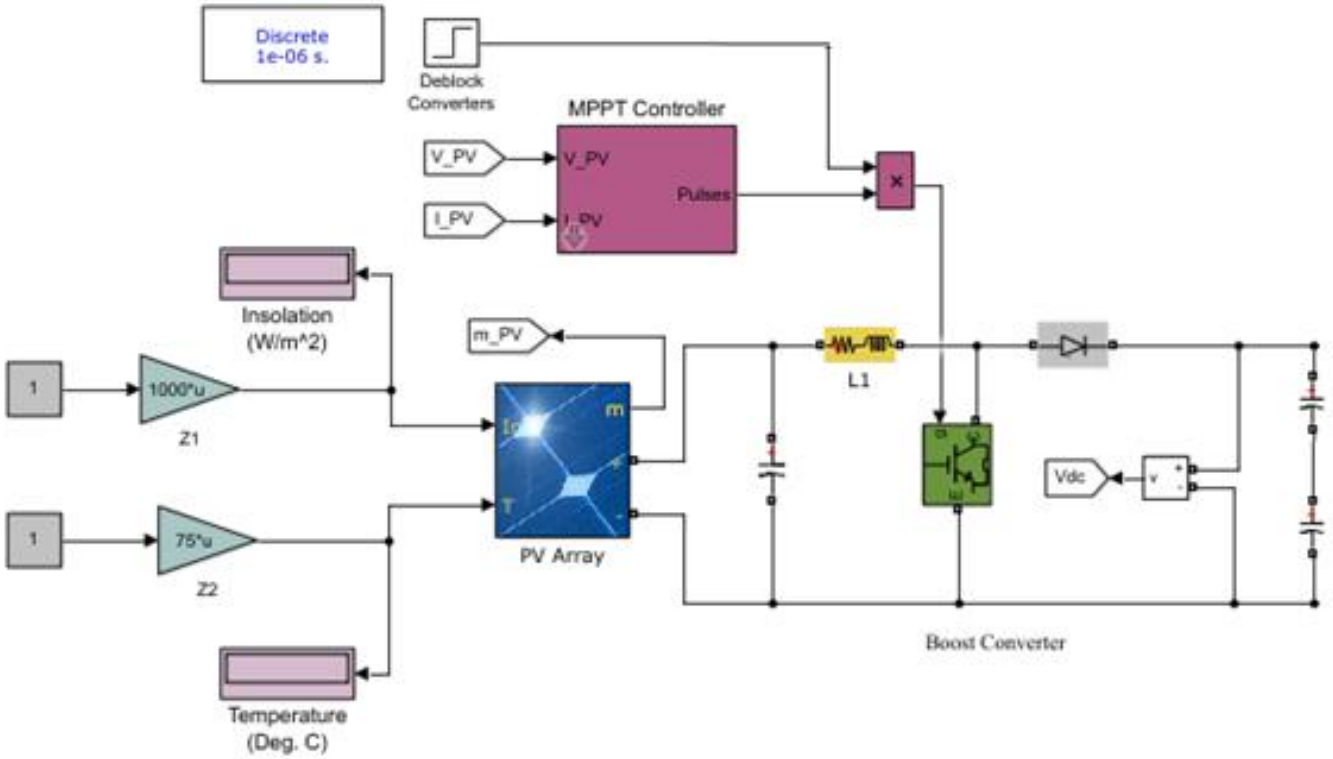

Figure 3.13: Matlab/Simulink model implementation of photovoltaic system

3.2.3 Modelling and Operating Principle of Wind Energy System

Power from the wind can be used to drive an electrical generator, i.e. electricity is produced by wind turbines. Wind generates lift and exerts a turning force as it passes over the blades. Blades spin the shaft within the nacelle, which is connected to the generator. Wind turbine systems can use both synchronous and induction generators [109]. Nevertheless, a gearless technique in the variable speed multi-pole permanent magnet synchronous generators (PMSG) is mostly used due to its improved performance as compared to other wind turbine generators. The variable speed multi-pole permanent magnet makes PMSG considered as the most effective and reliable system since it can work on a wide range of wind speeds [10]. In this research, PSMG is deployed due to its improved performance as compared to other wind turbine models.

In addition, some climate conditions are taken into consideration, i.e. continuous accessibility of the wind energy source.

Energy generated E_W by wind turbine and the rated output power P_W is given by the equations (3.17) and (3.18):

$$P_W = \frac{1}{2}\rho_W A v^3 C_p \mu_g \mu_t \tag{3.17}$$

$$E_W = E_W \times T \tag{3.18}$$

Where: E_W is energy generated by the wind turbine, P_W is output power, ρ_W is density of air in Kg/m^3, A is a swept area of rotor blades, C_p is the power coefficient representing generator and turbine efficiency, μ_g is generator efficiency and μ_t is turbine efficiency.

The power coefficient can be expressed by the following equation:

$$C_p = \frac{1}{2}\left(\delta - 0.022\beta^2 - 5.6\right)e^{-0.17\delta} \tag{3.19}$$

(Where β , is the pitch angle of blades in degree and δ is the tip speed ratio of turbines)

The high speed shaft is modelled by an inertia and a damper. The sum of inertia of the high speed shaft, rotor of the generator and gearbox; the friction of the high speed shaft bearings, the aerodynamic torque, generator torque and gear ratio are demonstrated in Figure 3.14. Figure 3.14 shows that a two-mass model system is used to define the wind turbine system which basically consists of blades, the gear train and the generator[110].

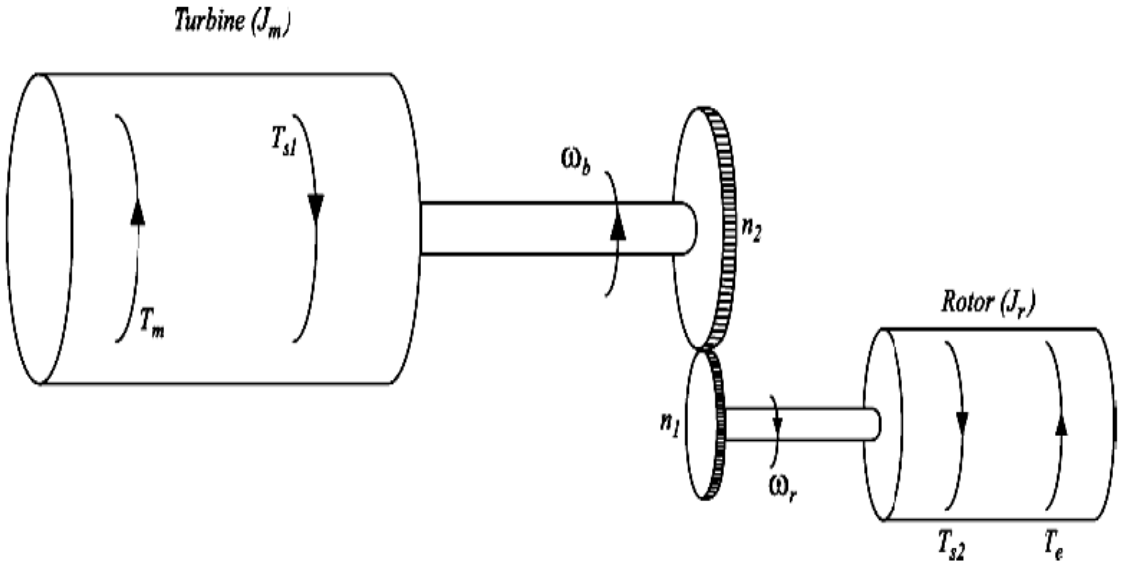

Figure 3.14: Two-mass Model for wind turbine [110]

The turbine torque Tm (produced by the wind) accelerates the turbine inertia and is counter-balanced by the shaft torque T_{S1} (produced by the torsional action of the low speed shaft). It is represented by the following expression in equation (3.20):

$$T_m - T_{S1} = J_m \frac{\partial \omega b}{\partial t} \tag{3.20}$$

3.2.3.1 Rectifiers

A rectifier is an electrical system made up of single or more diodes that permits the flow of current in one direction only. It is used to convert alternating current (AC) into direct current (DC) [111]. In this research study wind generation produces AC and it has to be converted to a desired DC output voltage. The AC voltage can be altered into DC voltage by a component named the PN junction diode. Rectification of AC to DC is mostly achieved by the application of a PN junction diode which acts as a rectifier. A PN junction diode allows electric current only in one direction, i.e. forward bias condition, and blocks electric current in reverse bias conditions. There are different types of rectifiers, categorized into two types, namely: Single phase and three-phase rectifiers. Furthermore, rectifiers are categorized into three types, namely: uncontrolled, half controlled and controlled rectifiers [112].

3.2.3.1.1 Half-wave Rectifier

When an alternating current supply is applied at the input, one positive half-cycle is visible across the load while the negative half-cycle is obscured. A single diode is required in a single-phase supply, while three diodes are required in a three-phase supply. It is incapable because only half of the input waveforms make it to the output. More filtering is required to lessen the ripples of the AC frequency from the output in a half-wave rectifier circuit. Figure 3.15 represents the equivalent circuit for a half-wave rectifier. The rectification only takes place during half-periods. Figure 3.16 shows the half-wave output waveforms of voltage at the secondary and of the current in the load. Since the load is a resistance, then voltage on the load is proportional to the current. Load current $i_L(t)$ flows in the same direction in the secondary winding.

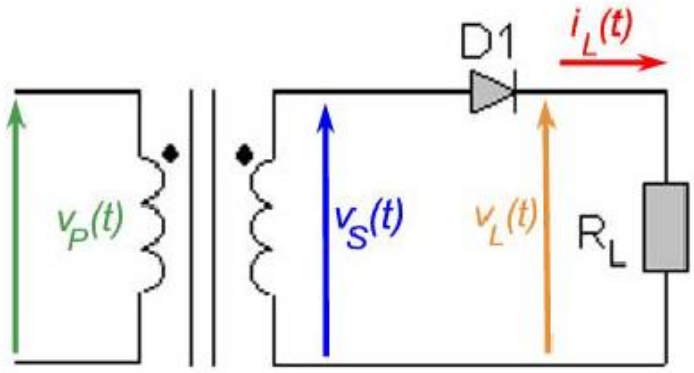

Figure 3.15: Half-wave Rectifier circuit

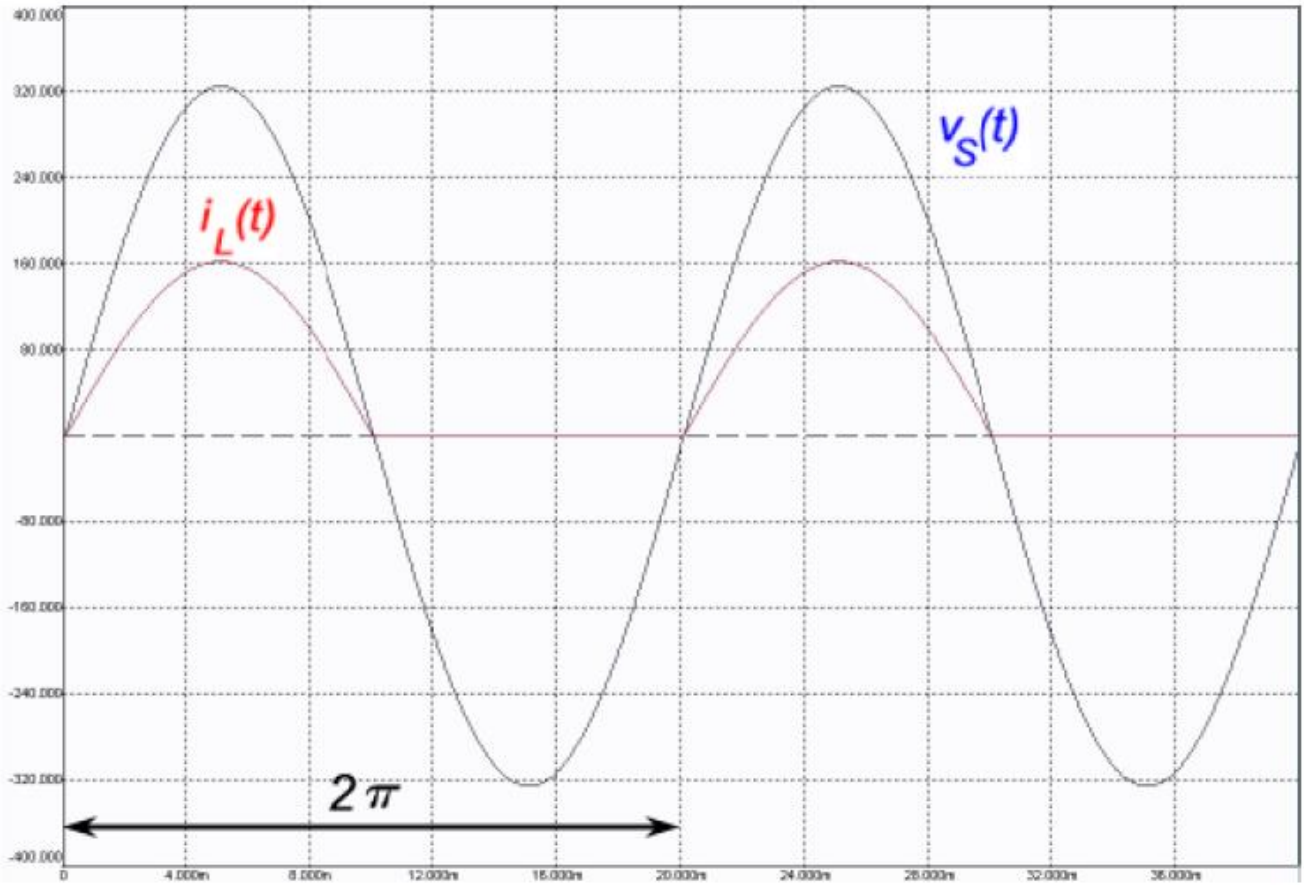

Figure 3.16: Half-wave rectifier waveform output

Using the definitions reported and explained by waveform, with equation (3.21) to equation (3.24), the following calculations result:

$$V_{DC} = \frac{1}{T}\int_0^T V_L(t)\,dt = \frac{1}{2\pi}\int_0^\pi V_S \sin(\omega t)\,dt = \frac{V_S}{\pi} \tag{3.21}$$

Similarly, one can calculate the other parameters:

$$V_L = \sqrt{\frac{1}{T}\int_0^T {V_L}^2(t)\,dt} = \sqrt{\frac{1}{2\pi}\int_0^\pi {V_S}^2 \sin^2(\omega t)\,dt} = \frac{V_S}{2} \tag{3.22}$$

$$I_{DC} = \frac{V_{DC}}{R_L} = \frac{V_S}{\pi.R_L} \tag{3.23}$$

$$I_L = \frac{V_L}{R_L} = \frac{V_S}{2.R_L} = I_S \tag{3.24}$$

3.2.3.1.2 Centre-Tap Full-wave Rectifier

This type of rectifier circuit uses two diodes connected in such a way that each one consumes one-half of the input AC voltage. To perform rectification, one diode uses the alternating current voltage shown on the upper half of the secondary winding, while the other diode uses the alternating current voltage shown on the lower half of the secondary winding. Because the AC supply powers both halves, the output and efficiency of this circuit are high. Figure 3.17 represents the equivalent circuit for a centre-tap full-wave rectifier. Figure 3.18 shows centre tapped output waveforms of voltage at the secondary and of the current in the load.

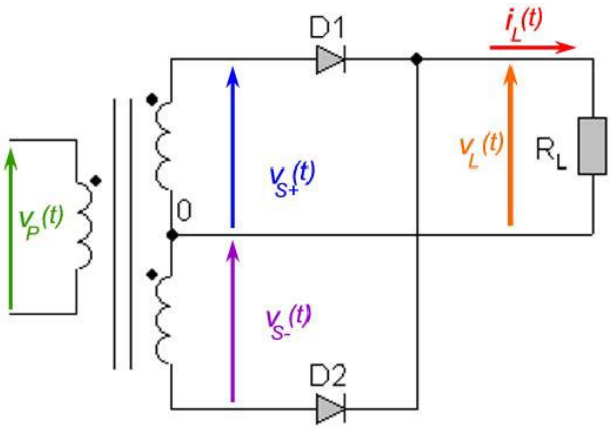

Figure 3.17: Centre-tap full-wave rectifier circuit

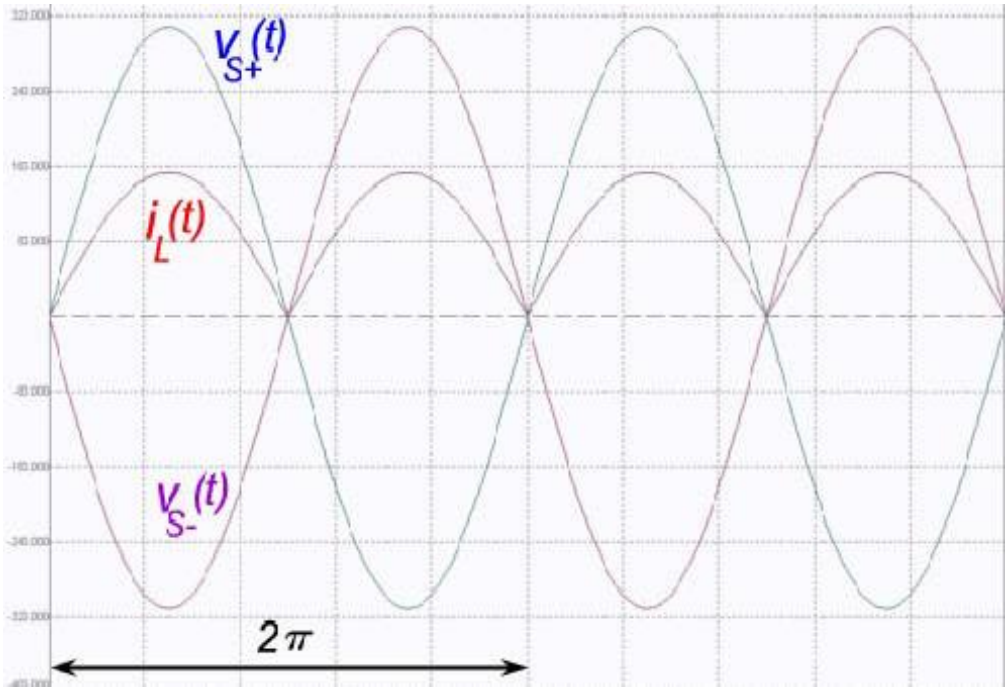

Figure 3.18: Centre-tap full-wave rectifier output waveform

It has been noted that the current flows in the same direction through the halves of the secondary winding in the presented simulation results. Using the definitions reported in the previous section and the symmetries expressed in equation (3.25) to equation (3.31), the following results are obtained:

$$V_{DC} = \frac{1}{T}\int_0^T V_L(t)\,dt = \frac{2}{2\pi}\int_0^\pi V_S \sin(\omega t)\,dt = \frac{2.V_S}{\pi} \tag{3.25}$$

$$V_L = \sqrt{\frac{1}{T}\int_0^T {V_L}^2(t)\,dt} = \sqrt{\frac{1}{\pi}\int_0^\pi {V_S}^2 \sin^2(\omega t)\,dt} = \frac{V_S}{\sqrt{2}} \tag{3.26}$$

$$I_{DC} = \frac{V_{DC}}{R_L} = \frac{2.V_S}{\pi.R_L} \tag{3.27}$$

$$I_L = \frac{V_L}{R_L} = \frac{V_S}{\sqrt{2}.R_L} \tag{3.28}$$

$$FF = \frac{V_L}{V_{DC}} = \frac{\pi}{2.\sqrt{2}} = 1.11 \tag{3.29}$$

$$\eta = \left(\frac{1}{FF}\right)^2 = 0.81 \tag{3.30}$$

$$RF = \sqrt{{FF}^2 - 1} = 0.483 \tag{3.31}$$

3.2.3.2 Matlab/Simulink model development of a wind power system

Figure 3.19 shows the Matlab/Simulink model implantation of a wind system consisting a wind model wind turbine and rectifier model. The AC output generated from wind energy is converted to DC output power by means of a rectifier.

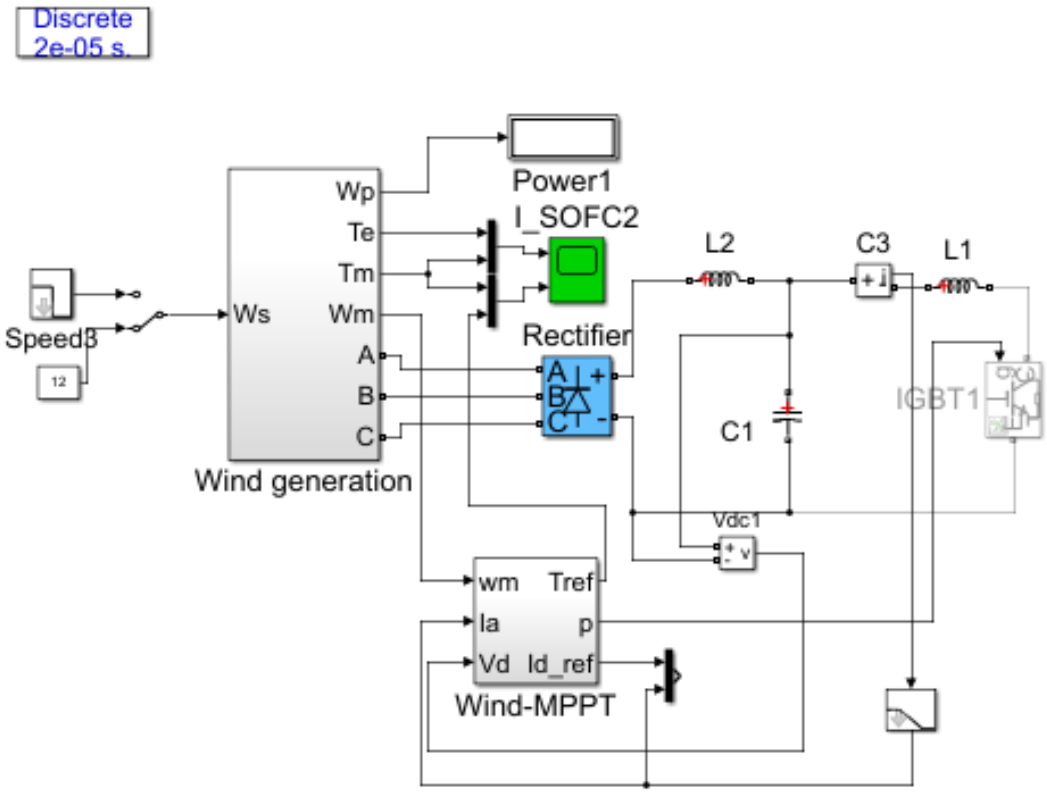

Figure 3.19: Matlab/Simulink model implementation of wind system

3.2.4 Modelling of a Battery

The battery will charge if the energy produced by wind energy or the PV array and the power exceeds the local load demand at any point during the day [113]. Moreover, in the event where the load is greater than the energy generated by the both sources of PV Solar and wind energy, the battery is discharged to support the insufficiency of power in the system. This can be expressed in the following equation:

$$SOC(k+1) = SOC(k) - \frac{\Delta t \eta}{E_{nominal}} \sum_{i=1}^{K} P_4(k) \tag{3.32}$$

Where SOC is the state of charge of the battery; $P_4(k)$ is the power flow from the battery (discharge); $E_{nominal}$ is a nominal energy; and η is the battery efficiency. The following general equation derived from equation (3.32) applies to the battery dynamics:

$$SOC(k+1) = SOC(0) - \frac{\Delta t \eta}{E_{nominal}} \sum_{i=1}^{K} P_4(k) \tag{3.33}$$

This is regarded as the initial SOC of the battery and $\frac{\Delta t \eta}{E_{nominal}} \sum_{i=1}^{K} P_4(k)$ is the amount of power discharged by the battery at a given point in time. The capacity of the usable battery bank must not fall below the minimum permissible capacity and must not exceed the maximum permissible capacity, to express this, the restriction use equation (3.34) [114]:

$$SOC^{min} \leq SOC(k) \leq SOC^{max} \tag{3.34}$$

Equation (3.34) can be translated into equation (3.35), the result of which the lower limit for the SOC of the battery bank cannot exceed at the time of discharging SOC^{min}. This may be expressed in the following equation [114]:

$$SOC^{min} = (1 - DOD).SOC^{max} \tag{3.35}$$

3.2.5 Modelling and principle of hybrid solar-wind

3.2.5.1 Matlab/Simulink model development of a hybrid solar-wind system

The microgrid is made up of a photovoltaic system and wind energy system. Figure 3.20 displays the Matlab model implementation of a hybrid system. Both sources, the PV system and wind energy, are embedded in the system. A battery is included for stability and a DC-DC converter of a battery will also act as the MPPT of the PV system.

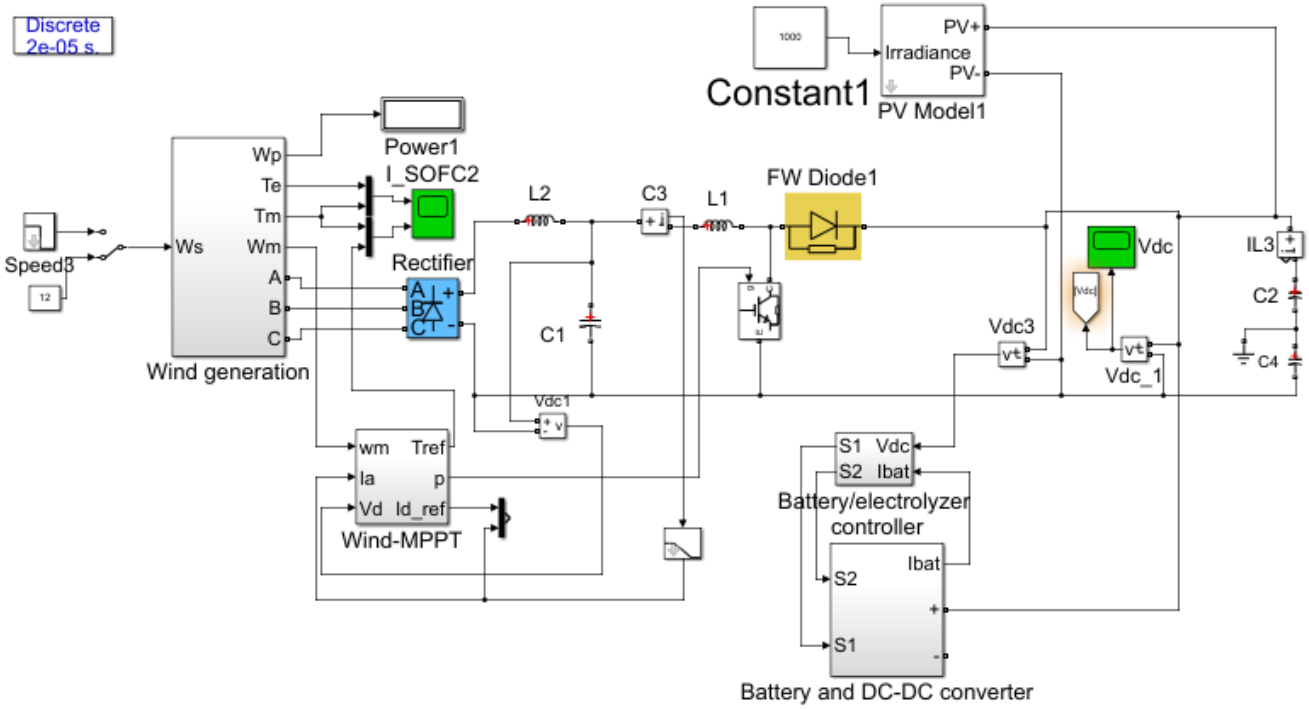

Figure 3.20: Matlab/Simulink model implementation of a hybrid system

Chapter Four
Results and Discussion of Results

4.1 Introduction

This chapter presents all the simulation results of the designed microgrid using hybrid sources PV system and wind energy on MATLAB/SIMULINK. The aim is to conduct a power flow analysis by reviewing the steady state of power and voltage. It also conducts fault analysis in a hybrid DC microgrid using MATLAB/SIMULINK. Steady state performance during faults are analysed using power flow study and transient studies respectively. The power flow analysis is done to comparatively evaluate the steady state stability of the base case combined system. The transient stability study is carried out on a PV system and wind energy system. DC faults are analysed.

4.2 Simulations Model and System Description

A DC microgrid model is based on direct current (DC) that is a standalone. The individual components of the microgrid are planned and simulated using a DC-DC converter. In order to extract maximum power from the resources, power electronic converters were designed and simulated for use with wind energy, while photovoltaic (PV) modules were used with MPPT. "Perturb and Observe" technique to vary the voltage across the terminals of the PV array and wind in order get the maximum possible power. The charge controller successfully controlled the DC-DC converter, permitting power to flow from/to the battery to attain voltage stabilization. A battery plays a crucial role as the most cost-effective option for integration into the microgrid. Wind energy is used and AC output from wind turbines converted to DC output by means of rectifiers. Since the power produced by a wind turbine is proportional to the cube of the wind speed, wind turbines should be located in areas where the mean annual wind speed

is high. Wind turbines begin to generate electricity at wind speeds of around 3-4 m/s and stop at wind speeds of around 20-25 m/s [115], [116].

The designed hybrid DC microgrid is made up of PV system, wind energy, energy storage and power converters to DC output. Rectifiers are used to produce DC from AC supplied by generators and feed the power to DC bus. The DC-DC boost converter's output is connected to the DC microgrid, which is where the load is connected. The DC-DC boost converter, which also controls the DC connection voltage, represents the battery. For stability purposes, the battery and DC-DC converter of battery is used and also acts as the MPPT of the PV system. Figure 4.1 represents a block diagram of the DC microgrid with PV system and wind energy system. The system is a standalone hybrid system.

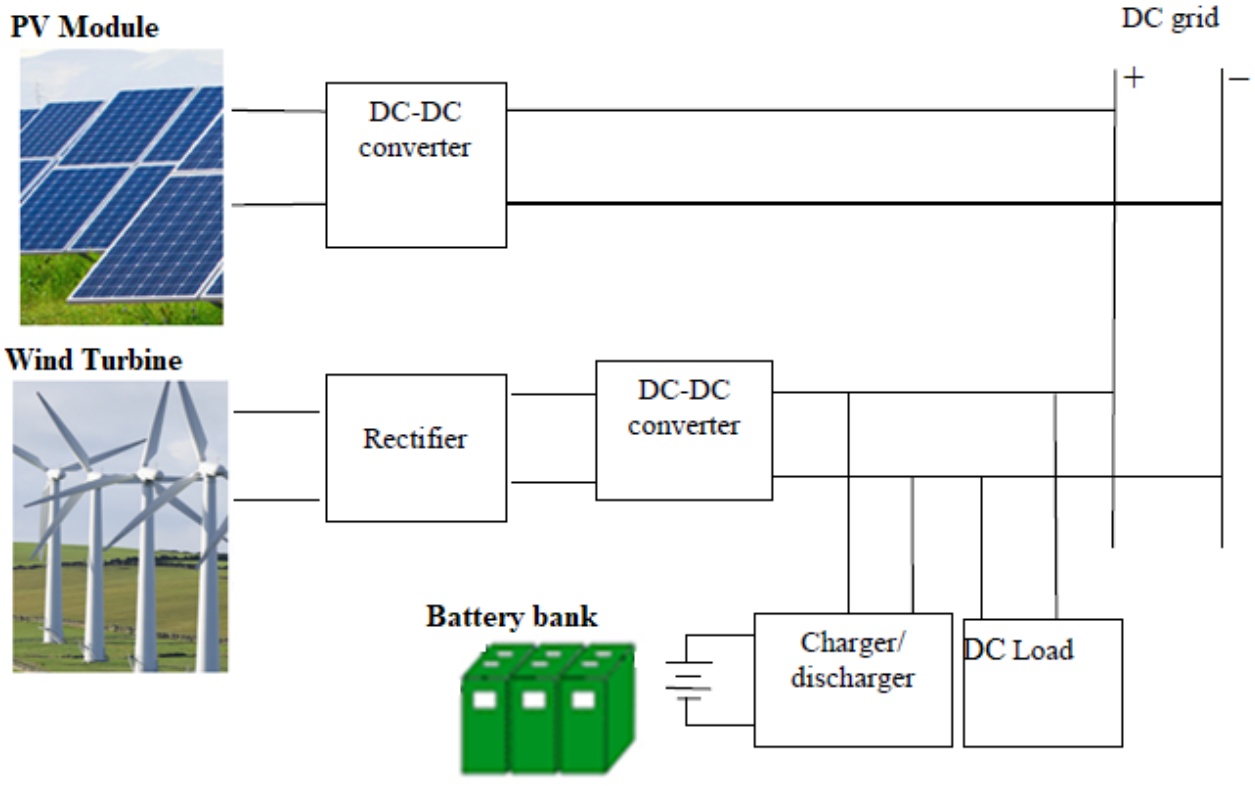

Figure 4.1: Block diagram of the DC microgrid with PV system and wind energy system

The objective is to design a hybrid DC microgrid, conduct power flow and a fault analysis in a system constructed on MATLAB/SIMULINK. Figure 4.2 shows a designed hybrid DC microgrid system supplied by PV and wind energy system on MATLAB/SIMULINK.

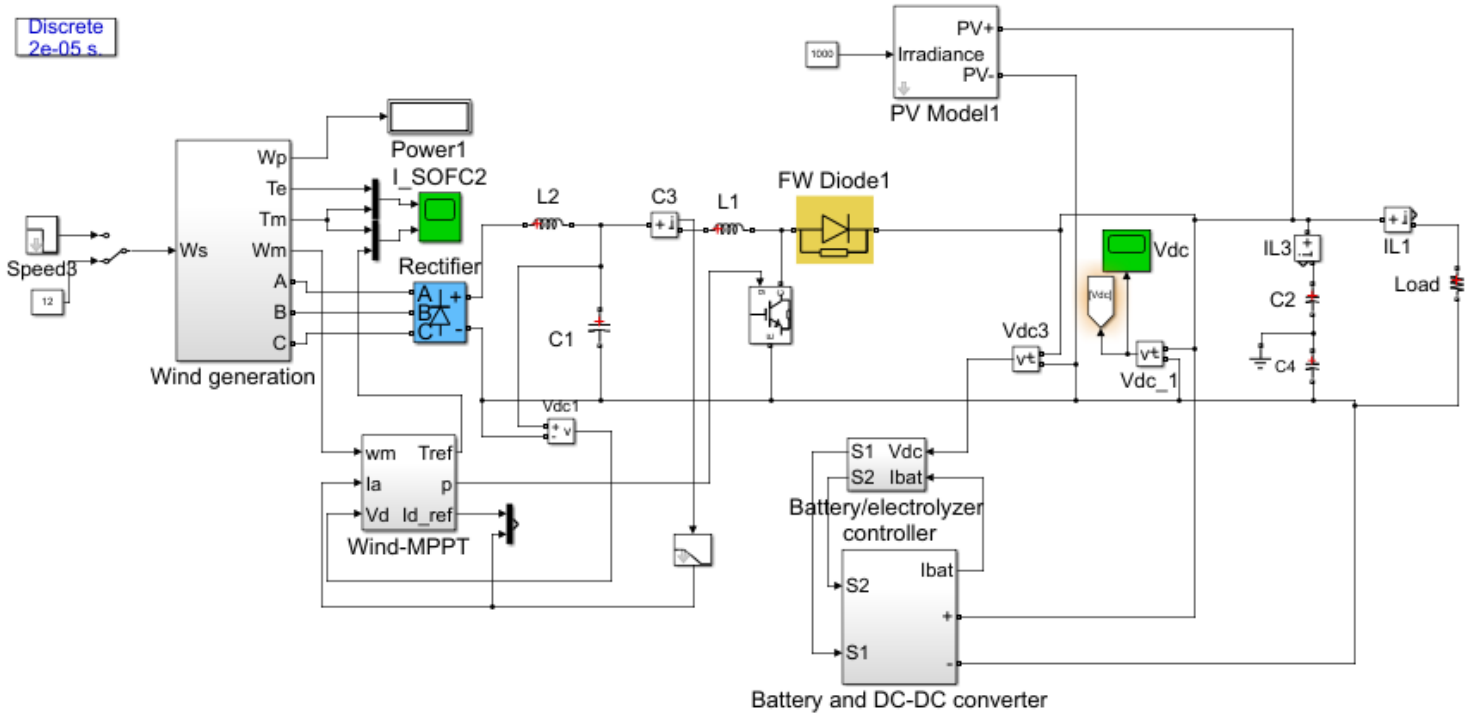

Figure 4.2: Hybrid DC microgrid simulation model in Matlab/Simulink

In this research, the coordination, control strategies of the DC microgrid and computer simulations were carried out using MATLAB/SIMULINK. A Power flow analysis of a hybrid DC microgrid and fault analysis of a hybrid DC microgrid is conducted. In the designed hybrid DC system, there are hidden internal components. Appendix A shows wind generation; Appendix B 2-Masse Drive Train1 Model; Appendix C- Pitch Angle-Controller and Appendix D shows a clear view of a hybrid DC microgrid system designed on MATLAB. In a designed hybrid DC microgrid, when the power produced by the PV system and wind turbine exceed the required load and the battery is below the maximum, then the excess power charges the battery.

4.3 Power Flow Analysis overview of a Hybrid DC Microgrid

The objective of power flow analysis is to determine the load power utilization, active and reactive power at each bus in an electrical power system. It is necessary in the planning and operation of power systems to analyse the steady-state operation of a power system under varying conditions and to consider the effect of variations in the configuration of equipment. Power flow analysis is a basic tool used in power system studies. With the use of flow study results, the compliance of system power and voltages to the allowable maximum and minimum limits at different points in the network under various operating conditions can be determined [117]. The essential purpose of power flow analysis is to define the line flow of active voltage, current and power in each section of the power system and the total power losses in the system.

4.3.1 Power Flow Analysis Bus Classification

Generators lines and loads are linked to a bus. In each node or bus node of a power system, there are four quantities such as magnitude of phase angle of voltage, reactive power and true or active power [118]. The buses are categorized into three kinds as follows:

4.3.1.1 Load bus

The real power and reactive power are specified in this bus. It is desired to find out the voltage magnitude and phase angle with the aid of load flow. It is necessary to obtain Pd and Qd at such bus since at a load bus, voltage can be permitted to vary within the tolerable values.

4.3.1.2 Generator bus or voltage controlled bus

The voltage magnitude corresponding to the real power Pg and generator voltage corresponds to the ratings that are identified. There is a necessity to determine the phase angle of the bus voltage and power generation Qg.

4.3.1.3 Slack (swing) bus

The voltage magnitude and phase Q are anticipated, while the actual and reactive powers, Pg and Qg are calculated using the power flow solution.

4.3.1.4 Gauss iterative method using Ybus

The assumptions are made on voltages for all buses except the voltage on slack bus due to that specified voltage remaining stable and as a result, that resolves the load flow. The currents must be calculated using the relevant method for all buses except the slack bus, derived from the following equation (4.1):

$$Ip = \frac{\left(P_p - jQ_p\right)}{E^*_p} \qquad p \neq s \;\; \& \;\; p = 1, 2 \ldots\ldots, n \tag{4.1}$$

Where n is the number of buses in the network, the performance of the network can be attained using equation (4.2):

$$I_{BUS} = Y_{BUS}\, E_{BUS} \tag{4.2}$$

Selecting the ground as the reference bus, a set of (n-1) simultaneous equations can be written in the following form, i.e. equation (4.3):

$$E_p = \frac{1}{Y_{pp}} \left(I_p - \sum_{\substack{q=1 \\ q \neq p}}^{n} Y_{pq}\, E_q \right) p \neq s \;\&\; p = 1, 2 \ldots\ldots, n \tag{4.3}$$

The bus currents calculated from equation (4.1), the slack bus voltage and the estimated bus voltages are substituted into equation (4.2) to obtain a new set of bus voltages. The new voltages are used in equation (4.3) to re-calculate bus currents from the following solution of equation (4.4). This procedure is repeated until all bus voltage variations are insignificant. The slack bus power that also occurs in the line can be found after obtaining the voltage solution. The network equation (4.1) and the bus loading equation (4.3) can be combined to obtain E_p in equation (4.4):

$$E_p = \frac{1}{Y_{pp}} \left(\frac{P_p - jQ_p}{E^*_p} - \sum_{\substack{q=1 \\ q \neq p}}^{n} Y_{pq} E_q \right) \quad p \neq s \;\&\; p = 1, 2 \ldots, n \tag{4.4}$$

The bus voltage is only included as a variable. Expressing the load flow problem in this method results in a set of non-linear equations that can be resolved by an iterative method. Carrying out numerous arithmetic processes as possible before initiating the iterative calculation plays a vital role in reducing computing time, finding solutions. Letting:

$$\frac{1}{Y_{pp}} = L_p \tag{4.5}$$

When substibuting equation (4.4), it gives equation (4.5), which can be written as follows:

$$E_p = \frac{\left(P_p - jQ_p\right) L_p}{E^*_p} - \sum_{\substack{q=1 \\ q \neq p}}^{n} Y_{pq} L_p E_q \quad where\ p \neq s \;\&\; p = 1, 2 \ldots, n \tag{4.6}$$

Letting

$$(P_p - jQ_p) L_p = KL_p \tag{4.7}$$

And

$$Y_{pq} L_{pq} = YL_{pq} \tag{4.8}$$

Then substituting the bus voltage equations (4.5) and (4.8), becomes equation (4.9)

$$E_p = \frac{KL_p}{E^*_p} - \sum_{\substack{q=1 \\ q \neq p}}^{n} YL_{pq} E_q \tag{4.9}$$

The load flow study takes up a stable system and utilises a single-phase demonstration corresponding to the positive sequence network. Many of the matrix elements were found to be zero due no common coupling and that gives a bus admittance matrix.

4.3.2 Simulation Result of Power flow in a DC PV solar system and DC wind energy system

The configuration of the DC microgrid system and control methods of distributed generation are expressed. Moreover, focus is on the source side, transmission side and load side. Figure 4.3 shows a simulation diagram of a hybrid DC microgrid in MATLAB/Simulink.

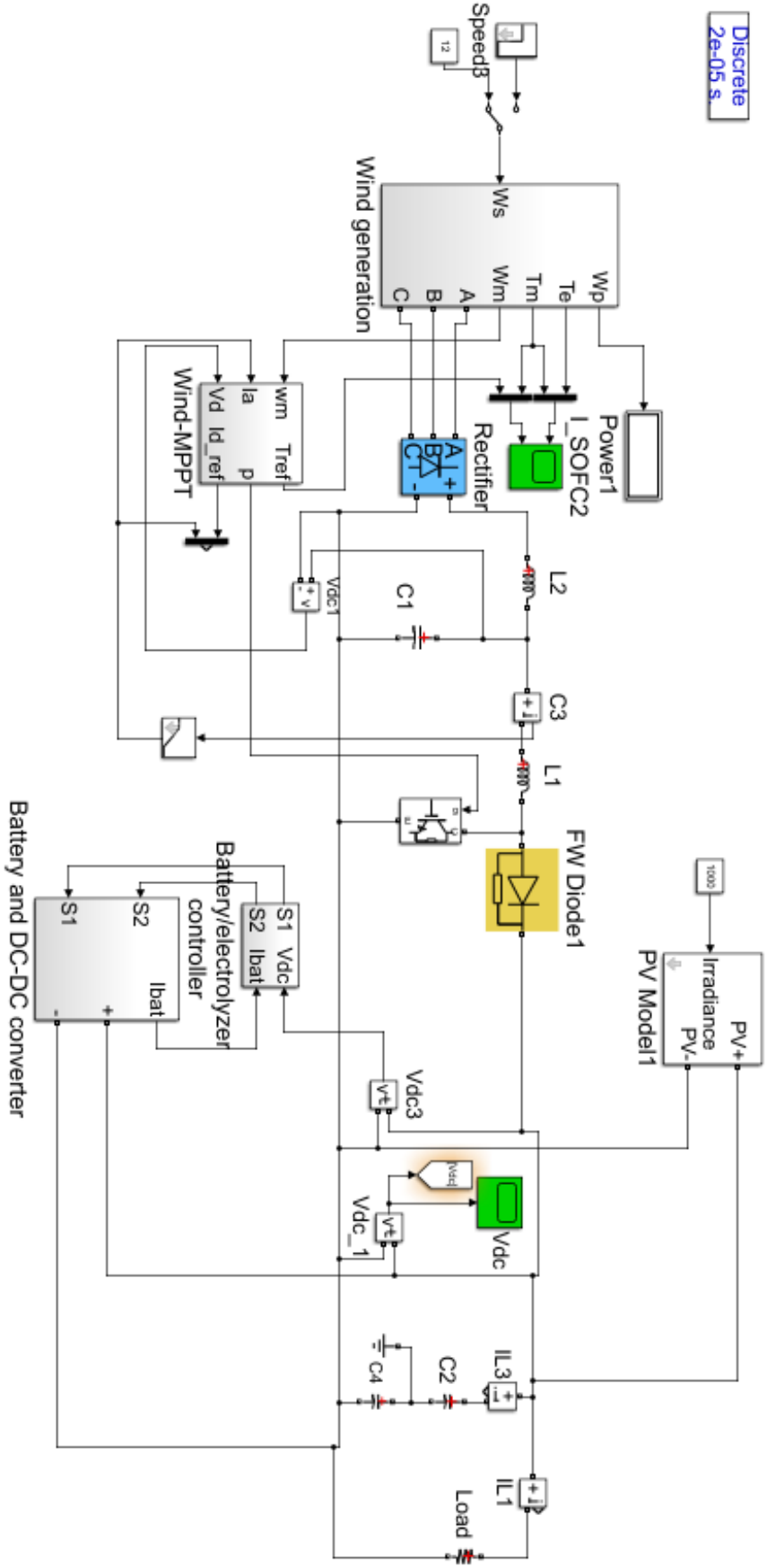

Figure 4.3: Simulation Diagram of DC microgrid in MATLAB/Simulink

Figure 4.4 presents the PV model1 main block parameters. It consist of 22 modulus connected in series at 30.3 V maximum, 30.3 V x 22 gives 666.6 V maximum voltage. Short-circuit current, open-circuit and current at Pmax values are all shown in the block parameters. The short-circuit current is 8.01 A. The PV system is a primary source that supplies the DC microgrid. Solar energy is transformed into electricity using a solar panel. PV arrays are connected through a boost converter to simulate DC sources in the designed system. The output voltage of a PV system is not ideal because it is dependent on temperature, irradiation, and load characteristics.

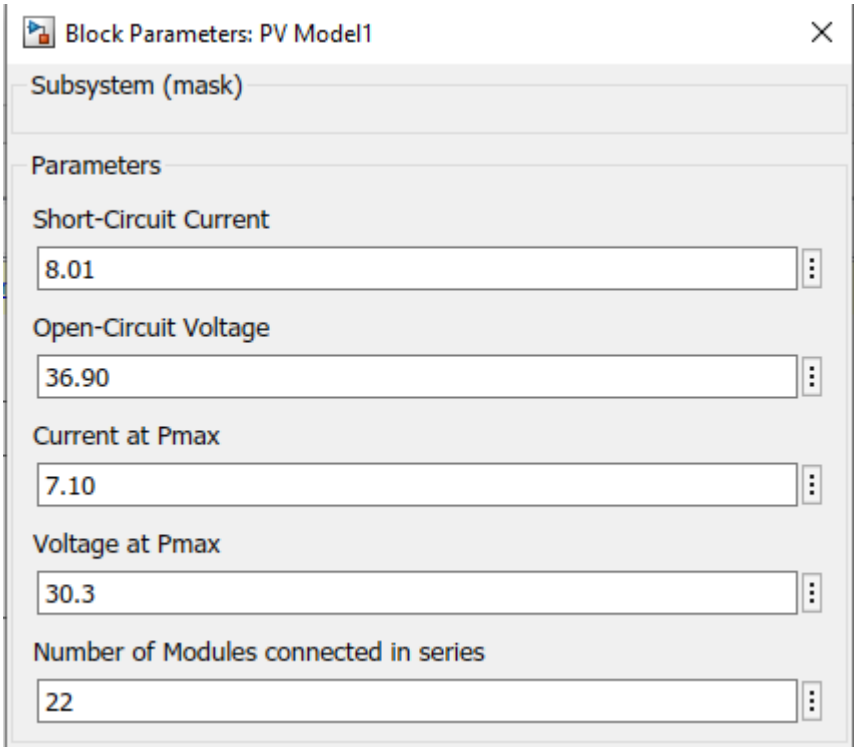

Figure 4.4: PV Model1 main block parameters

From Figure 4.5 below which shows DC grid voltage (Vdc_1), it is observed that PV voltage is above 665 V, almost at maximum voltage of 666.5 V. At first within 0.2 seconds, the voltage reaches the maximum and after 0,3 seconds it is now at 661 V below the maximum expected voltage. Hence the DC is operating delivering load to the consumers and continues running at

a constant voltage. The results revealed that output from the module is constant with increasing voltage until a certain voltage is reached and the demand is met since the output voltage is at maximum. The PV cell's performance is sensitive to minor changes in series resistance but unaffected by changes in shunt resistance. Results display that DC grid voltage is at the maximum desired voltage at full load.

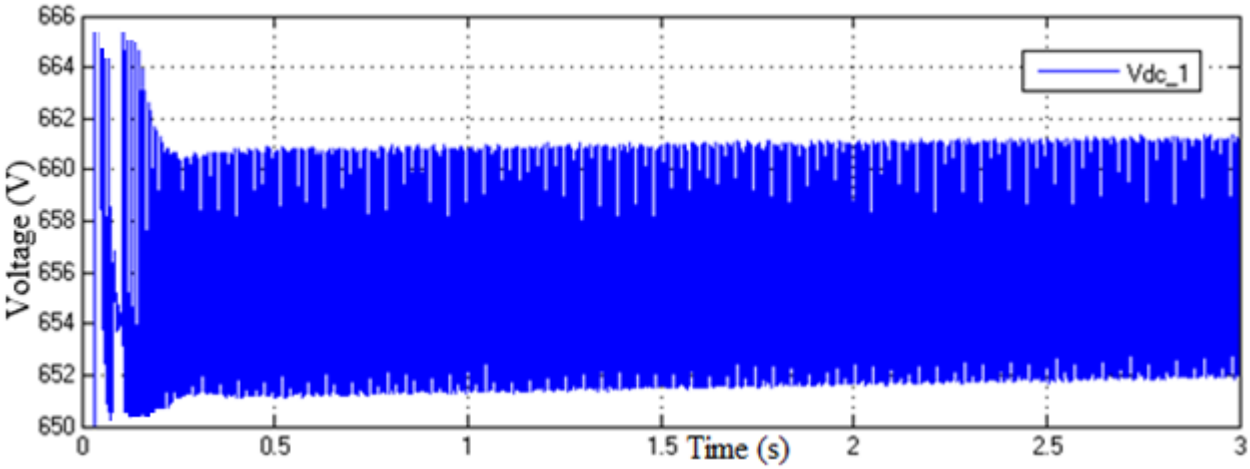

Figure 4.5: DC Grid voltage at full load

The maximum voltage is discussed in the main block parameters to be 666.6 V in Figure 4.4 presented. The charge controller is successfully controlled by the DC to DC converter, allowing power from/to the battery to achieve voltage stabilization. Without the battery storage, the system struggles to deliver the maximum required voltage. The simulations show that continuous performance of a PV DC without battery storage fails to reach desired voltage and is shown in Figure 4.6 where the DC grid is connected without battery storage below 666.6 V. It shows the decrease and instability in the output harvested voltage. At t=0.25 seconds, it spikes up to above expected output voltage. The spike reaches 690 V overvoltage, but after a few seconds it drops down to normal voltage.

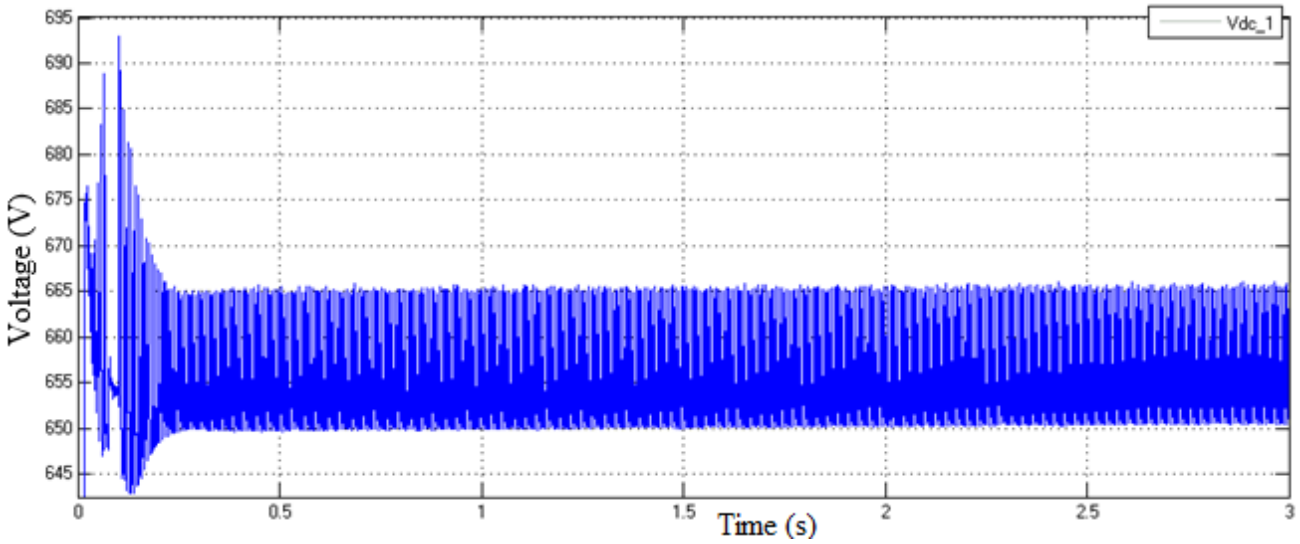

Figure 4.6: DC Grid voltage without battery storage connected

Figure 4.7 below presents the battery storage main block parameters. It presents a nickel-metal-hydride with 300 V nominal voltage and rated capacity of 6.5 Ah. DC/DC converter (average model) connected to the battery storage. Battery storage plays a crucial role in storing energy in a DC microgrid. A battery with the bi-directional DC/DC converter is connected to DC as energy storage. The energy storage system is a critical element on a microgrid that is centred on distributed energy resources to improve efficiency and maintain voltage stability.

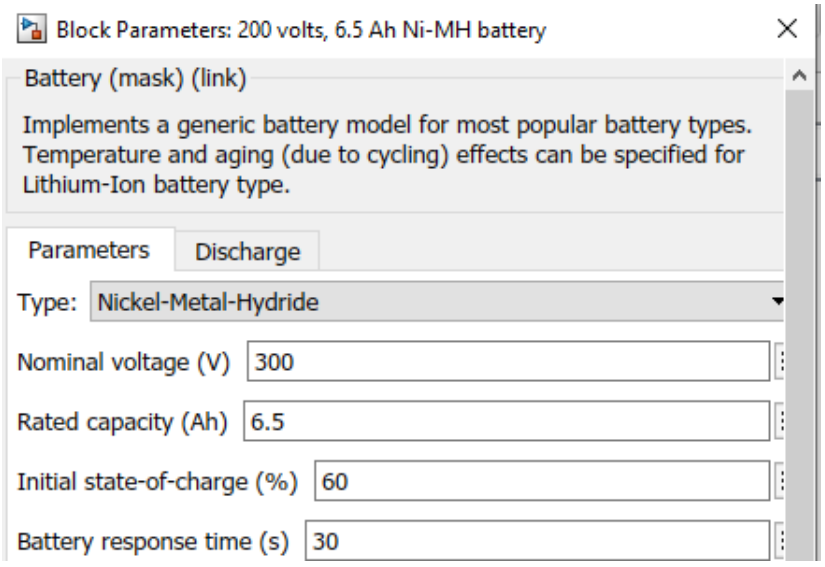

Figure 4.7: Battery storage main block parameters

Figure 4.8 shows DC voltage during normal operation. It is because of storage nominal voltage charging At t = 0.1 seconds that the is variation on the voltage is almost exceeding average, spiking to almost 700 V, but at t = 0.25 seconds it is at the normal maximum voltage. Energy storage is a critical component in the microgrid for power stability.The application of battery storage plays an essential role in achieving steadiness in the system. To advance the effectiveness of the power system, distributed generation is connected to DC lines through converters. The power flow of the system is satisfactory as it delivers the maximum voltage of 666.6 V, which is the expected voltage to the load. The results revealed great voltage stability in the system due to the battery arrangement.

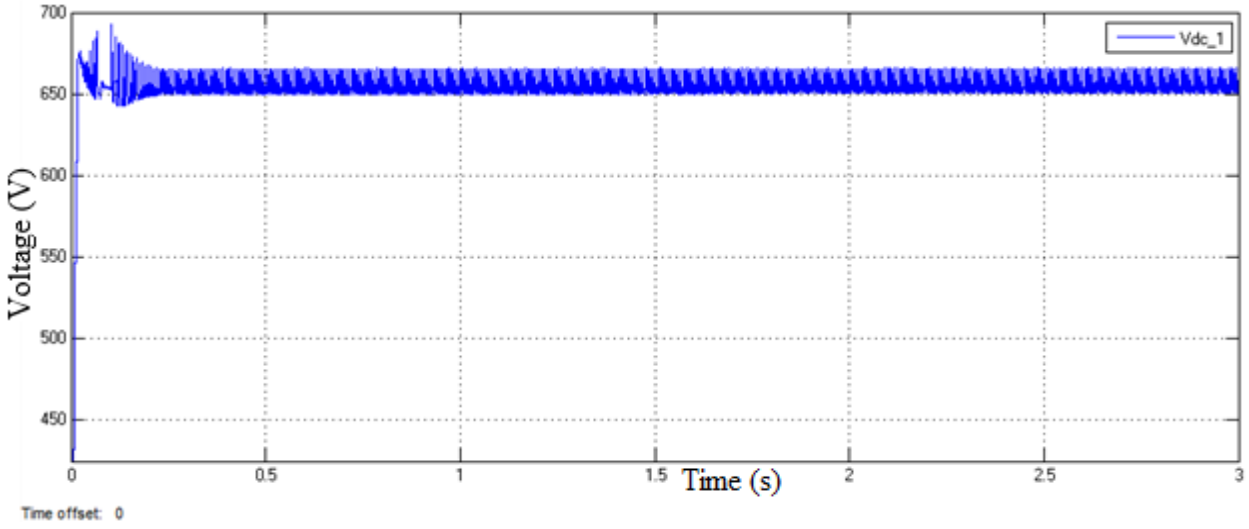

Figure 4.8: DC voltage during normal operation

Figure 4.9 presents wind turbine model block parameters, presenting all the values for nominal mechanical output power (W) at 0.8 Pu, base power of the electrical generators (VA) and base wind speed (m/s) of a wind turbine at 12 m/s. Wind energy is also used to supply the DC microgrid. The wind generation (alternating current) is converted by means of a rectifier to produce direct current, hence the aim of the study is to produce DC output. The wind speed is directly proportional to the power generated, while there is increases in wind speed and the power generation also increases. The power produced from the wind is fluctuating constantly. In order to obtain non-fluctuating power, one has to store in a battery and then provide it to the

load. The Tm and Te displayed in the simulations are the characteristics of wind turbine simulations results of wind turbines using PMSG.

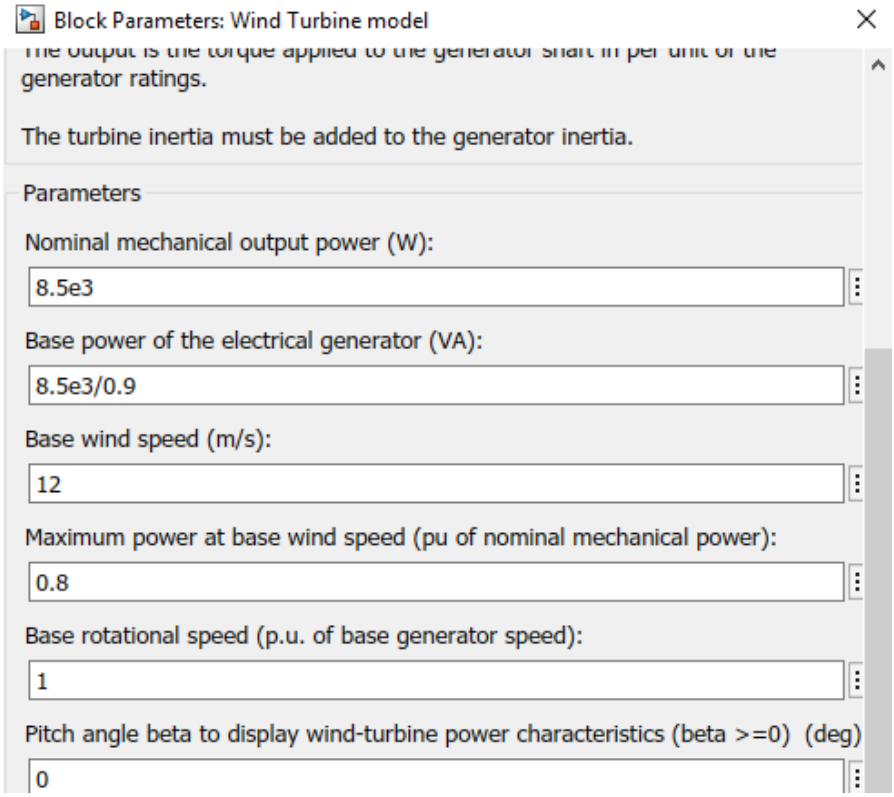

Figure 4.9: Wind Turbine model main block parameters

Figure 4.10 presents wind generation/Tm and wind-MPPT/1 without a battery. Due to the effectiveness of wind generation in the system designed, the system is able to pick up, but in the same pattern. The wind generation/Tm is at 43.5 kW above 43 kW and wind-MPPT/1 is at 42.5 kW below 43 kW. The wind generation/Tm is inversely proportional to wind-MPPT/1. When the wind generation/Tm drops, decreasing the wind-MPPT/1 rises, increasing to balance the output generated so that the system is sustained. When the fault occurs, the wind-MPPT/1 fluctuates radically and result not at equilibrium with wind generation/Tm due to the fault that occurred. The results are obtained at 12 m/s base wind speed. The wind generation delivers the maximum peak power. The maximum power point tracker plays a vital role to harvest the desired power from the wind generation side. If the wind speed is too high, pitch control can be used to minimize the blade speed by changing the angle of the blades.

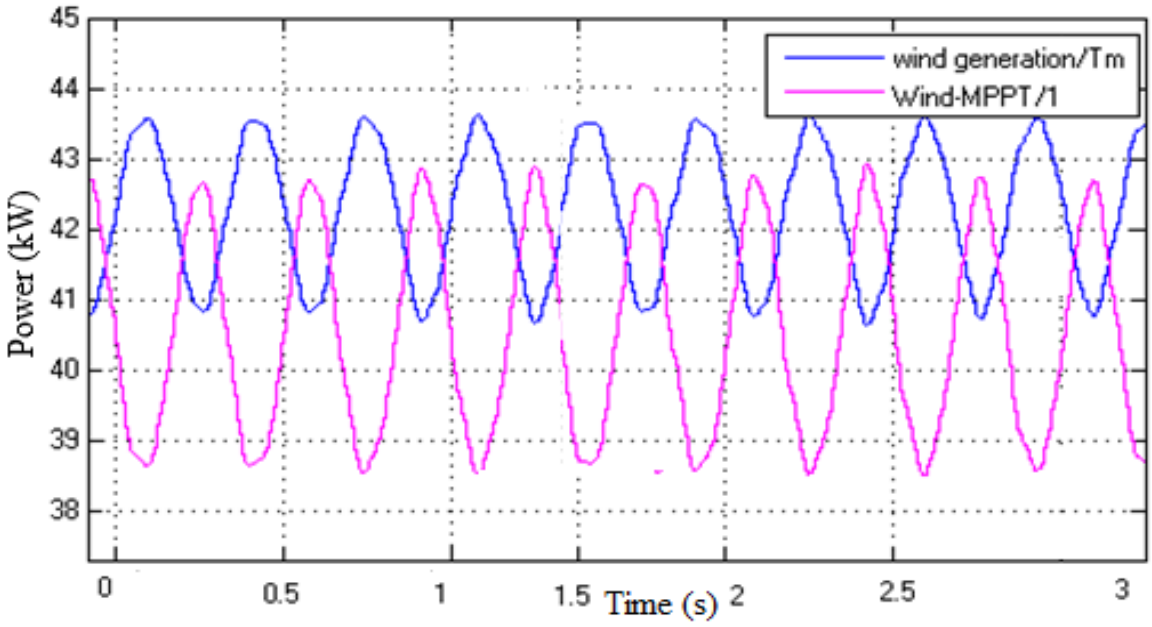

Figure 4.10: Wind generation/Tm with Wind MPPT/1 without a battery storage

Figure 4.11 illustrates the rectifier block parameters. The Rectifier plays a vital role in converting alternating current to direct current. The blades rotate at a variable speed to extract maximum power from the wind resource, therefore the power is converted from AC to DC at the specific frequency. The rectifier output is fluctuating DC voltage that has the same frequency as the AC input. Rectifier parameters are quite imperative since they are measure of the rectification process's efficiency. The forward voltage in the rectifier main is 0.8 V and it uses diode snubber resistance and capacitance as represented. The block main parameter of a rectifier display at snubber resistance is set at 100 ohms. The Snubber capacitance initial value is also displayed.

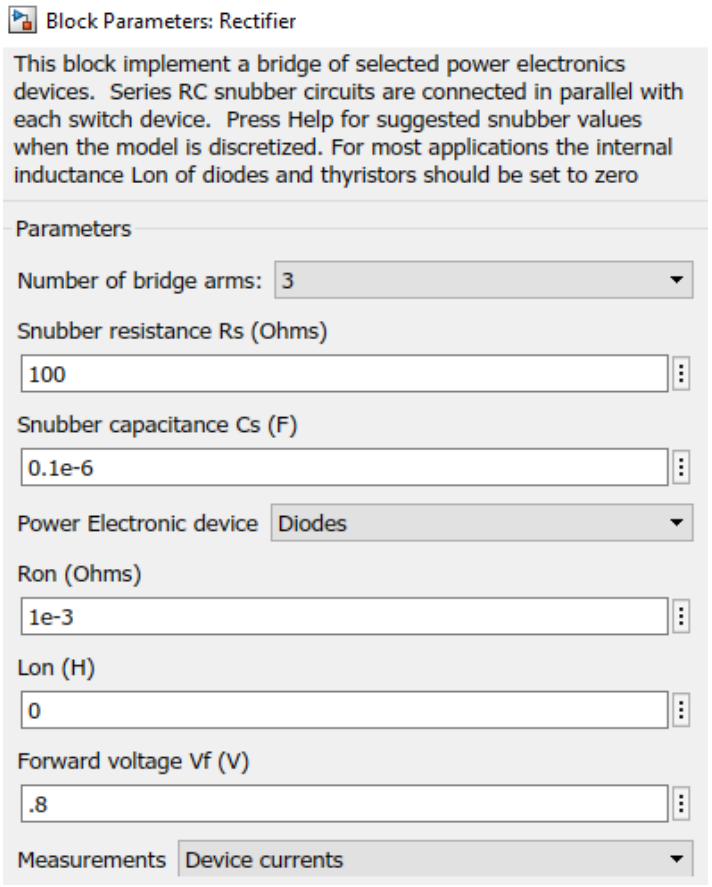

Figure 4.11: Rectifier block parameters.

The wind generation (alternating current) is converted by means of rectifier to a produce direct current, hence the aim of the study is to produce DC output. From Figure 4.12 wind generation with wind-MPPT/3 and Discrete 1st –Order Filter1 is presented. Maximum power point tracker (MPPT) is connected to the wind system to harvest maximum power. The wind MPPT/3 determines whether voltage needs to be increased or decreased in order to increase the output power, the outputs a change in the duty cycle which is converted to a pulse width modulation signal and fed to the boost converter so that the voltage can be increased or decreased. The pulsating unidirectional outputs of the different rectifier circuits is presented. They are suitable for charging storage cells. The discrete 1st order Filter1 is above 12 kW showing a vastly increased and smoothed levelling out the pulses and produce steady results leading to direct output. Wind-MPPT/3 is all most at 13.5 kW fluctuating. The peak Pm and ripple voltage is shown, ripple increase with load current.

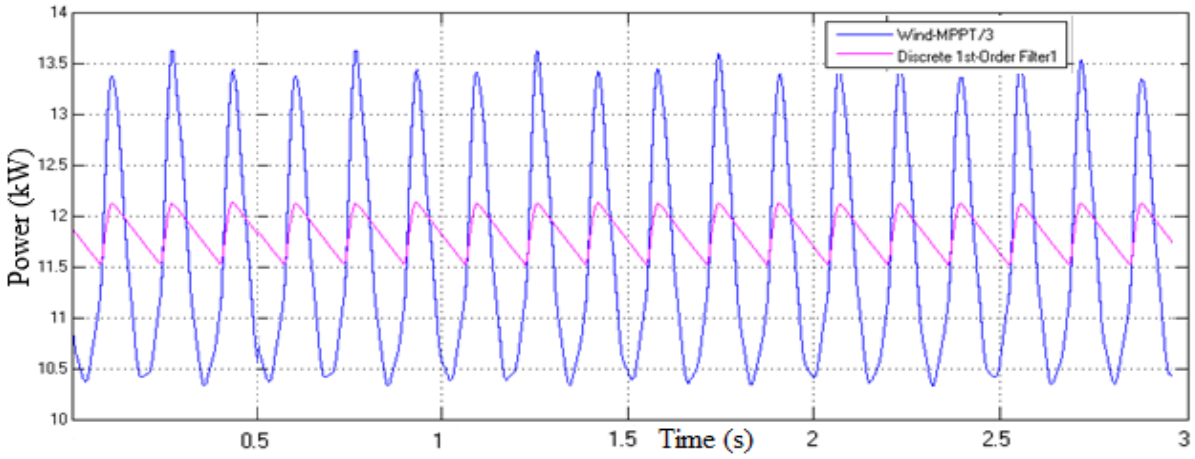

Figure 4.12: Wind generation with Wind-MPPT/3 and Discrete 1st –Order Filter1

Figure 4.13 presents the wind generation/Te with wind generation/Tm output during normal conditions and wind generation/Te with wind generation/Tm output during normal condition. These simulations show that before t = 0.2 seconds, there is no power stability as it spikes to 160 kW and at t = 0.25 seconds, there is power stability in wind generation as it is below 80 kW. Each boost is controlled by individual the Maximum Power Pointer Tracker (MPPT) in a variable speed operation system to achieve high efficiency in a wind power conversion system. Controllers are used based on the range in which rotor angular velocity control is needed, which varies depending on the turbine.

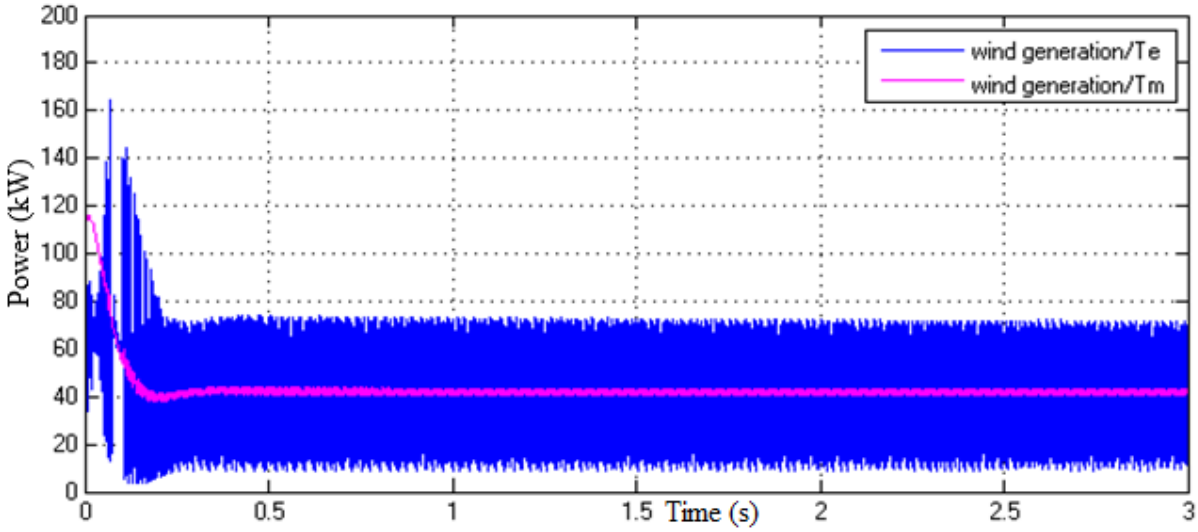

Figure 4.13: Wind generation/Te and wind generation/Tm output during normal conditions

The wind generation/Tm and wind-MPPT/1 output during normal condition at equilibrium are shown in Figure 4.14. Simulations are shown when wind-MPPT/1 is connected, before they

reach equilibrium at t = 0.25 seconds, the wind-MPPT/1 increases from 0 V and gets above 50 kW, while wind generation/Tm decreases from 120 kW until they both are at equilibrium reach 40 kW. For MPPT, the speed control rotor is performed within the wind turbine's operating range. Each boost is controlled by individual MPPT in a variable speed operation system to achieve high efficiency in a wind power conversion system.

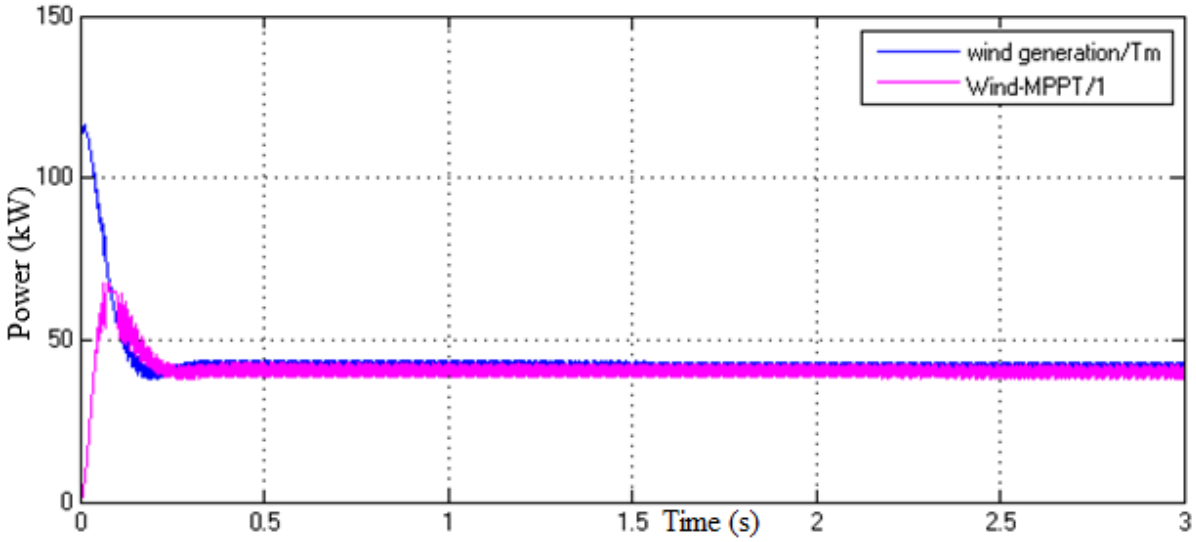

Figure 4.14: Wind generation/Tm and wind MPPT/1 output during normal condition

The wind generation/Te and wind generation/Tm without a storage component under normal state is shown in Figure 4.15. Wind turbines produce power at a wind speed of around base wind of 12 m/s. There is a speed variation in the wind generation. The maximum power at base wind speed is 0.8 pu of nominal mechanical power. During fault conditions, there is no stability in the output power. The output voltage of wind generation/Tm is reduced to less than 50 kW and wind generation/Te is above 70 kW, approximately 80 kW. The ripple factor measures the smoothness of the DC output of a rectifier. The ripple frequency is twice the supply frequency. The MPPT make use of “Perturb and Observe” technique to vary the voltage and harvest maximum possible power.

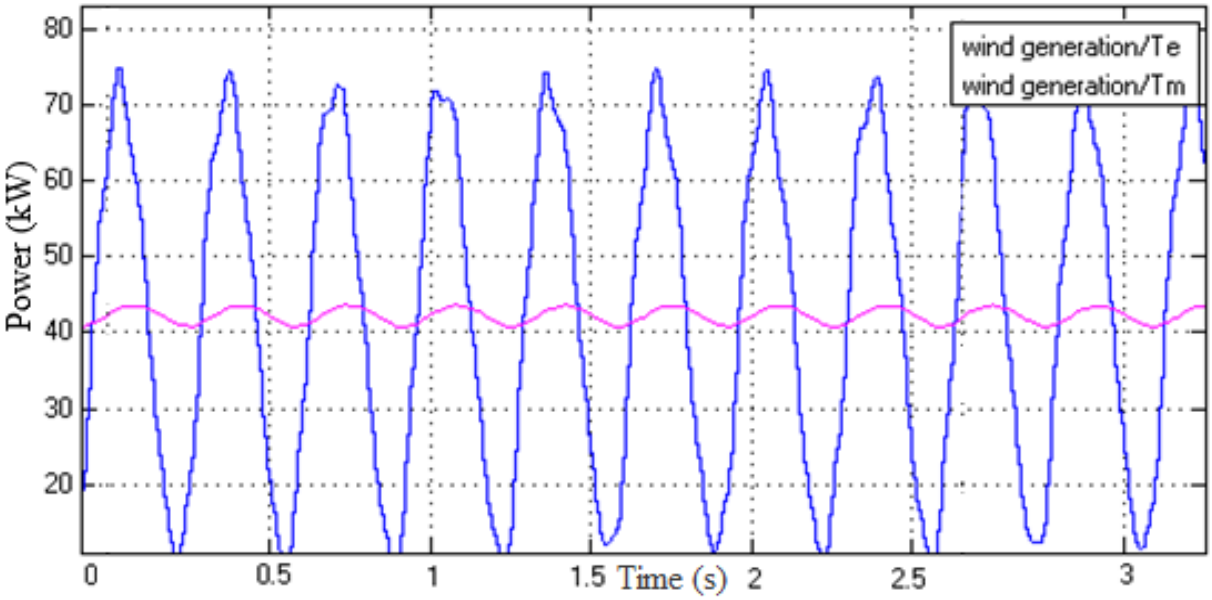

Figure 4.15: Wind generation/Te and wind generation/Tm without a battery storage

4.4 Fault Analysis of a Hybrid DC Microgrid

The arrangement of a hybrid DC microgrid system and distributed generation control methods are discussed. Also investigated are faults on source side, load side and DC transmission lines. Faults in DC transmission systems can occurs for number of reasons, they affect system stability by causing disruptions in parameters such as DC voltages, DC currents and voltages and currents of the coupled AC system. The following two DC faults are analysed:

a. DC line-to-ground fault.
b. DC line-to-line fault.

4.4.1 Simulation Results of a DC Fault Analysis in a DC PV solar system and DC wind energy system

Case 1- Faults on the generation side of the DC microgrid-DC line-to-ground Fault (L-G).

Figure 4.16 shows simulation results of wind generation/Tm and wind-MPPT/1 during DC line-to-ground on the generation side. The wind energy generation shifts significantly when compared to Figure 4.13 under normal conditions because of the line-to-ground fault that occurred. The wind MPPT/1 and wind generation on the waveform has shown great shift during the DC line-to-ground fault. It is not under equilibrium and delivers unstable output. At t = 0.1

seconds, it spikes up the wind MPPT/1 reaching 53 kW. As it continues at t = 0.25 seconds, the fault arises to reach 42 kW and the output delivered changes. Then both outputs are getting blurred and shift from its equilibrium point. Insulation failure between one DC conductor and ground of the system lead to DC line-to-ground faults. Pitch regulation, in which the angle of the blades is changed to minimize the speed of the blades, may be used if wind speeds are too high.

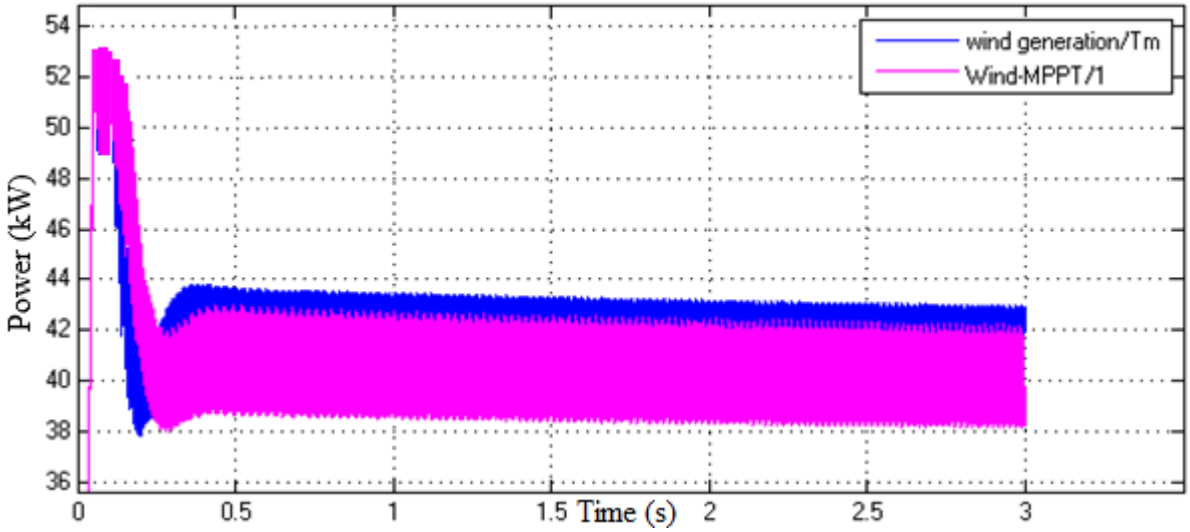

Figure 4.16: Wind generation/Tm and Wind-MPPT/1 during DC line-to-ground fault

Figure 4.17 shows simulation results of wind generation/Tm and wind-MPPT/1 during DC L-G fault at equilibrium. When the L-G fault occurs in the generation side, wind generation/Tm opposes wind-MPPT because of the poor module performance. When adjusting the temperature and irradiation settings, it is preferable to run the module at its highest power point so that the full power can be supplied to the load. The wind generation/Tm under this line-to-ground fault and the ripple effect are significantly seen throughout, as compared to Figure 4.10 under normal conditions. The output is constricted due to the fault that occurred in the system. Initially, the wind generation/Tm is at 43 kW, leading the wind-MPPT/1 at 41.5 kW. At 0.5 seconds, it is now vice versa. The wind generation/Tm starts leading increasing head above 43 kW, getting closer to 44 kW at t=1.5 seconds.

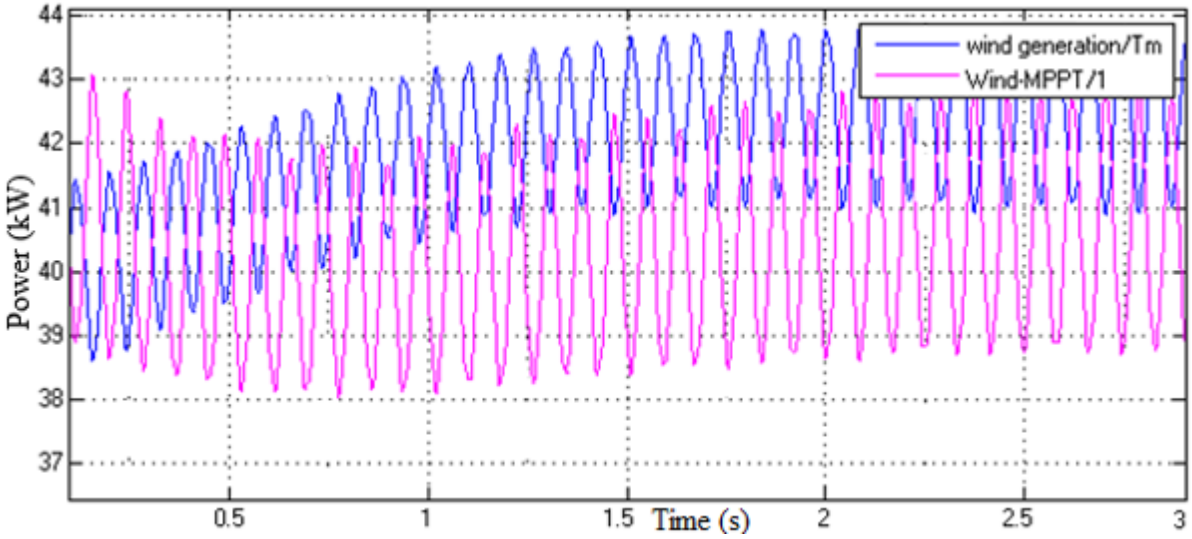

Figure 4.17: Wind generation/Tm and wind-MPPT/1 during DC line-to-ground fault at equilibrium.

Filtering is the significant measure after rectification to filter the unwanted remaining pulsating ripple voltage. Figure 4.18 presents DC current (C3) during the DC L-G fault. The three phase generation side acts as a primary source feeding the microgrid. C3 plays a vital role in the DC microgrid. It is seen that there is no stability and constant output. The diode starts to conduct when the output voltage reaches zero, and the load current flows through it. Another advantage of the diode is that it reduces voltage ripple and reactive power. Shunt capacitor C3 is considered as the most ingenious and effective apparatus in the system. The results obtained at C3 shows the output at the maximum of 100 V from 0 V after rectification took place and the cycle is recurrent.

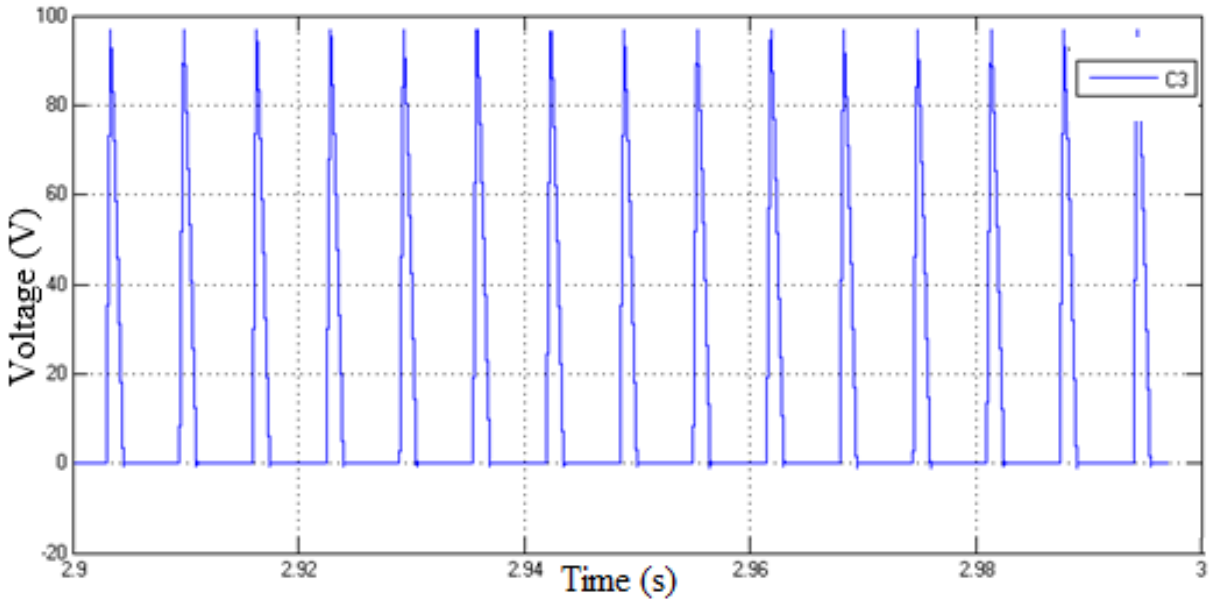

Figure 4.18: DC voltage (C3) during DC line-to-ground fault

Case 2- Faults on the generation side of the DC microgrid- DC line-to-line Fault (L-L)

Figure 4.19 presents the wind generation/Te and wind generation/Tm during DC line-to-line fault. As seen, wind generation/Te displays enormous fluctuation and as a result, it is no longer at equilibrium with wind generation/Tm due to the line-to-line fault that occurs in the system. The fluctuation of wind generation/Te is above 60 kW, while the wind generation/Te is fluctuating at 40 kW, showing unevenness impending at the rectification point. The output from the rectifier contains an undesirable ripple and different unwanted effects appear in the system. A DC line-to-line fault occurs when there is insulation failure amongst two DC conductors. Wind-MPPT plays a crucial role in the generation three-phase side. As the results show, wind-MPPT/1 is at equilibrium state during normal equation.

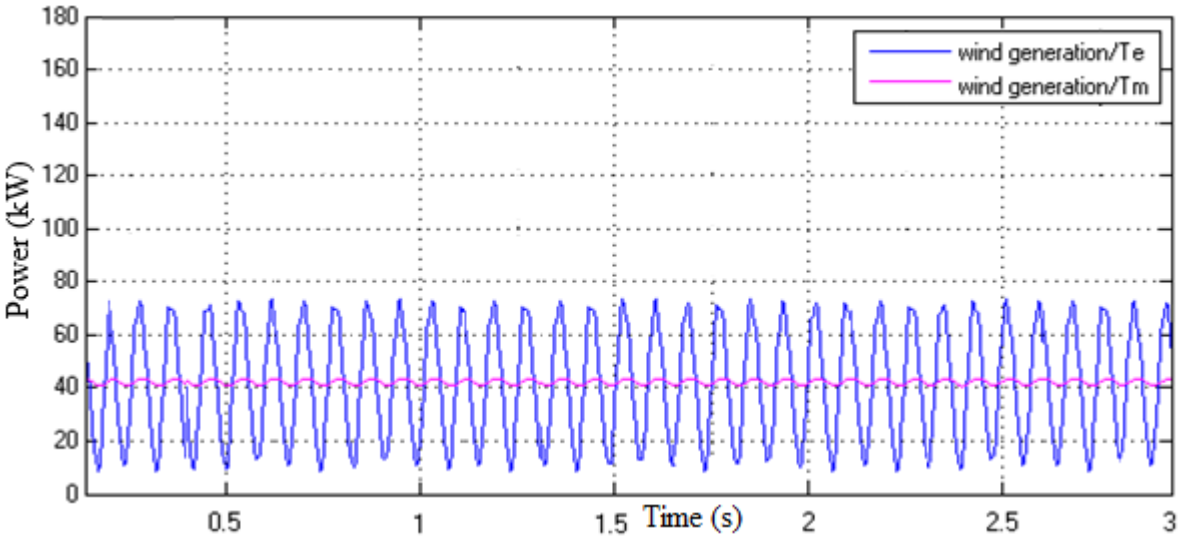

Figure 4.19: Wind generation/Te and wind generation/Tm during DC line-to-line fault

Figure 4.20 represents wind-MPPT/3 and discrete 1st order filter1 during the DC line-to-line fault. The discrete 1st order filter1 shows a very low ripple and high stability. Load regulation and line regulation output change as the one draws different amounts of current and as a result, the AC amplitude changes. The filter converts the pulsating DC into pure DC and a capacitive filter is deployed. The filter is used to limit the ripple voltage. The wind-MPPT/3 shows the MPPT harvesting the maximum possible power and supply the system. At Wind-MPPT/3, the output is constant but one spike after a while and the discrete 1st-order filter1 increases slowly from 12 kW at t=2.9 seconds, increasing up to 20 kW.

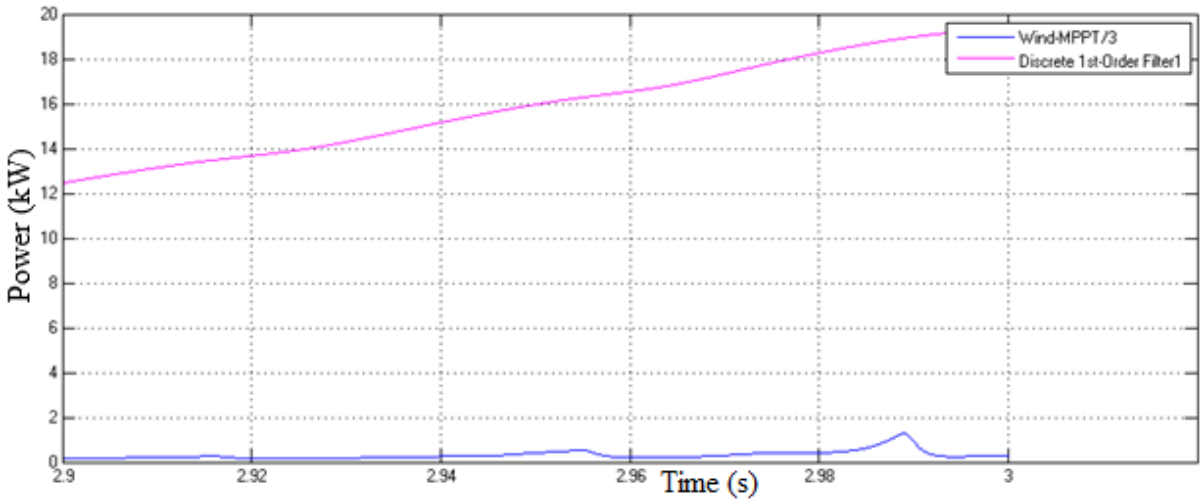

Figure 4.20: Wind-MPPT/3 and discrete 1st order filter1 during DC line-to-line fault

Figure 4.21 presents wind generation/Te and wind generation/Tm with no battery at the line-to-line fault. At t = 0 seconds, the output is below 200 kW. From there, it gradually increases to a peak value of 700 kW below 800 kW. At t= 0.5 seconds, the wind generation changes and decreases to below 200 kW on a negative cycle, hence there is no energy storage system at the time. The generation continues as the wind picks up, but there is no stability and steadiness on the output due to the fault disturbing the system, struggling to reap the maximum power as it is supposed to attain the highest possible output.

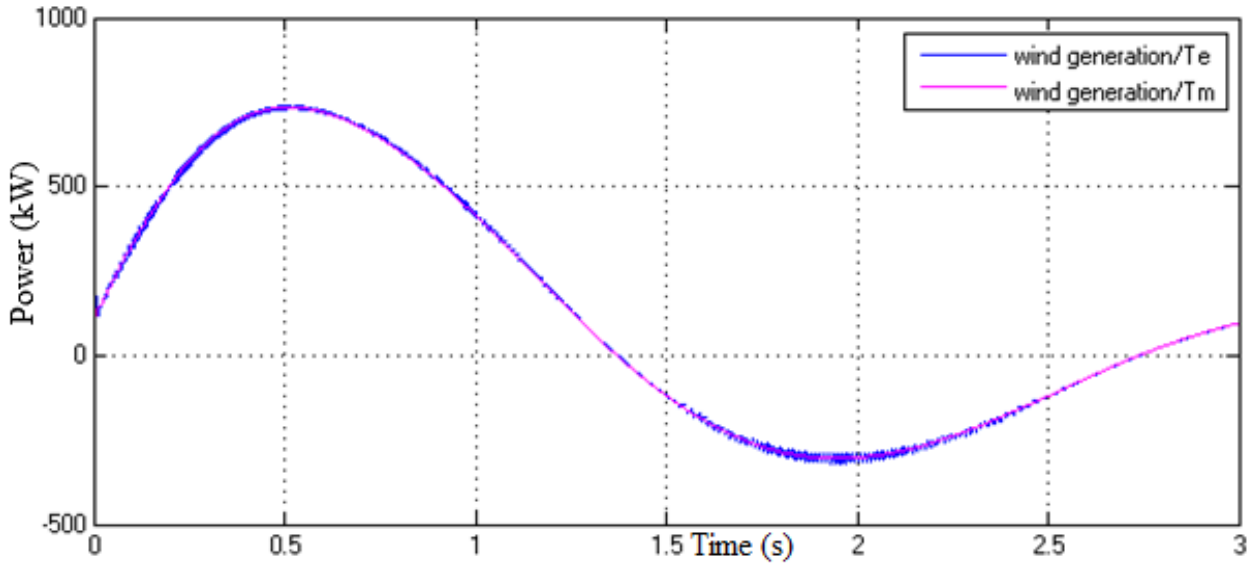

Figure 4.21: Wind generation/Te and wind generation/Tm with no battery at line-to-line fault

Case 3-Faults on the load side of the DC microgrid- DC line-to-ground Fault (L-G)

Figure 4.22 shows a DC voltage (Vdc_1) output during a DC line-to-ground fault. Voltage in per unit is fluctuating and blown, the ripples occurs severely on the DC voltage and consumer side because of fault. Initially, the voltage reaches the maximum output voltage of 20 V, but due to this DC line-to-ground fault, it ranges below 0 V. The rated value of this condition can never get back to stable because of the line-to-ground fault. When DC line to ground faults occur on the load side of the DC microgrid, the consumer's side will be rigorously affected.

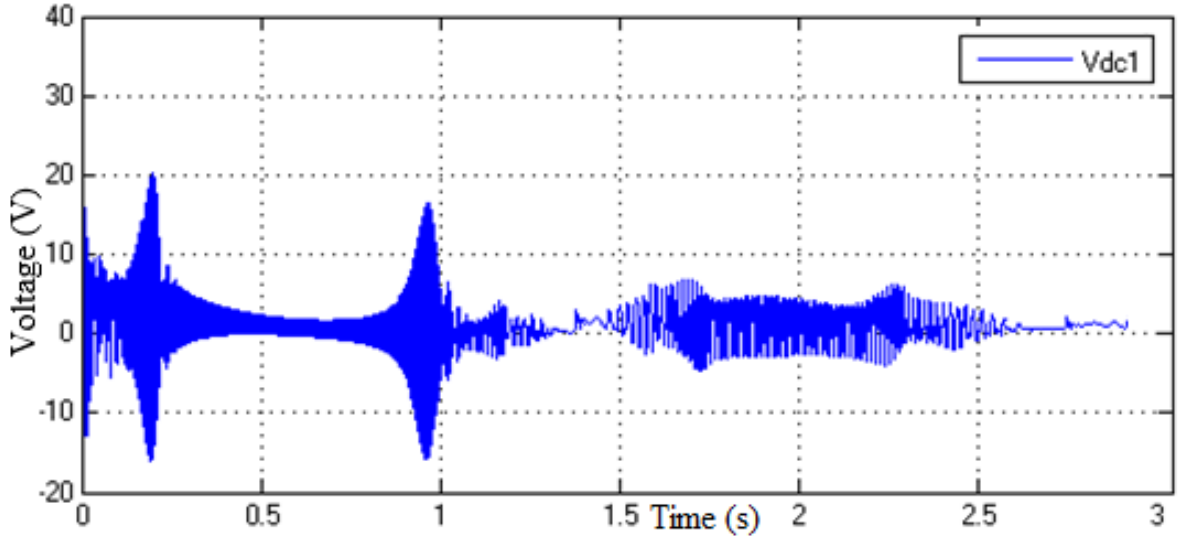

Figure 4.22: DC voltage (Vdc_1) during the DC line-to-ground fault on load side

As also presented in Figure 4.23, the DC voltage (Vdc3) is at full load during a DC line-to-ground fault. The output voltage under this fault does not deliver expected output voltage, but only delivers almost 665 V. The voltage fluctuation is diminished and output waveform is standardized less than 666.6 V. The output voltage at this level is between 664 V to 665 V. The irradiation and ambient temperature of PV arrays is operating abnormally under the line-to-ground fault condition. Maximum power is transferred when the load resistance is equal to the resistance of the PV array.

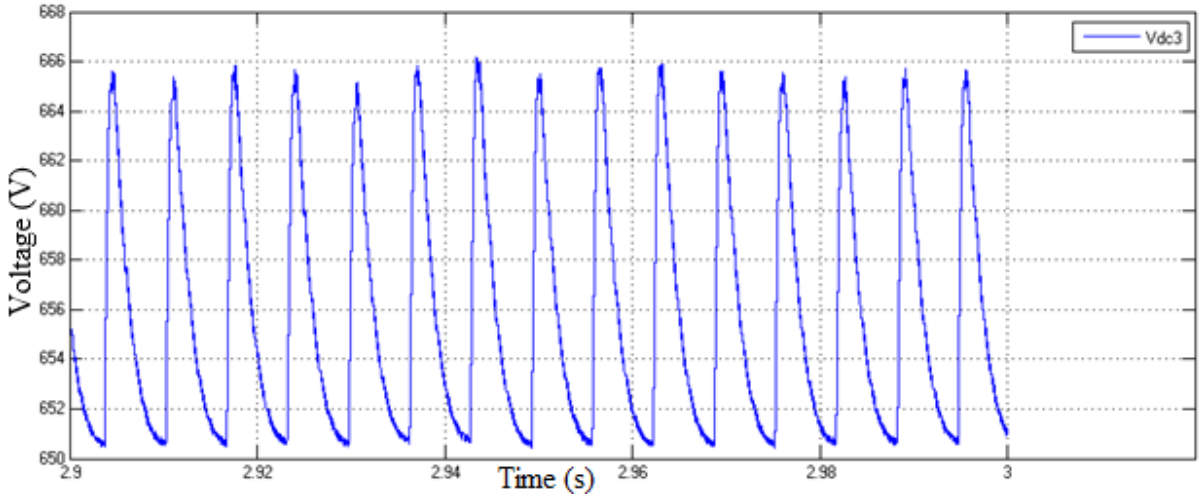

Figure 4.23: DC voltage (Vdc3) at full load during the DC line-to-ground fault

Figure 4.24 presents DC current (IL1) on the load side during an L-G fault. This is displayed on the Ideal current measurement (IL1) connected on the load side of the DC microgrid. The maximum current in the main parameters is 7.10 A. When this fault occurs, the current on the load side of the system falls down. It rises before it falls down. The consumer's side gets affected severely when attacked by a DC L-G fault. DC current (IL1) on the load side during L-G fault is shown in Figure 4.24. When this fault occurs, the current on the load side of the system fluctuates unceasingly. The consumer's side gets disturbed when a DC line-to-ground fault occurs. It falls down before it rises to peak value. This is displayed on the ideal current measurement (IL1) connected on the load side of the DC microgrid. The main parameters set short circuit current in the PV module1 at 0.801 A. The output current obtained under this condition is at 0.25 A. The current is shifting down, decreasing to 0.238 A as there is a line-to-ground fault.

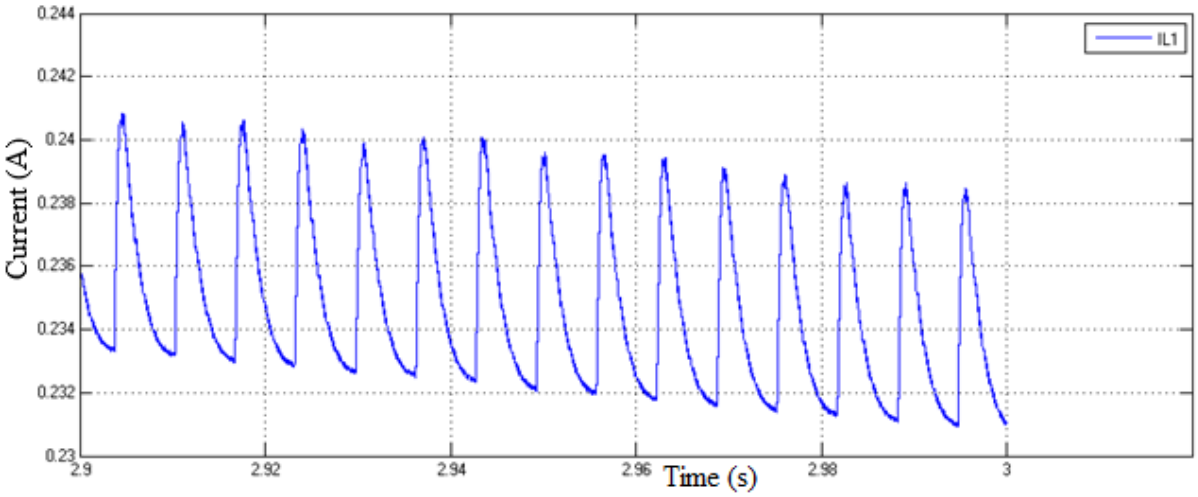

Figure 4.24: DC current (IL1) on the load side during a line-to-ground fault

Case 4-Faults on the load side of the DC microgrid- DC line-to-line Fault (L-L)

Figure 4.25 shows DC current (IL3) during a DC line-to-line fault. It is shown on the ideal current measurement (IL3) connected on the load side of the DC microgrid. The maximum current in the main parameters is 7.10 A per solar panel. When a DC line-to-line fault occurs,

the current on the load side of the system falls down. IL3 spikes and struggles to reach 100 A maximum and it decreases to below 40 A, showing no steadiness. The occurrence of DC line-to-line faults on the load side of the DC microgrid will bring deviation to the consumer's side and the whole system will be conscientiously disturbed.

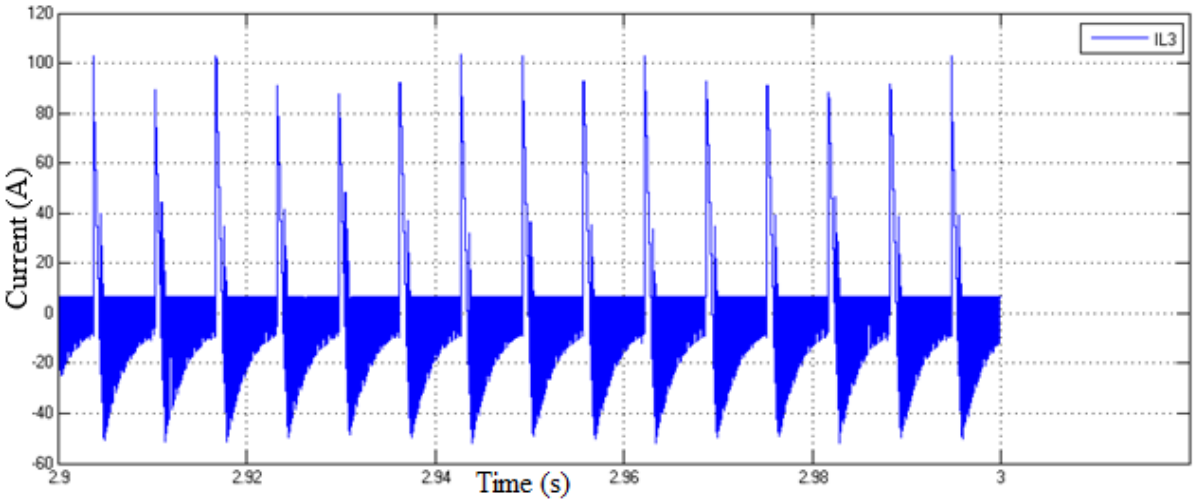

Figure 4.25: DC current (IL3) during DC line-to-line fault

DC current (C3) during a DC L-L fault is shown in Figure 4.26. When this fault occurs, the current on the load side of the system fluctuates continuously. The consumer's side gets disturbed when a DC L-L fault occurs. It falls down below 20 A before it rises to a 30 A value. It accumulates at the same pattern, climbing up and improving with the performance. This is displayed on the C3 linked on the load side of the DC microgrid. This fault has adverse impacts and requires the coordination of the system to be excellent so that it will not damage the system easily.

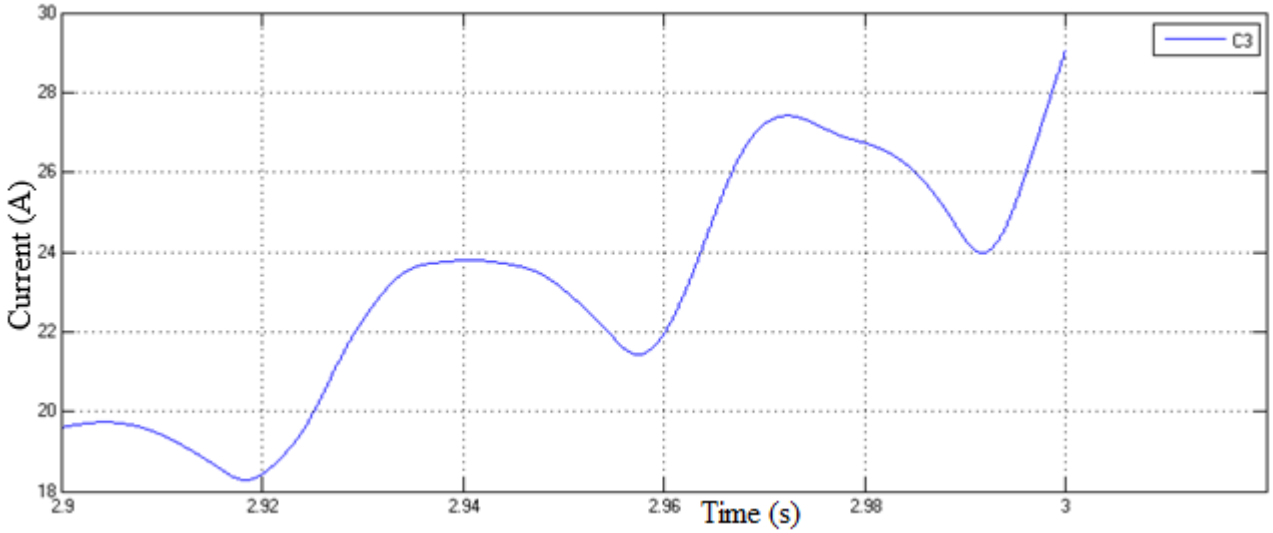

Figure 4.26: DC current (C3) during a DC line-to-line fault

4.5 Summary of Results

4.5.1 Model and System Description

All the results obtained are summarised and listed in the tables. The modelling and simulations parameters and all the important components are defined. The system description summary is shown in Table 4.1 presenting the input values in the main system, including PV Model1, battery model, wind turbine and rectifiers.

Table 4.1: Main parameters of the system.

PV Model1	Number of modules connected in series	22
	Short-Circuit Current	8.01 A
	Open-Circuit Voltage	36.90 V
	Current at Pmax	7.10 A
	Voltage at Pmax	30.3 V
Battery (Nickel-Metal-Hydride)	Nominal Voltage	300 V
	Rated Capacity	6.5 Ah
Wind Turbine Model	Nominal Mechanical Output Power	8.5e3 W
	Base power of the electrical generator	8.5e3/0.9 VA
	Base wind speed	12 m/s
	Maximum power at base wind speed	0.8 pu
Rectifier	Number of bridge arms	3
	Snubber Resistance Rs	100 ohms
	Snubber capacitance Cs	0.1e-6 F

4.5.2 Power Flow Analysis Results Summary

The summary of a hybrid DC microgrid under power flow is presented, Table 4.2 shows outputs results for a PV model voltages and Table 4.3 shows for a wind generation.

Table 4.2: Power flow results for PV model voltages

PV Model Voltages	
Condition	**Outputs**
DC Grid voltage at full load	Vdc_1 = 666.5 V
DC Grid voltage without battery storage connected	Vdc_1 = 665 V
DC voltage during normal operation	Vdc_1 = 700 V

Table 4.3: Power flow results for a wind generation

Wind Generation	
Conditions	**Outputs**
Wind generation/Tm with Wind MPPT/1 without a battery storage	Tm = 43.5 kW MPPT/1 = 42.5 kW
Wind Generation with Wind-MPPT/3 and Discrete 1st –Order Filter1	MPPT/3 = 13.5 kW 1st Order = 12 kW
Wind generation/Te and wind generation/Tm output during normal conditions	Te = 160kW Tm = 120 kW
Wind generation/Tm and wind MPPT/1 output during normal condition	Tm = 120 kW MPPT/1 = 70 kW Equilibrium = 40 kW
Wind generation/Te and wind generation/Tm without a battery storage	Te = 75 kW Tm = 44 kW

4.5.3 Fault Analysis Results Summary

The faults on the source side, load side and DC transmission lines it is where DC line-to-line faults and DC line-to-ground Faults are analysed. Table 4.4 – 4.7 shows the results summary of four (4) different scenarios for different cases under DC faults occurrence.

Table 4.4: Case 1- Faults on the generation side of the DC microgrid-DC line-to-ground Fault

Scenario 1	
Conditions	**Outputs**
Wind generation/Tm and Wind-MPPT/1 during DC line-to-ground fault	Tm = 53 kW MPPT/1 = 44 kW
Wind generation/Tm and wind-MPPT/1 during DC line-to-ground fault at equilibrium.	Tm = 44 kW MPPT/1 = 43 kW
DC voltage (C3) during DC line-to-ground fault	Vc3 = 100 V

Table 4.5: Case 2- Faults on the generation side of the DC microgrid- DC line-to-line Fault

Scenario 2	
Conditions	**Outputs**
Wind generation/Te and wind generation/Tm during DC line-to-line fault.	Te = 70 kW Tm = 44 kW
Wind-MPPT/3 and discrete 1st order filter1 during DC line-to-line fault	MPPT/3 = 1.5 kW 1st Order = 20 kW
Wind generation/Te and wind generation/Tm with no battery at line-to-line fault.	Te = 700 kW Tm = 700 kW

Table 4.6: Case 3-Faults on the load side of the DC microgrid- DC line-to-ground Fault (L-G)

Scenario 3	
Conditions	**Outputs**
DC voltage (Vdc_1) during the DC line-to-ground fault on load side	Vdc_1 = 20 V
DC voltage (Vdc3) at full load during the DC line-to-ground fault	Vdc_3 = 665 V
DC current (IL1) on the load side during a line-to-ground fault	IL1 = 0.24 A

Table 4.7: Case 4-Faults on the load side of the DC microgrid- DC line-to-line Fault (L-L)

Scenario 4	
Conditions	**Outputs**
DC current (IL3) during DC line-to-line fault	IL3 = 0.24 A
DC current (C3) during a DC line-to-line fault	IC3 = 29 A

CHAPTER FIVE
Conclusion and Recommendations

5.1 Conclusion

The performance of the hybrid DC microgrid system designed in MATLAB/SIMULINK is found to be satisfactory. The MPPT algorithm is used to coordinate the system and harness the full power from the sources. The surplus power from PV system and wind energy contribute to energy storage system, while the system is adequate to satisfy the load demand. The power from wind turbines is changed to direct current using rectifiers. In this research, the results of faults analysis are shown for the generation side, DC transmission and load side. The DC microgrid has revealed a high excellence distribution system. Because of the energy storage system and distributed generation system, when a faults occurrence on the generation side, there is no excessive effect on the consumer's load. When DC L-L and DC L-G faults take place in the load of the consumer's side, it is seen that it was not much influenced by the faults. In conclusion, the DC microgrid shows stable conditions in the demand side of the load since there is a minor effect. Since the power supply from PV and wind energy systems is sufficient to supply consumers, the system can deliver productive, excellent and dependable power system to consumers. To satisfy high efficiency in the system, power flow analysis is conducted and fault analysis is also performed under various conditions to understand the stability and reliability of the system. Faults are shown for the generation side, DC transmission and load side. The DC microgrid has revealed a high quality distribution system and simulations are carried out with MATLAB/SIMULINK software. In conclusion, DC microgrid shows stable conditions in the demand side of the load since there is a minor effect caused by the fault that occurs in the system.

The deployment of hybrid supplies in the system maximizes the efficiency from all of the sources and as a result improves stability in the DC microgrid. DC microgrid technology is persistently emerging and mainly implemented in renewable energy incorporation. Therefore, there is a wide-ranging focus area to overlook. DC line transmission experiences faults, imposing harmful effects on DC microgrid arrangement technique and leading to many damages to the mechanisms connected to the system. Applying high impedance grounding co-ordination realizes line-to–line faults in transmission lines and stabilise capacitors assist. The clearing current is low during this period so that the capacitor's voltage can withstand being deprived of any overcurrent stress.

Some significant conclusions that can be drawn from this work are:

- The overall effectiveness of the DC hybrid system is determined by the reduction of conversion losses and the expansion of the DC link.
- The PV system and wind energy combined with energy storage created a hybrid DC microgrid with high reliability, high efficiency, more efficient output power to consumers, and excellent load distribution performance.
- This hybrid system can be viable for small remote microgrids.
- Power electronic converters may be used in combination with solar modules and MPPT to increase the extracted energy from the solar resource by achieving impedance matching between the source and the load.
- A bi-directional converter can be used in between a microgrid and battery in order for power transfer to occur between the microgrid and battery. A PI controller can adequately control the operation of the bi-directional converter to attain a stable DC bus voltage with low steady-state error.

5.2 Recommendations

This research study has revealed the effectiveness of hybrid systems. The developed system is well suitable for isolated areas, act as a grid lock supply for domestic, industrial and agricultural systems. Future work may consider how to identify the exact location of the faults in the DC microgrid and how to protect the system from these faults when they occur. In addition, testing of the techniques on a real-life distribution system would provide a basis for confirming its effectiveness. The hybrid DC microgrid has proven that any power system functions well when it is supplied by two sources, the power stability and behaviour during faults occurrence is satisfactory. The PV system and wind energy system form a formidable hybrid DC microgrid that can be used in an isolated microgrids for rural communities and isolated industries. The increasing penetration of wind energy has been reviewed intermittently, in that way becoming more firm for renewable power plants. For that reason, it is needed for wind energy systems to advance the compensation of the generating plant to meet microgrid requirements.

References

[1] R. Banos, F. Manzano-Agugliaro, F. Montoya, C. Gil, A. Alcayde, and J. Gómez, "Optimization methods applied to renewable and sustainable energy: A review," *Renewable and sustainable energy reviews,* vol. 15, no. 4, pp. 1753-1766, 2011.

[2] A. Ali, W. Li, R. Hussain, X. He, B. Williams, and A. Memon, "Overview of current microgrid policies, incentives and barriers in the European Union, United States and China," *Sustainability,* vol. 9, no. 7, p. 1146, 2017.

[3] A. O. Akinrinde, A. Swanson, and R. Tiako, "Investigation of Temporary Overvoltage on Microgrid with Emphasis on Ferroresonance," in *International Journal of Engineering Research in Africa*, 2018, vol. 39: Trans Tech Publ, pp. 32-46.

[4] A. K. Khaimar and P. Shah, "Study of various types of faults in HVDC transmission system," in *2016 International Conference on Global Trends in Signal Processing, Information Computing and Communication (ICGTSPICC)*, 2016: IEEE, pp. 480-484.

[5] D. J. Feldman, A. Ebers, and R. M. Margolis, "Q3/Q4 2018 Solar Industry Update," National Renewable Energy Lab.(NREL), Golden, CO (United States), 2019.

[6] M. W. Siti, "Optimal energy control of a grid connected solar-wind based electric power plant," 2016.

[7] R. H. Lasseter and P. Paigi, "Microgrid: A conceptual solution," in *2004 IEEE 35th Annual Power Electronics Specialists Conference (IEEE Cat. No. 04CH37551)*, 2004, vol. 6: IEEE, pp. 4285-4290.

[8] B. M. Eid, N. Abd Rahim, J. Selvaraj, and A. H. El Khateb, "Control methods and objectives for electronically coupled distributed energy resources in microgrids: A review," *IEEE systems journal,* vol. 10, no. 2, pp. 446-458, 2014.

[9] E. Hossain, E. Kabalci, R. Bayindir, and R. Perez, "Microgrid testbeds around the world: State of art," *Energy Conversion and Management,* vol. 86, pp. 132-153, 2014.

[10] G. Salimath, N. K. Singh, and S. S. Badge, "Coordination and performance analysis of pumped hydro storage system integrated with solar, wind hybrid system," in *2017 International Conference on Energy, Communication, Data Analytics and Soft Computing (ICECDS)*, 2017: IEEE, pp. 160-164.

[11] K. Gowtham, C. Sivaramadurai, P. Hariprasath, and B. Indurani, "A Management of power flow for DC Microgrid with Solar and Wind Energy Sources," in *2018 International Conference on Computer Communication and Informatics (ICCCI)*, 2018: IEEE, pp. 1-5.

[12] S. Whaite, B. Grainger, and A. Kwasinski, "Power quality in DC power distribution systems and microgrids," *Energies,* vol. 8, no. 5, pp. 4378-4399, 2015.

[13] P. A. Madduri, J. Poon, J. Rosa, M. Podolsky, E. Brewer, and S. Sanders, "A scalable dc microgrid architecture for rural electrification in emerging regions," in *2015 IEEE Applied Power Electronics Conference and Exposition (APEC)*, 2015: IEEE, pp. 703-708.

[14] U. Manandhar, A. Ukil, and T. K. K. Jonathan, "Efficiency comparison of DC and AC microgrid," in *2015 IEEE Innovative Smart Grid Technologies-Asia (ISGT ASIA)*, 2015: IEEE, pp. 1-6.

[15] R. Bayindir, E. Hossain, E. Kabalci, and R. Perez, "A comprehensive study on microgrid technology," *International Journal of Renewable Energy Research (IJRER),* vol. 4, no. 4, pp. 1094-1107, 2014.

[16] S. N. Backhaus *et al.*, "DC microgrids scoping study. Estimate of technical and economic benefits," Los Alamos National Lab.(LANL), Los Alamos, NM (United States), 2015.

[17] A. R. Inversin, "Mini-grid design manual," 2000.
[18] S. Oliver and V. C. P. Line, "High-voltage DC distribution is key to increased system efficiency and renewable-energy opportunities," *Vicor White Paper,* 2012.
[19] T. Dragičević, X. Lu, J. C. Vasquez, and J. M. Guerrero, "DC microgrids—Part I: A review of control strategies and stabilization techniques," *IEEE Transactions on power electronics,* vol. 31, no. 7, pp. 4876-4891, 2015.
[20] J. Burkleo, "HVDC: The key to revolutionizing the renewable energy grid," *RenewableEnergyWorld. com,* 2013.
[21] S. Willems *et al.*, "Sustainable Impact and Standardization of a DC Micro Grid," in *Proceedings of Ecodesign 2013 International Symposium*, 2013.
[22] K. P. Vijayaragavan, "Feasibility of DC microgrids for rural electrification," ed, 2017.
[23] O. Alarfaj, "Modeling and Control of Low-Voltage DC Microgrid With Photovoltaic Energy Resources," University of Waterloo, 2014.
[24] Z. Jian, Z. He, J. Jia, and Y. Xie, "A review of control strategies for DC micro-grid," in *2013 Fourth International Conference on Intelligent Control and Information Processing (ICICIP)*, 2013: IEEE, pp. 666-671.
[25] D. Chen and L. Xu, "Autonomous DC voltage control of a DC microgrid with multiple slack terminals," *IEEE Transactions on Power Systems,* vol. 27, no. 4, pp. 1897-1905, 2012.
[26] L. Zhang, T. Wu, Y. Xing, K. Sun, and J. M. Gurrero, "Power control of DC microgrid using DC bus signaling," in *2011 Twenty-Sixth Annual IEEE Applied Power Electronics Conference and Exposition (APEC)*, 2011: IEEE, pp. 1926-1932.
[27] D. Chen, L. Xu, and L. Yao, "DC voltage variation based autonomous control of DC microgrids," *IEEE transactions on power delivery,* vol. 28, no. 2, pp. 637-648, 2013.
[28] T. Logenthiran, D. Srinivasan, A. M. Khambadkone, and H. N. Aung, "Multiagent system for real-time operation of a microgrid in real-time digital simulator," *IEEE Transactions on smart grid,* vol. 3, no. 2, pp. 925-933, 2012.
[29] C.-H. Yoo, W.-J. Choi, I.-Y. Chung, D.-J. Won, S.-S. Hong, and B.-J. Jang, "Hardware-in-the-loop simulation of DC microgrid with multi-agent system for emergency demand response," in *2012 IEEE Power and Energy Society General Meeting*, 2012: IEEE, pp. 1-6.
[30] H. Kakigano, A. Nishino, and T. Ise, "Distribution voltage control for DC microgrid with fuzzy control and gain-scheduling control," in *8th International Conference on Power Electronics-ECCE Asia*, 2011: IEEE, pp. 256-263.
[31] M. Mylrea and S. N. G. Gourisetti, "Blockchain for smart grid resilience: Exchanging distributed energy at speed, scale and security," in *2017 Resilience Week (RWS)*, 2017: IEEE, pp. 18-23.
[32] J. Karp, "Concentrating solar power: progress and trends," *Jacobs School of Engineering, University of California San Diego, Triton SPIE/OSA,* 2009.
[33] H.-T. Zhang and L. L. Lai, "Research on wind and solar penetration in a 9-bus network," in *2012 IEEE Power and Energy Society General Meeting*, 2012: IEEE, pp. 1-6.
[34] G. W. E. Council, "Global Wind Report Annual market update 2012, Belgium," ed, 2011.
[35] K. Grogg, "Harvesting the wind: the physics of wind turbines," *Physics and Astronomy Comps Papers,* vol. 7, 2005.
[36] D. M. Tagare, *Electricity power generation: the changing dimensions*. John Wiley & Sons, 2011.

[37] J. Reca, J. Martinez, R. Banos, and C. Gil, "Optimal design of gravity-fed looped water distribution networks considering the resilience index," *Journal of Water Resources Planning and Management,* vol. 134, no. 3, pp. 234-238, 2008.

[38] S. C. Savulescu and S. Virmani, "Half a century of computer methods in power system analysis, planning and operations: Part II: Glenn W. Stagg and his contributions to advancing the technology," in *2011 IEEE/PES Power Systems Conference and Exposition*, 2011: IEEE, pp. 1-8.

[39] P. Kumar and D. K. Palwalia, "Decentralized autonomous hybrid renewable power generation," *Journal of Renewable Energy,* vol. 2015, 2015.

[40] S. Tabish and I. Ashraf, "Simulation of partial shading on solar photovoltaic modules with experimental verification," *International Journal of Ambient Energy,* vol. 38, no. 2, pp. 161-170, 2017.

[41] C. Wang and M. H. Nehrir, "Power management of a stand-alone wind/photovoltaic/fuel cell energy system," *IEEE transactions on energy conversion,* vol. 23, no. 3, pp. 957-967, 2008.

[42] J. Li, X. Zhang, and W. Li, "An efficient wind-photovoltaic hybrid generation system for DC micro-grid," 2009.

[43] Y. Wang, Z. Zhang, Y. Fu, Y. Hei, and X. Zhang, "Pole-to-ground fault analysis in transmission line of DC grids based on VSC," in *2016 IEEE 8th International Power Electronics and Motion Control Conference (IPEMC-ECCE Asia)*, 2016: IEEE, pp. 2028-2032.

[44] J. Stevens and B. Schenkman, "DC energy storage in the CERTS microgrid," *Sandia National Laboratories,* 2008.

[45] S. Grillo, V. Musolino, L. Piegari, E. Tironi, and C. Tornelli, "DC islands in AC smart grids," *IEEE Transactions on Power Electronics,* vol. 29, no. 1, pp. 89-98, 2013.

[46] K. Hu and C. Liaw, "On the flywheel/battery hybrid energy storage system for DC microgrid," in *2013 1st International Future Energy Electronics Conference (IFEEC)*, 2013: IEEE, pp. 119-125.

[47] S. M. Kalaskar, "Seminar Report," *Fault Analsysis in HVDC & HVAC Transmission Line,* 2016-2017.

[48] Y. M. Soe, S. S. E. Aung, and Z. Linn, "Analysis on Performance of DC Microgrid under Fault Condition," *American Scientific Research Journal for Engineering, Technology, and Sciences (ASRJETS),* vol. 26, no. 3, pp. 1-12, 2016.

[49] D. Paul, "DC traction power system grounding," *IEEE Transactions on Industry Applications,* vol. 38, no. 3, pp. 818-824, 2002.

[50] M. M. Rahman, M. F. Rabbi, M. K. Islam, and F. M. Rahman, "HVDC over HVAC power transmission system: Fault current analysis and effect comparison," in *2014 International Conference on Electrical Engineering and Information & Communication Technology*, 2014: IEEE, pp. 1-6.

[51] W. Leterme and D. Van Hertem, "Classification of fault clearing strategies for HVDC grids," in *CIGRE, Date: 2015/05/27-2015/05/28, Location: Lund*, 2015.

[52] P. Zhao, Q. Chen, and L. Xing, "DC fault analysis of VSC-HVDC and DC cable protection principle," in *2015 IEEE PES Asia-Pacific Power and Energy Engineering Conference (APPEEC)*, 2015: IEEE, pp. 1-5.

[53] J. Lagorse, D. Paire, and A. Miraoui, "Sizing optimization of a stand-alone street lighting system powered by a hybrid system using fuel cell, PV and battery," *Renewable Energy,* vol. 34, no. 3, pp. 683-691, 2009.

[54] M. Deshmukh and S. Deshmukh, "Modeling of hybrid renewable energy systems," *Renewable and sustainable energy reviews,* vol. 12, no. 1, pp. 235-249, 2008.
[55] M. Kalantar, "Dynamic behavior of a stand-alone hybrid power generation system of wind turbine, microturbine, solar array and battery storage," *Applied energy,* vol. 87, no. 10, pp. 3051-3064, 2010.
[56] S. I. Klychev, M. Mukhammadiev, R. Zakhidov, and K. Potaenko, "Technical and economic conditions for creation of combined solar-wind power plants," *Applied Solar Energy,* vol. 43, no. 4, pp. 214-217, 2007.
[57] F. Jurado and J. R. Saenz, "Neuro-fuzzy control for autonomous wind–diesel systems using biomass," *Renewable energy,* vol. 27, no. 1, pp. 39-56, 2002.
[58] Y. Katsigiannis, P. Georgilakis, and E. Karapidakis, "Multiobjective genetic algorithm solution to the optimum economic and environmental performance problem of small autonomous hybrid power systems with renewables," *IET Renewable Power Generation,* vol. 4, no. 5, pp. 404-419, 2010.
[59] A. Mahor, V. Prasad, and S. Rangnekar, "Economic dispatch using particle swarm optimization: A review," *Renewable and sustainable energy reviews,* vol. 13, no. 8, pp. 2134-2141, 2009.
[60] S. Brini, H. H. Abdallah, and A. Ouali, "Economic dispatch for power system included wind and solar thermal energy," *Leonardo Journal of Sciences,* vol. 14, no. 2009, pp. 204-220, 2009.
[61] F. N. Kanhukamwe, "Matching renewable energy to the South African electricity system," Stellenbosch: Stellenbosch University, 2019.
[62] R. Dufo-Lopez and J. L. Bernal-Agustín, "Multi-objective design of PV–wind–diesel–hydrogen–battery systems," *Renewable energy,* vol. 33, no. 12, pp. 2559-2572, 2008.
[63] B. O. Bilal, V. Sambou, P. Ndiaye, C. Kébé, and M. Ndongo, "Optimal design of a hybrid solar–wind-battery system using the minimization of the annualized cost system and the minimization of the loss of power supply probability (LPSP)," *Renewable Energy,* vol. 35, no. 10, pp. 2388-2390, 2010.
[64] A. Pachori and P. Suhane, "Modeling and simulation of photovoltaic/wind/diesel/battery hybrid power generation system," *International Journal of Electrical, Electronics and Computer Engineering,* vol. 3, no. 1, p. 122, 2014.
[65] F. G. Montoya, R. Baños, C. Gil, A. Espín, A. Alcayde, and J. Gómez, "Minimization of voltage deviation and power losses in power networks using Pareto optimization methods," *Engineering Applications of Artificial Intelligence,* vol. 23, no. 5, pp. 695-703, 2010.
[66] C. Cormio, M. Dicorato, A. Minoia, and M. Trovato, "A regional energy planning methodology including renewable energy sources and environmental constraints," *Renewable and Sustainable Energy Reviews,* vol. 7, no. 2, pp. 99-130, 2003.
[67] V. Courtecuisse, J. Sprooten, B. Robyns, M. Petit, B. Francois, and J. Deuse, "A methodology to design a fuzzy logic based supervision of Hybrid Renewable Energy Systems," *Mathematics and computers in simulation,* vol. 81, no. 2, pp. 208-224, 2010.
[68] T.-Y. Lee and C.-L. Chen, "Wind-photovoltaic capacity coordination for a time-of-use rate industrial user," *IET Renewable Power Generation,* vol. 3, no. 2, pp. 152-167, 2009.
[69] A. K. Kaviani, G. Riahy, and S. M. Kouhsari, "Optimal design of a reliable hydrogen-based stand-alone wind/PV generating system, considering component outages," *Renewable energy,* vol. 34, no. 11, pp. 2380-2390, 2009.
[70] R. Eke, O. Kara, and K. Ulgen, "Optimization of a wind/PV hybrid power generation system," *International Journal of Green Energy,* vol. 2, no. 1, pp. 57-63, 2005.

[71] G. Giannakoudis, A. Papadopoulos, P. Seferlis, and S. Voutetakis, "On the systematic design and optimization under uncertainty of a hybrid power generation system using renewable energy sources and hydrogen storage," in *Computer Aided Chemical Engineering*, vol. 28: Elsevier, 2010, pp. 907-912.

[72] E. Sreeraj, K. Chatterjee, and S. Bandyopadhyay, "Design of isolated renewable hybrid power systems," *Solar Energy,* vol. 84, no. 7, pp. 1124-1136, 2010.

[73] J. L. Bernal-Agustín and R. Dufo-Lopez, "Simulation and optimization of stand-alone hybrid renewable energy systems," *Renewable and Sustainable Energy Reviews,* vol. 13, no. 8, pp. 2111-2118, 2009.

[74] M. Martiskainen and J. Coburn, "The role of information and communication technologies (ICTs) in household energy consumption—prospects for the UK," *Energy Efficiency,* vol. 4, no. 2, pp. 209-221, 2011.

[75] T. Senjyu, D. Hayashi, A. Yona, N. Urasaki, and T. Funabashi, "Optimal configuration of power generating systems in isolated island with renewable energy," *Renewable energy,* vol. 32, no. 11, pp. 1917-1933, 2007.

[76] P. Balamurugan, S. Ashok, and T. Jose, "Optimal operation of biomass/wind/PV hybrid energy system for rural areas," *International Journal of Green Energy,* vol. 6, no. 1, pp. 104-116, 2009.

[77] P. Nema, R. Nema, and S. Rangnekar, "A current and future state of art development of hybrid energy system using wind and PV-solar: A review," *Renewable and Sustainable Energy Reviews,* vol. 13, no. 8, pp. 2096-2103, 2009.

[78] R. Dufo-Lopez, J. L. Bernal-Agustín, and J. Contreras, "Optimization of control strategies for stand-alone renewable energy systems with hydrogen storage," *Renewable energy,* vol. 32, no. 7, pp. 1102-1126, 2007.

[79] R. S. Garcia and D. Weisser, "A wind–diesel system with hydrogen storage: Joint optimisation of design and dispatch," *Renewable energy,* vol. 31, no. 14, pp. 2296-2320, 2006.

[80] E. Koutroulis, D. Kolokotsa, A. Potirakis, and K. Kalaitzakis, "Methodology for optimal sizing of stand-alone photovoltaic/wind-generator systems using genetic algorithms," *Solar energy,* vol. 80, no. 9, pp. 1072-1088, 2006.

[81] H. Yang, W. Zhou, L. Lu, and Z. Fang, "Optimal sizing method for stand-alone hybrid solar–wind system with LPSP technology by using genetic algorithm," *Solar energy,* vol. 82, no. 4, pp. 354-367, 2008.

[82] A. Arce, C. Bordons Alba, and A. d. Real Torres, "Optimization strategy for element sizing in hybrid power systems," *Journal of Power Sources, 193, 315-321.,* 2009.

[83] J. L. Bernal-Agustín and R. Dufo-López, "Efficient design of hybrid renewable energy systems using evolutionary algorithms," *Energy Conversion and management,* vol. 50, no. 3, pp. 479-489, 2009.

[84] P. Zervas, H. Sarimveis, J. Palyvos, and N. Markatos, "Model-based optimal control of a hybrid power generation system consisting of photovoltaic arrays and fuel cells," *Journal of power sources,* vol. 181, no. 2, pp. 327-338, 2008.

[85] S. Diaf, M. Belhamel, M. Haddadi, and A. Louche, "Technical and economic assessment of hybrid photovoltaic/wind system with battery storage in Corsica island," *Energy policy,* vol. 36, no. 2, pp. 743-754, 2008.

[86] S. Hakimi and S. Moghaddas-Tafreshi, "Optimal sizing of a stand-alone hybrid power system via particle swarm optimization for Kahnouj area in south-east of Iran," *Renewable energy,* vol. 34, no. 7, pp. 1855-1862, 2009.

[87] J. A. Razak, K. Sopian, Y. Ali, M. A. Alghoul, A. Zaharim, and I. Ahmad, "Optimization of PV-wind-hydro-diesel hybrid system by minimizing excess capacity," *European Journal of Scientific Research,* vol. 25, no. 4, pp. 663-671, 2009.

[88] S. Chakraborty, T. Senjyu, A. Y. Saber, A. Yona, and T. Funabashi, "Optimal thermal unit commitment integrated with renewable energy sources using advanced particle swarm optimization," *IEEJ transactions on electrical and electronic engineering,* vol. 4, no. 5, pp. 609-617, 2009.

[89] J. Matevosyan, M. Olsson, and L. Söder, "Hydropower planning coordinated with wind power in areas with congestion problems for trading on the spot and the regulating market," *Electric Power Systems Research,* vol. 79, no. 1, pp. 39-48, 2009.

[90] E. D. Castronuovo and J. P. Lopes, "On the optimization of the daily operation of a wind-hydro power plant," *IEEE Transactions on Power Systems,* vol. 19, no. 3, pp. 1599-1606, 2004.

[91] R. Dufo-López and J. L. Bernal-Agustín, "Design and control strategies of PV-Diesel systems using genetic algorithms," *Solar energy,* vol. 79, no. 1, pp. 33-46, 2005.

[92] J. Anagnostopoulos and D. Papantonis, "Simulation and size optimization of a pumped–storage power plant for the recovery of wind-farms rejected energy," *Renewable Energy,* vol. 33, no. 7, pp. 1685-1694, 2008.

[93] A. Anarbaev, R. Zakhidov, and R. Avezov, "Schematic and parametric optimization of solar+ fuel boiler installations," *Applied Solar Energy,* vol. 44, no. 1, pp. 20-23, 2008.

[94] C. V. RAO, B. S. SAW, V. VENKATESH, B. S. KUMAR, and G. Y. NAIK, "Solar PV System Precise by Using P&O for Maximum Output."

[95] M. Sheraz and M. Abido, "An efficient fuzzy logic based maximum power point tracking controller for photovoltaic systems," in *International Conference on Renewable Energies and Power Quality*, 2013, pp. 4-10.

[96] L. Piegari and R. Rizzo, "Adaptive perturb and observe algorithm for photovoltaic maximum power point tracking," *IET Renewable Power Generation,* vol. 4, no. 4, pp. 317-328, 2010.

[97] M. Patil and A. Deshpande, "Design and simulation of perturb and observe maximum power point tracking using matlab/simulink," in *2015 International Conference on Industrial Instrumentation and Control (ICIC)*, 2015: IEEE, pp. 1345-1349.

[98] L. Ashok Kumar, S. Sumathi, and P. Surekha, "Solar PV and wind energ conversion systems: An introduction to theory, modeling with MATLAB/SIMULINK, and the role of soft computing techniques," ed: Springer, 2015.

[99] H.-L. Tsai, C.-S. Tu, and Y.-J. Su, "Development of generalized photovoltaic model using MATLAB/SIMULINK," in *Proceedings of the world congress on Engineering and computer science*, 2008, vol. 2008: San Francisco, USA, pp. 1-6.

[100] A. Oi, "Design and simulation of photovoltaic water pumping system," *California Polytechnic State University,* 2005.

[101] G. M. Masters, *Renewable and efficient electric power systems*. John Wiley & Sons, 2013.

[102] D. Hohm and M. E. Ropp, "Comparative study of maximum power point tracking algorithms," *Progress in photovoltaics: Research and Applications,* vol. 11, no. 1, pp. 47-62, 2003.

[103] G. Yu, Y. Jung, J. Choi, and G. Kim, "A novel two-mode MPPT control algorithm based on comparative study of existing algorithms," *Solar Energy,* vol. 76, no. 4, pp. 455-463, 2004.

[104] R. Pena, R. Cardenas, R. Blasco, G. Asher, and J. Clare, "A cage induction generator using back to back PWM converters for variable speed grid connected wind energy system," in *IECON'01. 27th Annual Conference of the IEEE Industrial Electronics Society (Cat. No. 37243)*, 2001, vol. 2: IEEE, pp. 1376-1381.
[105] A. D. Hansen, P. Sorensen, L. H. Hansen, and H. Bindner, "Models for a stand-alone PV system," *Roskilde: Rio National Laboratory,* 2000.
[106] Y. Ito, Y. Zhongqing, and H. Akagi, "DC microgrid based distribution power generation system," in *The 4th International Power Electronics and Motion Control Conference, 2004. IPEMC 2004.*, 2004, vol. 3: IEEE, pp. 1740-1745.
[107] J. Grant, "Design and Simulation of a DC Microgrid for a Small Island in Belize," *Iceland School of Energy,* 2018.
[108] D. W. Hart, *Power electronics*. Tata McGraw-Hill Education, 2011.
[109] J. Zhao, K. Graves, C. Wang, G. Liao, and C.-P. Yeh, "A hybrid electric/hydro storage solution for standalone photovoltaic applications in remote areas," in *2012 IEEE Power and Energy Society General Meeting*, 2012: IEEE, pp. 1-6.
[110] J.-N. Paquin, J. Moyen, G. Dumur, and V. Lapointe, "Real-time and off-line simulation of a detailed wind farm model connected to a multi-bus network," in *2007 IEEE Canada Electrical Power Conference*, 2007: IEEE, pp. 145-152.
[111] S. Aldhaher, D. C. Yates, and P. D. Mitcheson, "Load-independent class E/EF inverters and rectifiers for MHz-switching applications," *IEEE Transactions on Power Electronics,* vol. 33, no. 10, pp. 8270-8287, 2018.
[112] in *Elprocus Electrical project Focus*, ed.
[113] M. W. Siti and R. Tiako, "Optimal Energy Control of a Grid-Connected Solar Wind-Based Electric Power Plant Applying Time-of-Use Tariffs," *International Review of Electrical Engineering (IREE),* 2015.
[114] A. A. El-Hady, S. H. Arafa, M. N. Nashed, and S. G. Ramadan, "Modeling and Simulation for Hybrid of PV-Wind system," *International Journal of Engineering Research,* vol. 4, no. 4, pp. 178-183, 2015.
[115] F. Mohamed, "Microgrid modelling and simulation," *Helsinki University of Technology, Finland,* 2006.
[116] Y.-K. Chen, Y.-C. Wu, C.-C. Song, and Y.-S. Chen, "Design and implementation of energy management system with fuzzy control for DC microgrid systems," *IEEE Transactions on power electronics,* vol. 28, no. 4, pp. 1563-1570, 2012.
[117] A. A. Aduragba, "Investigating the application of Static Synchronous Compensator (STATCOM) for mitigating power transmission line losses," 2017.
[118] D. Q. Zhou, U. D. Annakkage, and A. D. Rajapakse, "Online monitoring of voltage stability margin using an artificial neural network," *IEEE Transactions on Power Systems*, vol. 25, no. 3, pp. 1566-1574, 2010.

APPENDIX A: Wind Generation

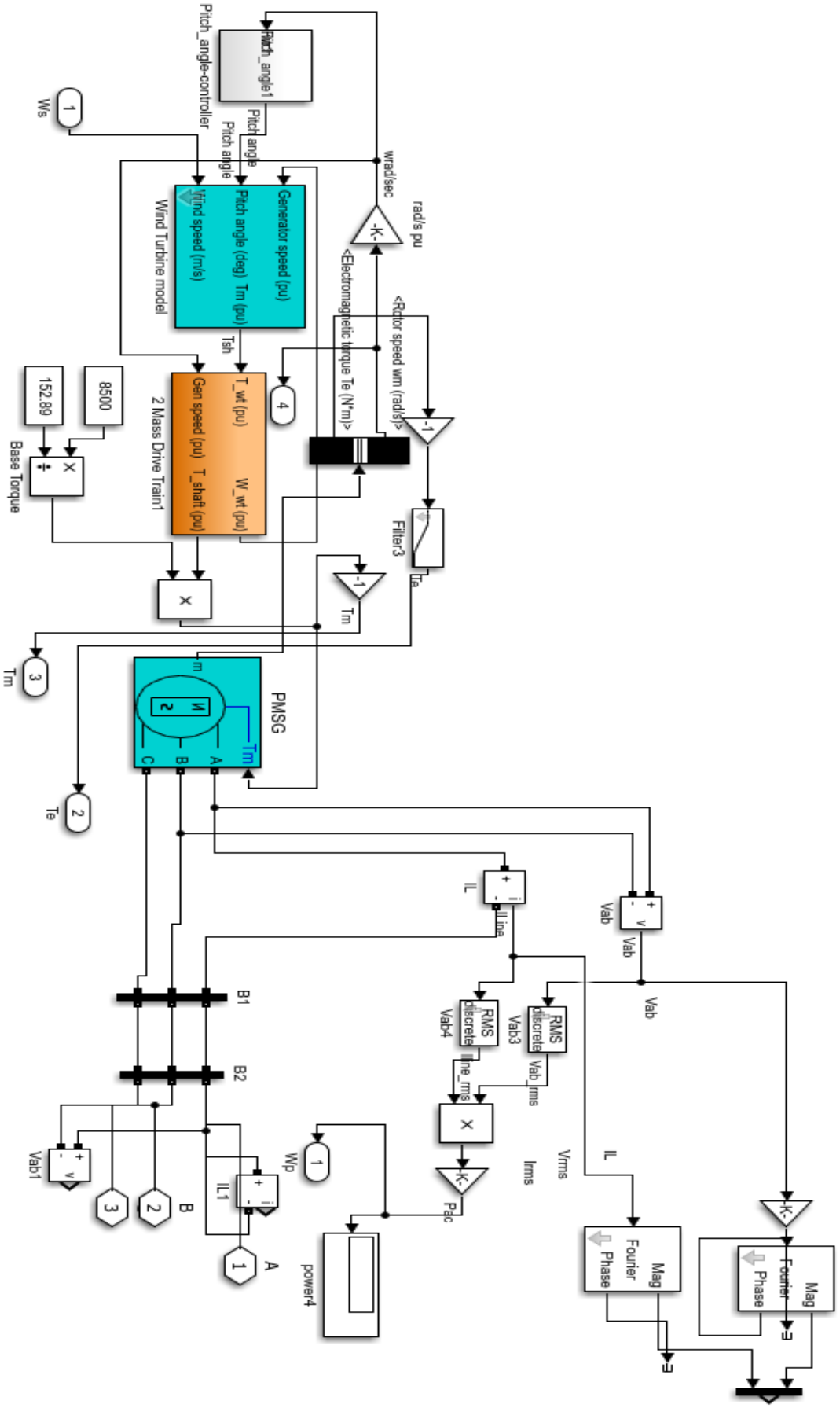

APPENDIX B: 2-Masse Drive Train1 Model

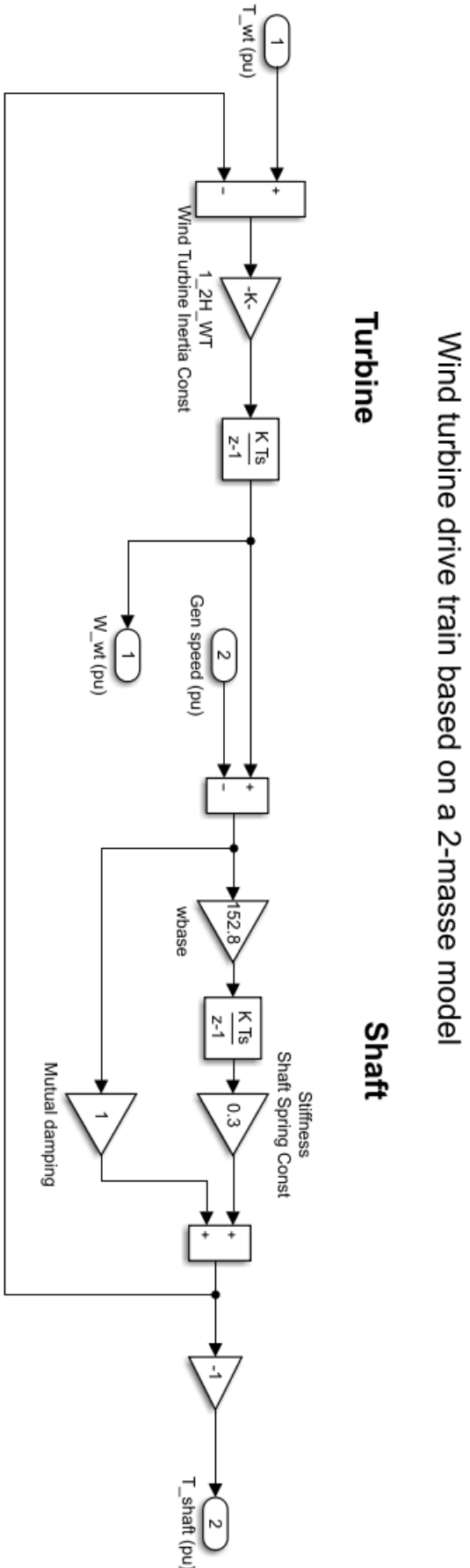

APPENDIX C: Pitch Angle-Controller

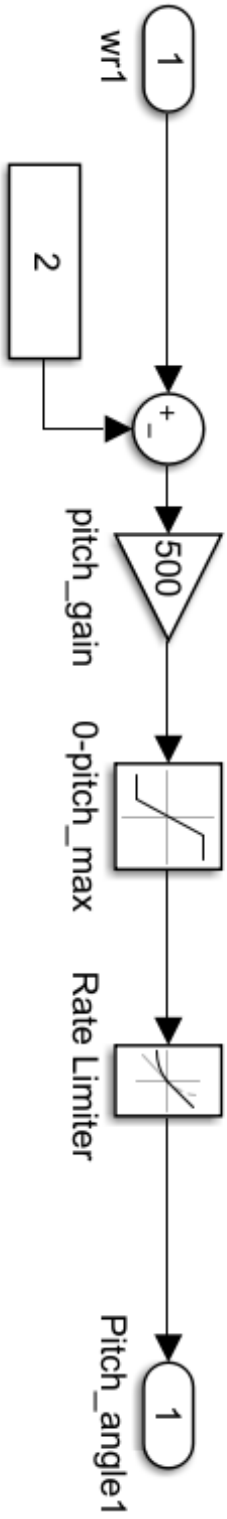

APPENDIX D: Hybrid DC Microgrid: PV System and Wind Energy System